The Pharmacokinetics of Local Vascular Drug Delivery: Demonstration with a Model Vasotherapeutic Compound, Heparin

by

Mark A. Lovich

B.S. Mechanical Engineering
Columbia University, 1988

M.S. Mechanical Engineering
University of California at Berkeley, 1990

SUBMITTED TO THE HARVARD-M.I.T. DIVISION OF HEALTH SCIENCES AND TECHNOLOGY
IN PARTIAL FULFILLMENT OF THE REQUIREMENTS FOR THE DEGREE OF

DOCTOR OF PHILOSOPHY IN
MEDICAL ENGINEERING AND MEDICAL PHYSICS
AT THE
MASSACHUSETTS INSTITUTE OF TECHNOLOGY

JUNE, 1997

Signature of Author: _____
Division of Health Science and Technology
January 7, 1997

Certified by: _____
Elazer R. Edelman
Hermann Von Helmholtz Associate Professor of
Health Sciences and Technology
Thesis Supervisor

Certified by: _____
Martha L. Gray
J.W. Kieckhefer Associate Professor of
Electrical Engineering and Computer Science
Co-Director, Health Sciences and Technology

The Pharmacokinetics of Local Vascular Drug Delivery:
Demonstration with a Model Vasotherapeutic Compound, Heparin

by

Mark A. Lovich

Submitted to the Harvard-M.I.T. Division of Health Sciences and Technology on January 7, 1997 in Partial Fulfillment of the Requirements for the Degree of Doctor Of Philosophy In Medical Engineering And Medical Physics

ABSTRACT

Aim: To predict vascular deposition and distribution of exogenous regulatory compounds.

Motivation: The hyperproliferative response to vascular injury is the greatest limitation to the potential of mechanical revascularization. Tissue and animal models have defined classes of compounds that might combat these diseases, yet none work clinically. One limitation of extrapolating from tissue culture to humans is the uncertainty of whether such failure is from a resistant human arteriopathic lesion or simply a limitation of drug residence within the vessel. Only detailed pharmacokinetic models describing drug-tissue interactions can differentiate between these failures. Detailed analyses are especially important for the development of local vascular drug delivery strategies which impart large dynamic drug concentration gradients across tissues.

Transport and Binding Properties: A series of experiments elucidated the mechanisms of deposition and distribution. Diffusive and convective transport, and binding in each arterial layer were characterized for a model inhibitor of smooth muscle cell growth, heparin. The molecular diffusivity of heparin in media and adventitia, and the transendothelial resistance were measured with *in vitro* perfusion experiments. Both the adventitia and endothelium were shown to exert minimal resistance to heparin transport. Theoretical predictions and perfusion studies showed that diffusion outweighs convection in controlling transmural transport in thin arteries, but these forces are more balanced in thicker vessels or following endothelial injury. The density of all binding sites, their average dissociation constant, and the fractional available space were measured with an equilibrium distribution technique. More heparin binding sites were identified in arterial media than adventitia, the latter with higher affinity. The transport of drug to the vessel wall from the perivascular space was characterized through inulin clearance and arterial heparin deposition studies. Most of the perivascularly released inulin was shown to be cleared by extramural capillaries, and yet most of the heparin deposited in arteries diffuses directly from the exterior.

Pharmacokinetics: Computational models of intramural drug deposition and distribution were constructed based on the accumulated data. Augmentation of animal data with simulations has helped overcome limitations of standard labeled-drug deposition assays by providing high spatial and temporal resolution and by predicting transmural concentration profiles of soluble, bound and internalized drug. The simulations suggest that heparin is not retained in the arterial wall for appreciable periods, implying that sustained modes of delivery are needed to treat vascular disease.

Conclusions: Definition of the physical interaction between soluble compounds and vascular tissues has shed light on the mechanisms of proliferative vascular disease and its therapy. The same principles can be applied to any therapeutic, physiologic, and pathophysiologic process where cells communicate through soluble signals.

Thesis Committee: Prof. Elazer R. Edelman (Supervisor)
Prof. Roger D. Kamm
Prof. Morris J. Karnovsky
Prof. Robert S. Langer
Prof. Douglas A. Lauffenburger

ACKNOWLEDGEMENTS

I wish to thank first and foremost my thesis supervisor Prof. Elazer R. Edelman for single-handedly creating a field for me to work in, and for pouring his heart and soul into my education as a scientist and my professional development. He has never been less than 100% supportive of all of my goals and needs, and has always been available to me for any issue or concern, professional and personal, 24 hours a day. He has been the model mentor to me, giving me tremendous latitude while teaching experimental design, laboratory skills, and most importantly how to present my work in a manner that is intuitive and highlights the scientific impact. He has been a role model to me and I will always consider him my teacher.

I would like to pay special tribute to my thesis committee members, Profs. Morris J. Karnovsky, Robert S. Langer, Douglas A. Lauffenburger, and Roger D. Kamm. I am fortunate to have had the support and guidance of the world's leaders in vascular biology, controlled-release technology, receptor kinetics and trafficking, and modeling of physiology. I thank Prof. Karnovsky for tutoring me in heparin biochemistry and transendothelial transport, and Prof. Langer for his insightful suggestions and for giving me access to all of the resources in his laboratory. I thank Prof. Lauffenburger for making me think through the finest details of my work and helping my studies gain acceptance outside MIT, and Prof. Kamm who has been a part of this project since day one and has met with me countless times to help with the quantitative aspects of my work. Each member has shaped the direction of this project and has contributed directly to my education. I have profound reverence and admiration for them all and am honored by their interest and input.

Many of the members of Prof. Edelman's laboratory have sacrificed much of their time to help me and to teach me. All of them have brought a unique set of skills and expertise and I have benefited tremendously from their perspectives. Drs. Larry Brown, Campbell Roger, and Edward Koo have all taken inordinate amounts of time from their own projects to work with me in the laboratory and I thank them for their selflessness. I also wish to acknowledge the many hours that Drs. Aruna Nathan, Iveta Dinbergs, David Ettenson, Martin Sirois, and David Tseng have spent

educating me and helping me navigate through many fields so distant from my background. Jim Squire has been a consistent resource for the quantitative aspects of the project and has reviewed every manuscript. Wade Wan deserves special thanks for helping making the code for the simulations in this thesis into a user friendly tool that is now used by many in the lab. Anna Browne has always supported my work logistically and looked out for my interests. I owe thanks to Philip Seifert for teaching technical skills, staying late to assist me, and always seeking to improve my methods. Some of the work in this thesis was performed with the assistance of Renata Yang and Carmen Berg, and they have my thanks.

Much of the work in my thesis was performed using equipment belonging to Dr. Fred Bowman and he has my gratitude. His graduate student, Greg Martin, was a great resource to me in the early stages of my thesis.

Several of the analyses in this work could not have been possible without the financial and laboratory assistance of many employees Focal Interventional Therapeutics. I am grateful to our Industrial Collaborators: Mike Philbrook, Ed Weselcouch, Pat Campbell, Shawn Sawyer, Michelle Gallant, and Larry Roth.

A special thanks to Dr. Roger Mark for steering me towards Dr. Edelman's laboratory.

This work has been supported by the NIH, the Whitaker Foundation, the Dorothy Poitras Foundation, Focal Interventional Therapeutics, and Sterling Winthrop, Inc.

My pursuit of the PhD could not have been possible without the enthusiasm and blessings of my wife, Debbie. I thank her for letting me indulge myself while she worked hard to support us and now our family. I want to thank our daughter Danielle for being so cute and making everything that much more enjoyable.

CONTENTS

1. BACKGROUND AND INTRODUCTION

1.1. Anatomy of the Blood Vessel Wall

A brief review of arterial architecture and content will put into context many of the terms and concepts used throughout this work. Arteries are living tubes composed of three concentric tunics or layers, each with distinct structure, cell types, and functions: 1) The innermost layer is the *tunica intima* and consists of a monolayer of endothelial cells supported by the internal elastic lamina, a layer of connective tissue comprised mostly of elastin. The endothelial cells are interconnected through intercellular tight junctions, forming an intact monolayer wherein each cell is aligned along the axis of flow in the artery. In many blood vessels in humans and higher animal species, the subendothelial space, just luminal of the internal elastic lamina, may contain vascular smooth muscle cells. 2) The middle layer is the *tunica media* and consists of alternating sublayers or lamellae of circumferentially oriented vascular smooth muscle cells and thin sheets of collagen and elastin. These cells provide the contractile force required to modulate vessel diameter and alter perfusion to downstream tissues. 3) The outermost layer is the *tunica adventitia*, which consists primarily of type I collagen with scattered fibroblasts and adipocytes. Coursing through this layer in arteries approximately 0.5 mm thick or greater are *vasa vasorum*, also referred to as the blood vessels of the blood vessel wall.[1] In many arteries, the extent of the adventitia is less well-defined than the intima or media, and further away from the lumen it gradually blends into layers of fascia and fat.

The cells within the arterial wall communicate and regulate each other through biochemical paracrine signals. Endothelial cells, for example, are sensitive to shear stress and respond by releasing factors such as Endothelial Derived Relaxing Factor (EDRF) which causes medial smooth muscle cells to relax leading to vasodilation and enhanced regional blood flow.[2-4] Endothelial cells and smooth muscle cells also secrete compounds that promote and inhibit each others' growth, both in quiescent states and in states of dysregulation and repair. For example, injured vascular smooth muscle cells release compounds such as basic fibroblast growth factor (bFGF) which are

mitogenic to both endothelial and smooth muscle cells, possibly in attempt to repair the vessel wall.[5-9] On the other hand, confluent endothelial cells secrete soluble inhibitors of vascular smooth muscle cell growth, such as heparan sulfate proteoglycans, that may provide negative feedback on the reparative process and limit the hyperplasia initiated by wound healing.[10-13] Thus, the cells of the blood vessel wall are constantly communicating through soluble signals in order to optimally regulate vascular function and homeostasis.

1.2. Proliferative Vascular Diseases

It has been postulated that injury to the endothelial monolayer and underlying smooth muscle disrupts the normal arterial homeostasis and initiates a cascade of cellular and molecular events that culminate in vascular hyperproliferation.[14-16] Endothelial injury leads to platelet aggregation, thrombus formation, inflammation, activation of macrophages and the local release of cytokines.[8,17] Direct injury to the arterial media kills a substantial fraction of smooth muscle cells, releasing growth factors and other mediators that stimulate their proliferation, in an attempt to heal the blood vessel.[7-9,18] Many of these mediators promote their own synthesis and release from neighboring cells in a self-amplifying manner, which stimulates DNA synthesis and cell division throughout the injured artery in a synchronized fashion. Several days after injury, under the influence of other chemotactic agents, smooth muscle cells begin migrating towards the lumen of the artery, some dividing once within the expanded intima.[18] These smooth muscle cells in the lumen change to a synthetic rather than contractile phenotype, produce extracellular matrix and proliferate further.

Cardiovascular diseases, which derive from chronic forms of injury and endogenous repair, account for over 1 million deaths each year in the United States and almost 1.5 million interventions. Currently, the only available therapies are mechanical revascularizations such as percutaneous transluminal coronary angioplasty, venous interposition and prosthetic grafting, endovascular stent placement, and atherectomy. Unfortunately, all of these mechanical attempts at alleviating the symptoms of low coronary flow rates are beset by accelerated vascular disease of their own. For example, 30 - 40% of coronary angioplasty patients will require another

angioplasty or bypass surgery within 3-6 months.[16] The mean lifetime of a saphenous vein interposition graft is seven years and 10% are occluded within two weeks after surgery, 20% at one year and 35% at five years.[16] Endovascular stenting can increase luminal diameter, prevent elastic recoil, and yet is associated with a similar rate of clinical failure. All of these mechanical interventions expand the functional lumen of the artery, but as a byproduct they also injure the blood vessel wall, and initiate the cellular and molecular events described above and culminate in a space occupying lesion within the arterial lumen that consists primarily of vascular smooth muscle cells.[16] This injury and proliferative response is referred to as intimal hyperplasia or restenosis.

Randomized clinical trials on patients following revascularization and subsequent arterial injury have included readily available cardiovascular drugs that in theory should modulate the molecular mechanisms involved in forming the restenotic lesion. Antiplatelet agents, anticoagulants, calcium channel blockers, angiotensin converting enzyme inhibitors, lipid lowering agents, steroids, growth inhibitors, and antiproliferative compounds have all been unsuccessful in limiting human accelerated arteriopathies.[19,20] Efficacy of these agents at regulating the proliferative response to injury is therefore limited to the animal, and is not demonstrable in the human, or is only evident at doses and for exposure times much greater than previously utilized. The lack of an "off-the-shelf" pharmacologic solution to the restenosis problem has sparked numerous cell culture investigations to find inhibitors of vascular smooth muscle cell proliferation and migration.[11,12,21-25] Animal models of arterial injury have been used to evaluate the antiproliferative effects of heparin,[10,13,26,27] Hirulog,[28] anti-inflammatory drugs such as dexamethasone,[29,30] angiotensin converting enzyme inhibitors,[31] antimitotic inhibitors of tubulin polymerization such as colchicine,[32,33] anti-platelet drugs such as forskolin,[34] antineoplastic antibiotic agents such as mitomycin c[35] or gamma interferon,[36] antisense oligonucleotides directed against cell cycle proteins,[37-39] and cytotoxic compounds directed against growth factor receptors.[40] Although these investigations showed promising results, many of these compounds are non-specific inhibitors of cell growth and therefore cause inadvertent injury to other tissues, such as the rapidly proliferating gut epithelium and lymphoid cells. Systemic levels of other compounds have

profound toxic effects independent of their antiproliferative properties. For example steroid hormones are associated with hypertension, diabetes, immunosupression, and profound systemic morphologic effects.[41] Heparin in large concentrations can cause hemorrhage, osteoporosis, alopecia, electrolyte shifts and thrombocytopenia.[42,43] Furthermore, for many of these compounds the concentration in injured arterial tissues need to be elevated for days to weeks to achieve inhibition of intimal hyperplasia, however, their rapid plasma clearance and denaturation require continuous administration, which can be clinically burdensome. Lastly, some of the above compounds are extraordinarily expensive. For example, at current commercial rates, a single intravenous bolus of antisense oligonucleotides large enough to elevate plasma levels high enough to treat a 70 kg man would cost approximately $1.4 million. Therefore, for any of these compounds to be effective and practical, a route of delivery is required that minimizes systemic concentrations and side effects, that allows drug to reach target tissues and act before it is cleared or denatured, and minimizes waste by not loading unnecessary tissues. Recent pharmacologic strategies have evolved to deliver these compounds to the immediate vicinity of the diseased blood vessel segment, in an attempt to elevate concentrations in target tissues while minimizing systemic levels.[26-30,32-35,37-40]

1.3. Local Delivery

Several technologies have evolved that can deliver compounds locally to the environment of the blood vessel wall in an attempt to achieve the goals stated above, and are shown schematically (Fig. 1.1). These can be organized into two groups: systemic administration and local release. Systemic administration through intravenous injection or infusion, intramuscular injection, transdermal patch or subcutaneous polymeric controlled-release implants delivers drug to all tissues in the organism, requiring drug to circulate to the target tissue. Local modes of release preferentially load adjacent tissues over systemic sites can be classified either as bolus delivery, such as through permeable and double balloon catheters, or as sustained or controlled-release modes of delivery. Several generations of permeable balloons have been designed with various sizes, numbers, and configurations of holes that transmit soluble drug to the endovascular aspect

of blood vessel wall.[33,44-47] Local sustained delivery methods typically utilize erodable or nonerodable polymeric release devices which are implanted on or near either the endovascular or perivascular aspect. Perivascular delivery devices have been formed into a number of shapes, to release drug from a slab, a point source or a complete circumferential wrap. Endovascular sustained release has been accomplished by crosslinking hydrogels to the intimal surface,[48,49] deploying more rigid polymeric sheets,[50] or from mechanotherapeutic expandable endovascular stents.[34,51,52]

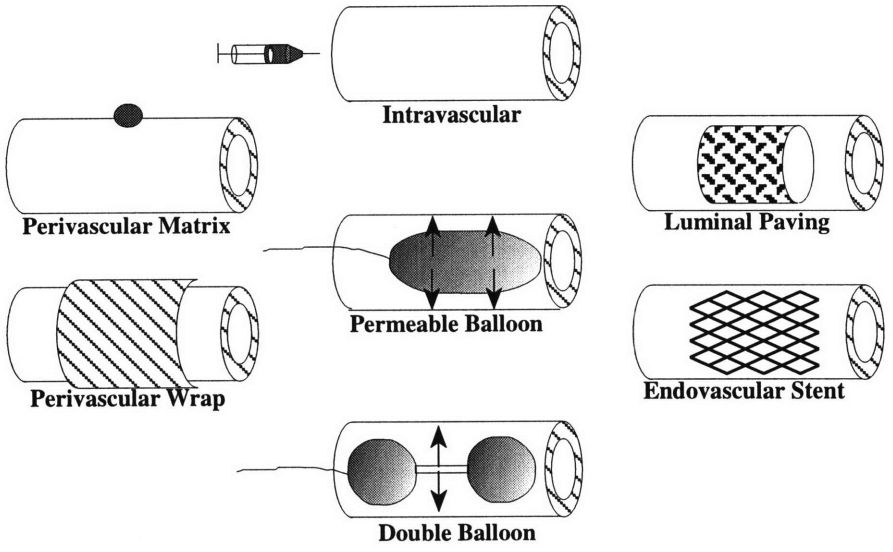

Figure 1.1 Modes of local vascular drug delivery.

1.4. Pharmacokinetic Framework

Despite the theoretical advantages of local delivery systems to treat proliferative vascular diseases, only a small group of antiproliferative compounds have shown benefit in animal models and none in clinical trials. The central hypothesis of this work is that the application of local vascular release systems to inhibit restenosis requires sophisticated coupling of both pharmacokinetic and pharmacodynamic processes. The former describes the fate of a drug within an organism and the latter describes the biologic effect of that drug in tissues where it is distributed.

It is the goal of this work to determine drug deposition and distribution following any mode of

vascular drug delivery. With this ability, one could predict *a priori* whether a drug delivery strategy maintains arterial concentrations adequately for a sufficient duration to achieve the desired biologic effect. Alternatively, the ability to predict tissue concentrations of drug could be used to correlate biological effect with vascular delivery experiments, to determine the duration and local concentration required to modulate injured blood vessel repair. A traditional pharmacokinetic approach will be used to provide a quantitative framework by which to establish vascular drug deposition and distribution and to compare these modalities. Classic pharmacokinetics quantitatively describe the administration, distribution, and elimination. It should be noted that the analysis of local delivery described in this thesis differs from classical pharmacokinetic studies as the compartment of interest is not the systemic circulation, extracellular fluid, or the entire organism but rather the blood vessel wall. Therefore, in the context of local delivery, administration refers to release from implanted polymer matrices or catheters and transport to the perivascular and endovascular boundaries of the blood vessel wall (Fig. 1.2). Similarly, distribution refers to the transport of soluble drug, and potential binding into an immobile phase. Elimination includes dissociation from binding sites, transport through the vessel wall and out the boundaries, cellular internalization, and local degradation.

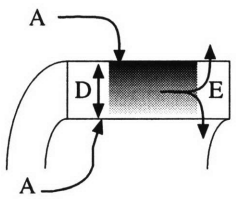

Fig. 1.2. Local vascular pharmacokinetics describes the administration (A) to, the distribution (D) through, and the elimination (E) from the blood vessel wall.

1.5. Foundations of Local Vascular Pharmacokinetics

The vascular administration, distribution and elimination of drugs is highly dependent on mechanisms of soluble drug transport and deposition (Fig. 1.3). Forces of solute transport include diffusion which results from random molecular collisions and Brownian motion, and convection which arises from the physiologic transmural hydrostatic pressure gradient and the hydraulic

conductivity of the arterial wall. Anatomical barriers such as the endothelium or adventitia inhibit the distribution of solutes. The deposition of drug is influenced by reversible binding to both biologically active as well as nonspecific sites, and endocytotic and transmembrane cellular internalization. Classical ligand binding studies include steps to eliminate nonspecific binding and therefore, little quantitative information exists on the magnitude of these effects for any compound, let alone vasoactive substances in arterial tissues.[53] The transvascular transport of soluble compounds, however, has been studied extensively with respect to the infiltration of atherogenic substances. The entry of plasma born macromolecules, such as low-density lipoprotein (LDL), into the arterial wall has been implicated as a causative process in the long-term development of atherosclerosis.[54,55] The precise mechanisms of transmural molecular transport has been the subject of intensive experimental and theoretical study over the last 50 years and continues to be so today. Much attention has focused on quantifying transendothelial permeability[56-62] and subsequent arterial distribution by diffusive and convective mechanisms,[63-74] of LDL and more convenient representative macromolecules such as serum albumin[75-90] and horseradish peroxidase (HRP).[91-96] Many theoretical treatises have described the transmural transport in terms of several physicochemical properties of the compound in the tissue.[97-102] Although many of the compounds used in atherogenic studies, such as LDL, albumin, and HRP bear little resemblance to vasoactive compounds, the same principles potentially govern the transport of exogenous drug in vascular structures. Application of atherogenic-transport models to soluble vasotherapeutic agents might simply require applying the correct physicochemical properties of the drug in arterial tissues.

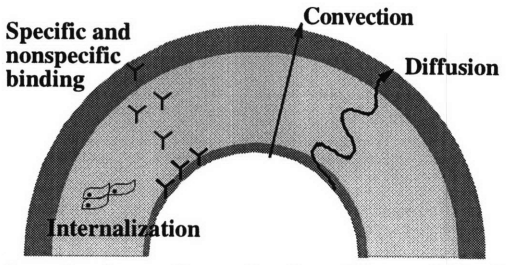

Figure 1.3 Potential mechanisms of vascular deposition and distribution of drug.

1.6. Review of Atherogenic Transvascular Transport Models

A review of the evolution of atherogenic transport models is presented and forms the basis of the local vascular pharmacokinetic framework. Rather than recapitulate every transvascular transport model in detail, a few analyses are presented which represent significant developments or specific classes of models.

1.6.1. Lumped Parameter Models

One of the first models was developed by Duncan et al. to help explain radiolabeled albumin uptake by various segments of the canine aorta and other peripheral tissues.[81] The artery and plasma were each considered well mixed compartments, where the solute in the plasma crossed into the tissue according to first order kinetics (k_1), and was degraded or cleared also by first order kinetics (k_2). A mass balance of the tissue compartment yields:

$$\frac{d}{dt}(c_T) = k_1 c_p - k_2 c_T$$

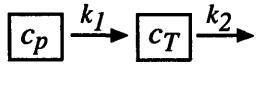

Following the injection of the solute, the serum concentration (c_p) was empirically measured and fit to a double exponential decay. The rate constants k_1 and k_2 were fit to experimental tissue concentration (c_T) data at various locations along the aorta. Interestingly, the rate of vascular uptake, k_1, decreased along the length of the aorta where the arterial segments are progressively thinner. Another two compartment model presented by Ghosh et al.,[67] in contrast to the previous one by Duncan et al., allowed for solute to exchange freely between the plasma and tissue pool, but did not allow for degradation. Rate constants were determined for LDL, albumin, and gamma-globulin, however, no correlation was found between the constants and the molecular weight of the compounds. This led them to hypothesize that the arterial uptake mechanisms were significantly different for each compound. Krishnan et al. extended this analysis to a three compartment model including plasma, extracellular, and intracellular tissues.[103] The rate constants were not determined due to an inability to distinguish intracellular from extracellular solute.

1.6.2. Continuum Models

All of the lumped parameter models, such as the one proposed by Duncan et al.,[81] are

empirical and offer little insight into the mechanisms of vascular solute uptake, and are thus not extendible to other arterial systems or compounds. Alternatively, a continuum approach, which views the arterial wall as an infinite number of concentric and infinitesimally thin homogeneous compartments, was first proposed by Weinbaum and Caro.[101] In this approach, the concentration across the vessel wall is described continuously, and thus local changes in transport properties are evident as altered concentration gradients. They modeled the diffusive transport and internalization of labeled macromolecules in a hypothetical *in vitro* perfusion preparation, by first defining the following dimensionless groups:

$$\chi = x/l, \qquad \tau = tD/l^2, \qquad \beta = Pl^2/D$$

where l is the thickness of the artery, x is a spatial coordinate oriented from the intima to the adventitia, t is time, and β is a dimensionless cell permeation parameter based on a cell membrane permeability, P. Note that the diffusion coefficient, D, is the effective molecular diffusivity of the solute and is lower than in aqueous solutions due to tortuosity in the solute pathway, the porosity of the tissue, and steric and charged interactions. The following governing equation then represents solute accumulation, diffusion in the extracellular phase, and permeation into the intracellular phase:

$$\alpha_{ec}\frac{\partial c_{ec}}{\partial \tau} - \frac{\partial^2 c_{ec}}{\partial \chi^2} = \beta(c_{ic} - c_{ec})$$

where c_{ec} and c_{ic} are concentrations in the extracellular and intracellular phases, respectively, normalized by the perfusate concentration, and α is the volume fraction of each phase. The rate of accumulation inside cells was equated with the permeation into this compartment:

$$\alpha_{ic}\frac{\partial c_{ic}}{\partial \tau} = \beta(c_{ec} - c_{ic})$$

The boundary conditions assumed that the concentration at the adventitia was zero, and that transport across the endothelial monolayer was exclusively through vesicles:

$$c_{ec}(1,\tau) = 0 \quad \text{at} \quad \chi = 1$$

$$-\frac{\partial c_{ec}}{\partial \chi} = \sigma[1 - c_{ec}] \quad \text{at} \quad \chi = 0$$

The dimensionless parameter $\sigma = \phi_R V_v L/D$, is a ratio of the transendothelial vesicular transport

rate to the diffusive transport rate in arterial media, where ϕ_R is the transendothelial vesicle number flux and V_v is the internal vesicular volume. Initially there was no solute in the tissue. These solutions were solved to predict transmural concentration profiles of solute in this hypothetical preparation.

1.6.3. More Complete Models and Parameter Estimation

Although the early continuum model of Weinbaum and Caro neglected solute convection, binding, and degradation, it was an important first application of continuum engineering principles to the transvascular transport of solutes. Bratzler et al. proposed a model that also included convection, reversible binding, dissociation, and intracellular degradation.[97] Furthermore, the boundary conditions allowed for solute to cross the endothelium in intercellular junctions as well as in vesicles. This model is more representative of transport *in vivo* than the model of Weinbaum and Caro because the adventitial boundary condition was non-zero, accounting for diffusion and vesicular transport into lymphatics and additional vesicular transport from *vasa vasorum*. The governing equation for free unbound solute in the soluble phase (*subscript s*) was described:

$$\underset{\textit{Accumulation}}{\frac{\partial c_s}{\partial t}} = \underset{\textit{Diffusion}}{D\frac{\partial^2 c_s}{\partial x^2}} - \underset{\textit{Convection}}{\frac{U}{\varepsilon}\frac{\partial c_s}{\partial x}} - \underset{\textit{Internalization}}{P(c_s - c_{ic})} - \underset{\textit{Binding}}{k_1 c_s} + \underset{\textit{Dissociation}}{k_2 c_b}$$

Where U is the superficial filtration flow velocity, ε is the tissue porosity, k_1 the first order binding rate constant, and k_2 the first order dissociation rate constant from those binding sites. Additional governing equations describe bound (*subscript b*) and internalized (*subscript ic*) solutes, respectively.

$$\underset{\textit{Accumulation}}{\frac{\partial c_b}{\partial t}} = \underset{\textit{Binding}}{k_1 c_s} - \underset{\textit{Dissociation}}{k_2 c_b}$$

$$\underset{\textit{Accumulation}}{\frac{\partial c_{ic}}{\partial t}} = \underset{\textit{Degradation}}{-k_3 c_{ic}} + \underset{\textit{Internalization}}{P(c_s - c_{ic})}$$

where k_3 is a first order rate constant describing the degradation of internalized solute. The intimal boundary condition (x=0) was described as follows:

$$Uc_p(1-r_e)+K_e\left(c_p-\frac{c_f}{\varepsilon}\right)= \quad Uc_f \quad - \quad D\frac{\partial c_f}{\partial x}$$

Intercellular Endothelium | *Vesicular Endothelium* | *Convection Media* | *Diffusion Media*

where the terms represent from left to right: transport in interendothelial junctions, vesicular transport, convection in media, and diffusion in media. At the adventitial boundary condition ($x=l$):

$$Uc_f(1-r_L) \quad + \quad K_L\frac{c_f}{\varepsilon} \quad +K_c\left(\frac{c_f}{\varepsilon}-c_p\right) \quad = \quad Uc_f \quad - \quad D\frac{\partial c_f}{\partial x}$$

Intercellular Lymphatics | *Vesicular Lymphatic* | *Vesicular Vasa Vasorum* | *Convection Media* | *Diffusion Media*

and the terms represent from left to right: transport to lymphatics, vesicular transport from *vasa vasorum*, vesicular transport to lymphatics, convection in media, and diffusion in media. r_e and r_L are phenomenological reflection coefficients for the endothelium and lymphatics. K_e, K_c and K_L are vesicular mass transfer coefficients for endothelium, vasa vasorum, and lymphatics, respectively. The authors tried to fit this model to empirical data and demonstrated a fundamental limitation of parameter estimation by this technique. Even though they correctly assumed that binding and degradation were negligible for short-time tracer studies and set k_1, k_2, and k_3 equal to zero, they still had nine parameters (D, ε,V, P, K_e, K_c, K_L, r_e, r_L) to determine from one set of curves. Fitting this many parameters from data that expressed concentration as a function of space and time represents a mathematically unconstrained problem in which there is not one unique solution, i.e. many combinations of parameters fit the data with the same accuracy. The fewer the parameters the more constrained the curve-fit becomes, and they therefore tried to include independently-measured coefficients to increase the uniqueness of the solution and the confidence in the estimated parameters. Although they used premeasured values for the tissue porosity (ε) and they held the ratio of velocity to diffusivity constant, they still had seven independent parameters to estimate. In some cases, the parameters estimated varied by an order of magnitude, leading to ambiguous conclusions of the mechanisms of transvascular macromolecular transport.

Truskey et al. increased the sophistication of the above analysis even further by adding separate terms for diffusion and convection into and out of venous and arterial capillaries in the

adventitia.[100] Although these models are more complete from the point of view of potential mechanisms, they have even more parameters to fit than the model of Bratzler et al.[97] Fry was able to obtain unique parameter estimates from fitting transmural concentration profile data when the number of independent variables was limited to five or fewer.[98] Some have eliminated parameters to fit by restricting their models to very short times after solute injection.[99] In this time, the solute can not completely penetrate the arterial media and therefore this tissue can be considered mathematically semi-infinite. Thus, the parameters in the adventitial boundary conditions do not appear in the analysis. Much of the arterial uptake data in the atherogenesis literature is taken within thirty minutes of solute injection.[63,76,100] Furthermore, Saidel et al. and others have simplified the intimal boundary conditions with a single parameter describing permeability across this layer.[94,99,102,104,105] These analyses quantify intimal transport as the sum of several concentration driven processes, but make no attempt at discriminating between them.

Fry and Vaishnav presented a series of simple models and analytic solutions that build to incorporate the major mechanisms encountered in arterial uptake.[102] They first discussed steady-state diffusion across a homogenous slab, then successively added a second zone to form a composite slab, then a surface barrier, and then allowed for chemical reactions. The homogenous slab is analogous to arterial media, the surface barrier is analogous to the endothelial monolayer, and the chemical reaction represents contributions from first-order binding, degradation, and internalization. They repeated each of these process for non-steady state transvascular transport. This sequential approach shows, with a minimum of complexity, how each of these effects individually impacts the transmural distribution of solutes.

1.6.4. Endothelium and Intima

Fry and Vaishnav included solutions for transport into slabs with surface barriers because it is widely held that the endothelium is the organ that prevents plasma macromolecules from entering the arterial wall and contributing to the atherogenic process.[63,76,79,87,93,94,101,106,107] Many vascular transport models have attempted to elucidate the mechanisms of endothelial permeability to plasma proteins.[108-114] These works seek to explain the focal nature of endothelial permeability to

tracer molecules, which has been attributed to the normal physiologic turnover of endothelial cells, and has been called the "leaky junction hypothesis."[57-60,73,84,115,116] Sophisticated models have shown that the small gap in the otherwise tight intercellular junctions created by normal endothelial turnover can lead to substantial increases in the overall permeability of the monolayer to large proteins.[108-114] These analyses model two-dimensional transport both across the subendothelial space and radially outwards from the leaky cleft in the plane of the intima, in addition to transmural diffusion and convection. Experimental analyses focusing on the intima and endothelium have shown that this intact layer is the dominant barrier to transvascular transport of macromolecules.[63,76,79,87,93,94,101,106,107] This anatomic barrier function observed *in vivo* includes the ever present physiologic leaks in the endothelium that are caused by normal mitoses. Other analyses treat the intima as several discrete layers consisting of endothelial cells, subintimal matrix and internal elastic laminae, and have resolved the diffusive resistances of each of these structures.[95,117] For example, the internal elastic laminae has been shown to account for 25% of the diffusive resistance of the intima to HRP.[95]

1.6.5. Deformable Arterial Wall

All of the aforementioned models are based on rigid nondeformable blood vessels, yet the arterial wall is a clearly an elastic structure having internal stresses which depend on the transmural pressure.[118] For example, increased pressure will distend the lumen radius and decrease the wall thickness. These deformations cause the tissue to compact and may alter transport properties such as available tissue space for solute distribution or hydraulic conductivity.[65,89,119-122] Applied transmural pressure can potentially enhance convective transport or decrease available space, and these effects are difficult to distinguish in many experimental preparations. Building on the fiber matrix theories of Curry,[123-125] Kim and Tarbell derived a model for the impact of applied pressure on the effective molecular diffusivity and the available space for distribution of several solutes, and the hydraulic conductivity through the arterial wall.[126] They matched the results of their model to the data of Tedgui and Lever[88,119,120] to show that the available space increases towards the adventitia for macromolecules, but is independent of position for small molecules such

as sucrose. They noted that the fiber dimensions required to make the data fit the model suggested that molecules diffuse in the interstitium of arteries and circumvent smooth muscle cells. This elegant analysis illustrates the potential impact of *in vitro* manipulation of tissues on transport properties and highlights some of the more subtle physical phenomenon that influence distribution in the complex blood vessel wall.

1.7. Work In This Thesis

Much quantitative insight into transvascular transport and pharmacokinetics has been gained from studies motivated by lipid and protein uptake by the arterial wall during atherogenesis.[56-96] However, these studies are concerned almost exclusively with endovascular infiltration of atherogenic compounds such as LDL, marker compounds such as HRP, and inert compounds such as albumin. None of them bear great resemblance to vasotherapeutic molecules in size, charge, and steric conformation and therefore careful pharmacokinetic study of any potential compound is warranted. The experimental studies in this work examine vascular drug deposition and distribution of an actual vasotherapeutic compound, heparin, which is the gold standard for smooth muscle cell growth inhibitors.[11-13,127] Endothelial cells produce heparan sulfate proteoglycan and the ability of their cultured media to inhibit smooth muscle cell growth arises from a heparin-like product.[11,128] Exogenous heparin (10-100 μg/ml) rapidly inhibits DNA and RNA synthesis in growth arrested cells released from G_0 block.[12] Continuous intravenous infusion of heparin virtually abolishes intimal smooth muscle cell proliferation in the injured artery.[13] Knowledge of the local transport and distribution of these compounds may help to better understand the role they play in endogenous vascular repair and their potential as therapeutic agents.

The pharmacokinetic analyses in this work differ from the previous models of transvascular transport of atherogenic compounds in several additional ways. Rather than applying compounds to arteries, observing the distribution phenomenologically and attempting to infer the contribution of each potential mechanism of transport and binding simultaneously from a single set of experimental data, the experiments performed are the simplest possible that examine each

mechanism in isolation. All of the individual results are then assimilated in a unified model. Secondly, the effects of binding are not assumed to follow first order rate kinetics, which implies that the binding sites never approach saturation. The current models allow the examination of regimes where the binding sites fill, and furthermore explicitly incorporate the effects of nonspecific binding. Because transvascular transport of vasotherapeutic compounds potentially includes passage through the adventitia, this layer is studied in greater detail than many of the previous works which assume it is a loose layer with little impact. Finally, transmural concentration profiles are generated through computational simulations, which have the benefit of having entirely flexible boundary conditions which allow easy description of many of the modes of local vascular drug delivery.

1.8. Summary of Analyses

The following chapters in this work describe the measurement of intramural transport mechanisms, binding within the arterial wall, and the movement of drug in the vicinity of but external to the blood vessel wall. The results are combined into a computational model that predicts vascular deposition and distribution.

Chapter 2. The Mechanisms Of Soluble Heparin Transport

The diffusivity of heparin in arterial media and adventitia and the diffusive resistance of the endothelium have been quantified through transmural transport measurements in an *in vitro* rat abdominal aorta model. The relative contributions of convection and diffusion to transmural heparin deposition and distribution, as well as the barrier function of endothelium and adventitia have been evaluated in this and several other animal models including the calf carotid artery *in vitro* and the rabbit iliac artery *in vivo*.

Chapter 3 Tissue Average Binding And Equilibrium Distribution

The equilibrium distribution of heparin in arterial media and adventitia of porcine carotid arteries has been determined. The fractional volume of distribution, the total binding site density including specific and nonspecific association, and the average dissociation constant of these binding sites have been measured from these data.

Chapter 4 Drug Transport Around Local Arterial Environment

The pathways of drug clearance from the perivascular space to the systemic circulation and the pathways of drug incorporation into the blood vessel wall have been determined. The potential for drug to be lost to the lumen and extra-arterial capillaries has been compared.

Chapter 5 Computational Simulations Of Vascular Heparin Deposition And Distribution

A finite difference algorithm has been used to construct computational simulations of soluble, reversible, and internalized transmural concentration profiles of heparin. The model is verified with experimental data from a novel endovascular hydrogel delivery system, and as an example the ability of the arterial wall to retain heparin is assessed.

2. THE MECHANISMS OF SOLUBLE HEPARIN TRANSPORT

2.1. Introduction

Vascular pharmacokinetics depend on the movement of soluble drug through tissues, reversible binding, and cellular internalization. Forces of solute transport include diffusion, which results from random molecular collisions and Brownian motion, and convection, which arises from the physiologic transmural hydrostatic pressure gradient and the hydraulic conductivity of the arterial wall (Fig. 1.3). Structures at the borders of the arterial media, such as the endothelium or adventitia, potentially limit the transit of solutes into and out of the artery. This chapter describes the measurement of the diffusivity of heparin in arterial media and adventitia, and the transendothelial resistance to heparin transport. These measurements were made with a steady transvascular solute flux assay under conditions where transmural hydrostatic pressure gradients were eliminated. Thus, the heparin flux was exclusively driven by molecular diffusion. The rat abdominal aorta was used in these studies as this thin vessel allows steady-state transport to be established rapidly. Additional transmural transport experiments were performed with the addition of a physiologic transmural hydrostatic pressure gradient, to illustrate the impact of convective forces on the transvascular heparin flux in the rat abdominal aorta. These results compared favorably to theoretical predictions of the ratio of convective to diffusive forces generated by combining the diffusivity measurements with published correlations of arterial hydraulic conductivity.

The above experiments quantify the magnitude of transvascular transport mechanisms through transmural flux assays. The sum of all of these mechanisms define the deposition of applied drug. Arterial heparin deposition was measured *in vitro* in the calf carotid artery under varying conditions which highlighted individually the impact of convective forces, the presence of the endothelial monolayer, and the application of drugs directly to either the perivascular or endovascular surfaces. Theoretical predictions suggest that the ratio of convective to diffusive forces of transvascular heparin transport depends on the medial thickness. The calf carotid artery used in these latter

perfusion experiments is over ten times thicker than the rat abdominal aorta and was used to verify this prediction. Heparin was also delivered perivascularly to native and deendothelialized rabbit iliac arteries to examine the potential transendothelial resistance to transport *in vivo*.

2.2. Materials and Methods

2.2.1. Transvascular Flux Assay in the Rat Abdominal Aorta

2.2.1.1. Preparation of the Rat Abdominal Aorta

Sprague Dawley rats (320-360 g) were anesthetized with an intraperitoneal injection of ketamine (50 mg/kg) and xylazine (10 mg/kg). The abdominal aorta was exposed, cleaned of fat and excess fascia, and cannulated proximally just below the splenic vein and distally just above the iliac bifurcation. Ligatures were placed around each cannula so that the intermediate segment of artery was isolated from the rest of the circulation. All branch vessels were ligated and severed. The cannulas were clamped to a rigid frame so that the length of the isolated artery was preserved at its *in vivo* dimensions. The artery was excised and the length of the artery between the tips of cannula was measured under a dissecting microscope (0.99 ± 0.03 cm). Leaks from the artery were assessed by connecting one cannula to an elevated (100 cm) reservoir and closing the other cannula. The artery was inspected under the microscope and discarded if any leak was noted.

To assess the integrity of the vessel wall after dissection and to exclude arteries from the analysis where trauma might lead to potential artifact, each artery was pressurized to 125 cm H_20 by connecting an elevated bag of Ringer's solution with the other cannula closed. The artery was examined for leaks under a dissecting microscope, and the bag for flow for several minutes. In a separate experiment, the integrity of the endothelial monolayer of excised rat abdominal aortas was confirmed by perfusing an artery with 4% Albumin and Evan's Blue Dye in buffer.[88]

2.2.1.2. *In Vitro* Perfusion Apparatus

The artery was placed in an *in vitro* perfusion apparatus (Fig. 2.1), simulating plasma flow through the artery. The perfusate flowed from an upper reservoir through the artery, emptied into a lower reservoir, and was pumped back to the upper reservoir, forming a well mixed endovascular compartment (100 ml). The artery was immersed in a perivascular bath (4 ml), to which known concentrations of radiolabeled heparin were added, establishing a fixed transmural

concentration gradient. Krebs-Henseleit buffer (Sigma) was used as the perfusate in the endovascular compartment and in the perivascular bath. The transmural pressure gradient and the luminal volume flow rate were set by the height, or hydrostatic pressure head, of the upper reservoir, ΔH, and the downstream resistance to flow, which was adjusted through a throttle valve. An overflow line connected the upper and lower reservoirs directly, holding ΔH constant, regardless of pump speed. The entire perfusion system was placed within a closed cabinet maintained at 37°C and 100% relative humidity. Not shown are a stir bar in the perivascular bath, a thermally controlled water jacket surrounding the lower reservoir, and in the lower reservoir a thermometer, and a 95% O_2 and 5% CO_2 bubbler. The volume flow rate of perfusate was measured by counting the rate at which drops fell from an outflow needle. Drop volumes were determined before each experiment from the number of drops collected in a measured volume.

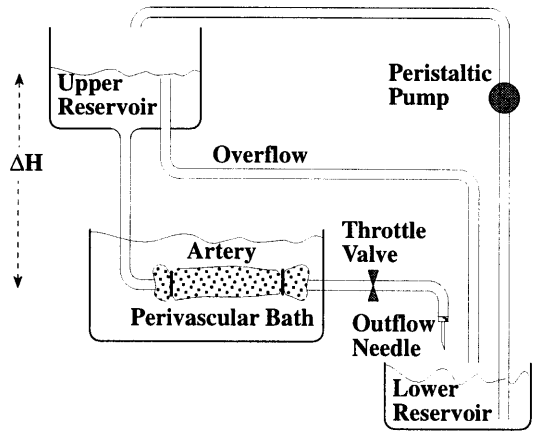

Figure 2.1. Schematic of the perfusion apparatus.

2.2.1.3 Rat Aorta Perfusion Protocol

Heparin was administered to the exterior of the artery by immersion in the perivascular bath containing ^{3}H-heparin (Du Pont-NEN) and unlabeled heparin (Hepar Industries) in buffer (2.5 mg/ml, 6 μCi/ ml). The artery was perfused for six hours at 37 °C. At one hour intervals, three 50-μl samples were taken from the lower reservoir and one 50-μl sample was removed from the perivascular bath. The perfusate volume flow rate, temperature, and pH were monitored hourly.

Nine rat aortas were perfused without a hydrostatic pressure head (ΔH = 0 cm), thus setting

the transmural pressure gradient (ΔP) to zero and establishing a scenario wherein all the measured mass transfer should have been governed solely by diffusion. The endothelium of four of these arteries were denuded with 3 passes of an inflated 2 French embolectomy catheter (Baxter Diagnostics).[129] Another 11 rat aortas were perfused with ΔH equal to 100 cm, mimicking a physiologic pressure gradient. Before each experiment the pressure just downstream of the artery was measured with a diaphragm manometer (Omega Engineering). The flow rate was adjusted with the throttle valve over a range that resulted in a physiologic pressure gradient of 99-103 cm H_20 (1±.25 ml/min). During the subsequent perfusions the flow rate remained within this range. Five of these arteries were also denuded of endothelium prior to cannulation.

At the end of the experiment, the perivascular bath was switched to a modified Bouin's fixative (53% EtOH, 4% formaldehyde, 2.5% glutaraldehyde, 7% acetic acid, 0.7% KCl) and the artery was perfused with fresh buffer for three hours. The artery was then immersion fixed for an additional 40 hours without perfusing, after which it was dehydrated and processed for paraffin embedding. Serial 10 μm cross sections were taken from one cannula tip to the other and stained with Verhoeff's elastin stain.

Computer assisted morphometric analysis was performed on cross sections taken at 1 mm intervals along the arterial length. The internal elastic lamina (IEL), the external elastic lamina (EEL), and outer edge of the adventitia were traced with image analysis software (IPLab Spectrum, Signal Analytics). The length of the IEL and EEL, and the area of the lumen, media, and adventitia were measured. The medial thickness of each cross section was calculated by dividing the medial area by the length of the IEL. The adventitial thickness of each cross section was calculated by dividing the adventitial area by the length of the EEL. Mean values for medial thickness, adventitial thickness, luminal area, and internal perimeter were calculated for each artery and used in subsequent calculations. The perivascular concentration was the average of the measurements at each time point. The transmural heparin mass transfer rate was defined as the time rate of change of heparin in the endovascular compartment and was calculated by a linear regression fit over the steady-state portion of the data.

2.2.2. Diffusivity of Heparin in Aqueous Solutions

The diffusivity of ^{3}H-heparin in water was measured using a standard diffusion cell (Crown Glass) with a porous hydrophilic membrane (GVWP, mean pore size 0.22 μm, Millipore) that separated two 3-ml chambers. ^{3}H-heparin was added to the source chamber and an equal concentration of unlabeled heparin was added to the sink chamber, to create iso-osmotic conditions. Each chamber was well mixed with magnetic stir bars and maintained at room temperature. 10-μl aliquots were taken from each chamber at 10 minute intervals for 90 minutes. The concentration gradient of ^{3}H-heparin was large enough so that it could be considered constant over the short time of the experiment, and approximated by the average concentration of heparin in the source chamber (c_{h*}). The time rate of change of heparin concentration in the sink chamber ($\partial c_h/\partial t$) was calculated by performing a linear regression over the steady-state portion of the sink chamber measurements. From a mass balance for the sink chamber, the diffusivity of heparin in aqueous solutions (D_{aq}):

$$D_{aq} = \frac{l_{mem} v_h}{A_o c_{h*}} \frac{\partial c_h}{\partial t} \tag{2.1}$$

where v_h is the volume of the sink chamber, A_o is the total open area of all of the pores and l_{mem} is the thickness of the membrane.

2.2.3. Arterial Heparin Deposition

2.2.3.1. Deposition in Calf Carotid Arteries *In Vitro*

Calf carotid arteries were excised at a slaughterhouse and immediately placed in phosphate buffered saline with 0.01 mM calcium and 0.1 mM magnesium (Sigma) at 4 °C, and stored for no more than 3 hours. The arteries were cleaned of excess fat and fascia, and approximately 1.5 cm long segments were cannulated at each end with polyethylene tubing (1.57 mm ID, 2.08 mm OD, Clay Adams). Just prior to cannulation, some arteries were denuded with 3 passes of an inflated 3 Fr embolectomy catheter (Baxter).[129] After cannulation, the integrity of the artery was assessed by connecting one cannula to an elevated bag of Ringer's solution, sealing the other cannula, and inspecting the artery for leaks under a dissecting microscope.[105] Both cannulas were clamped to a

rigid frame while the vessel was expanded under physiologic pressure so that the inflated length was maintained. The artery was then placed in the perfusion apparatus described above (Sec. 2.2.1.2).

^{3}H-heparin (0.12 μCi/ml, 0.7 mCi/mg, NEN-Dupont) was applied to either the perivascular or endovascular compartments and the artery was perfused for 1 hour. This time was insufficient for heparin to fully penetrate the arterial wall and therefore the drug deposition reflects the rate of entry into the artery.[63,76,99] The endovascular volume was 100 ml for all perfusions, while the perivascular volume was 12 ml for perivascular and 100 ml for endovascular administration. Three 50-μl samples were taken from both compartments at the start and end of each perfusion experiment. Following the perfusion, adsorbed drug was removed by either flushing 3 ml of fresh buffer through the lumen following endovascular delivery, or dipping the artery once in clean buffer following perivascular delivery. The artery was cut into five segments and the middle three were freeze-dried, weighed, solubilized with Soluene 350 (Packard), and prepared for measurement of deposited ^{3}H-heparin through liquid scintillation spectrometry with Hionic Fluor (Packard). Histologic frozen sections were cut from the two end arterial segments, and stained with Verhoeff's elastin stain.

Perfusion experiments were performed with all combinations of the following conditions: perivascular or endovascular administration of heparin, native or denuded arteries, and a transmural hydrostatic pressure gradient of 0 or 100 cm H_2O. Four arteries were perfused under each of these eight conditions, and deposition was measured three times for each vessel. The deposition is reported as the amount of drug normalized by both the dry mass of tissue and the average concentration of the applied drug. In a separate experiment, an artery was perfused with 4% Albumin and Evan's Blue Dye in buffer and no dense blue staining was observed on *en face* view, indicating the presence of endothelial cells.[88]

2.2.3.2. Deposition in Rabbit Iliac Arteries *In Vivo*

Heparin deposition was compared 2 hours after perivascular administration to native and denuded rabbit iliac arteries *in vivo*. Heparin releasing hydrogels were formed into hollow

cylindrical tubes by crosslinking a prepolymer solution using a photoreactive technique.[49] The prepolymer consisted of a backbone of polyethylene glycol (3.3 kD) with lactates on both ends (an average of 5 lactates per molecule) and capped with acrylate (Focal, Inc.). This prepolymer was dissolved in 90 mM triethanolamine (30% wt/wt, Aldrich) to which N-vinylpyrrolidone (VP, 2 μl/ml, Aldrich), and ^{3}H-heparin (20 μCi/ml, NEN-Dupont) were added. Just prior to crosslinking a photoinitiator, eosin Y (20 μg/ml, Sigma), was added to the prepolymer solution. This mixture was injected into a hollow cylindrical transparent molds (ID 2.08 mm, OD 3.35 mm, thickness 635 μm) and photopolymerized with an argon laser (488-514 nm, 70 mW/cm^2, American Laser). The resulting cylinders were cut into 7 mm long segments and slit longitudinally. The elasticity of the bulk-gelled hydrogel tubes allowed them to be placed around the iliac artery and retain their cylindrical shape.

Male New Zealand White rabbits (2.75 to 3.25 kg) were anesthetized with an intramuscular injection of ketamine (50 mg/kg) and xylazine (15 mg/kg) and were maintained with intravenous and intramuscular boluses as needed. The iliac arteries were exposed through a midline abdominal incision and displacement of the intestinal viscera, and arterial segments were isolated from the iliac bifurcation to the inguinal ligament. Heparin releasing hydrogel collars were made fresh before implantation. Two were applied to adjacent arterial segments such that each animal received four devices. The abdomen was sutured closed to prevent dehydration. The abdomen was reopened just prior to removal of each device and the corresponding iliac artery was clamped with a hemostat distal to the iliac bifurcation. This allowed for vessels to be removed without disrupting the flow to the contralateral artery, enabling drug delivery to persist for the duration of the experiment, and insuring that the adventitial surfaces would not become contaminated with blood. Just prior to implantation in a separate experimental group, both left and right iliac arteries were balloon denuded with three passes of an inflated 3 French embolectomy catheter passed retrograde from a femoral arteriotomy.[129]

Immediately following excision, the arteries were cut into proximal and distal segments and stored at -70°C. At the time of processing, they were freeze dried, weighed and solubilized with

Soluene-350, and prepared for measurement of deposited ^{3}H-heparin through liquid scintillation spectrometry with Hionic Fluor. Each experimental group consisted of 3 rabbits, and four segments of iliac artery were harvested from each, two on each side. The deposition is reported as the amount of drug normalized by both the dry mass of tissue and the initial concentration of the drug in the hydrogel release device.

2.3. Calculations

2.3.1. Diffusivities and Resistances of Heparin Within the Arterial Wall

The transvascular transport measurements on the rat abdominal aorta performed with no hydrostatic head (ΔH = 0 cm) had no transmural pressure gradient, and therefore no transmural hydraulic flux (Sec. 2.2.1.3). Thus, once steady state was established, the mass transfer data reflected diffusion alone. The arterial wall was modeled as a series of concentric cylindrical tubes (Fig. 2.2) and the medial and adventitial thicknesses were approximated as the average of those measured from all the histologic sections of an artery. Furthermore, the perivascular and endovascular compartments were well mixed so that the only concentration gradient existed in the transmural direction. The transport was modeled as four resistors in series, one each for the adventitia (R_{adv}), media (R_{med}), endothelium (R_{end}), and for the mass transfer boundary layer within the lumen flow (R_{bl}), which separate the potential or concentration gradient ($c_{pv} - c_{ev}$). Thus, by analogy to Ohm's law, the potential difference for diffusive mass transfer is the product of the flux and the series sum of these resistances:

(2.2) $$c_{pv} - c_{ev} = \left(\frac{j}{PL}\right)\left(R_{adv} + R_{med} + b_{end}R_{end} + R_{bl}\right)$$

j is the transmural heparin transfer rate, L is the length and P is the average perimeter of the lumen. The coefficient of R_{end} (b_{end}) is unitless and was 0 following a denuding injury, and 1 with intact native arteries.

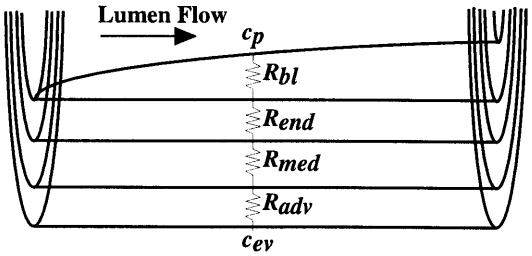

Figure 2.2. The transmural transport of heparin, when perfused with no transmural pressure gradient (ΔH=0 cm), is modeled as one dimensional. The thicknesses of the media and adventitia are assumed to be uniform along the length and circumference of the artery.

Since the mass transfer was purely diffusive in these perfusions performed at ΔH = 0 cm:

(2.3) $$R_{adv} = l_{adv}/D_{adv}$$

and

(2.4) $$R_{med} = l_{med}/D_{med}$$

l_{adv} and l_{med} are the adventitial and medial thicknesses, and D_{adv}, and D_{med} are the diffusivity of heparin within the adventitia and media, respectively. Note that the term "diffusivity" is a proportionality constant that equates the resulting mass flux to an applied concentration gradient. It is specific to a solute and the medium in which it moves. In a tissue such as an artery, the measured effective diffusivity will reflect molecular diffusion in the interstitium, tortuosity, steric and charged interactions, and potential active transcellular transport. Rearrangement of Equation 2.2 allows the unknowns, D_{med}, D_{adv}, and R_{end} to be determined by multiple linear regression:

(2.5) $$LP\left(c_{pv} - c_{ev}\right)/j - R_{bl} = l_{adv}/D_{adv} + l_{med}/D_{med} + b_{end}R_{end}$$

The boundary layer resistance (R_{bl}) results from solute that enters the lumen from points upstream and hinders the entry of solute from the wall at downstream locations (Fig. 2.2). The value of the boundary layer resistance can be determined from correlations that are specific for fluid momentum and mass transfer regimes encountered in the perfusion experiments. In all of the perfusion experiments, while fluid flow in the lumen was fully developed and laminar, the artery was not long enough to consider the mass transfer fully developed. The Sherwood number, Sh_d, is a nondimensional form of the resistance to mass transfer of the boundary layer.[130,131]

(2.6) $$Sh_d = \frac{d}{R_{bl}D_{aq}}$$

An appropriate correlation for the Sherwood number for fully developed fluid flow and non-fully developed mass transfer follows:[130,131]

(2.7) $$Sh_d = 3.66 + \frac{0.065(d/L)\mathrm{Re}_d\, \upsilon/D_{aq}}{1 + 0.04\left[(d/L)\mathrm{Re}_d\, \upsilon/D_{aq}\right]^{2/3}}$$

Where the Reynolds number is:

(2.8) $$\mathrm{Re}_d = \bar{v}_l d/\upsilon$$

and where $\bar{v}_l$ is the average fluid velocity in the lumen and equals the average volume flow rate of perfusate divided by the open area of the lumen (A_l), and υ is the kinematic viscosity. The

hydraulic diameter, d, helps describe the flow regime through non-circular ducts:

(2.9) $$d = 4A_l/P$$

2.3.2. Balance Between Diffusion and Convection in Transmural Transport

The physiologic hydrostatic pressure gradient gives rise to transmural convective currents which potentially "drag" drug through the artery. The ratio of the convective to diffusive forces of transmural transport of a given drug molecule is embodied in the Peclet number (Pe).[88,100,126] Pe much less than 1 implies that the transmural transport is purely diffusive, and conversely Pe much greater than 1 implies that the transport is purely convective. Pe about unity implies that both diffusive and convective effects play a role in drug transport. For heparin in arterial media:

(2.10) $$Pe = U_{med} l_{med} / D_{med}$$

U_{med} is the heparin drift velocity in arterial media and may be less than the hydraulic velocity (u) due to steric and charge interactions in the arterial tissue.[100,124] The degree of hindrance may differ for diffusive and convective mechanisms. The hindrance coefficient for diffusive flux of heparin in arterial media (f^D_{med}) is defined as the degree by which the diffusivity in arterial media is reduced from the diffusivity in aqueous solutions:[100,102]

(2.11) $$f^D_{med} = D_{med}/D_{aq}$$

Similarly, a hindrance coefficient for convective flux in arterial media (f^C_{med}) can be defined as the degree by which the solute drift velocity is reduced from the transmural hydraulic velocity (u)[102]

(2.12) $$f^C_{med} = U_{med}/u$$

The transmural hydraulic velocity (u) can be determined by modeling the media and endothelium as two conductors in series,

(2.13) $$u = \frac{\Delta P}{\frac{\mu l_{med}}{K_{med}} + \frac{b_{end}}{K''_{end}}}$$

where μ is the dynamic viscosity. K_{med} is the specific hydraulic conductivity of the media and has been measured to be 2×10^{-14} cm^2.[121] The intrinsic hydraulic conductivity of the intact endothelium, K''_{end}, is 8.2×10^{-11} cm^{2}s/g.[132] Recall that b_{end}, is 0 following a denuding injury, and 1 with intact

native arteries. By combining Equations 2.10 - 2.12:

$$Pe = \frac{f_{med}^{C}}{f_{med}^{D}} \frac{u\ l_{med}}{D_{aq}} \tag{2.14}$$

The hindrance coefficient for convection has not been explicitly measured for any solute in any model of arterial interstitium.[124] The physical constraints that generate the diffusive and convective restriction coefficients can be similar,[100] however, the media does not necessarily have to hinder convection. Thus, Pe can be framed within limits by assuming at one extreme that the hindrance for convection and are equivalent: $f_{med}^{D} = f_{med}^{C}$, and the other $f_{med}^{C} = 1$, such that:

$$u\ l_{med}/D_{aq} \leq Pe \leq u\ l_{med}/D_{med} \tag{2.15}$$

The Pe numbers were calculated for arteries over a range of medial thicknesses, for normal and deendothelialized arteries.

2.3.3. Pore Theory

As a further approximation of the Peclet numbers, the convective hindrance coefficient (f_{med}^{C}) was estimated from pore theory.[133,134] The drug movement across the arterial media was modeled as an unrotating, uncharged sphere that both diffuses and convects along the centerline of a transmural pore. The hydrodynamic interactions between a sphere and the wall of the pore have been described analytically and expressed as the convective (f_{med}^{C}) and the diffusive (f_{med}^{D}) hindrance coefficients which vary with the ratio of solute-to-pore radii (Fig. 2.3).[133,134] The diffusive hindrance coefficient for heparin defined by Equation 2.11 was used to estimate an effective solute-to-pore radii ratio, which was used to estimate the convective hindrance coefficient. The Peclet numbers for native and deendothelialized arteries were calculated over a range of medial thicknesses using Equation 2.13 and this convective hindrance coefficient.

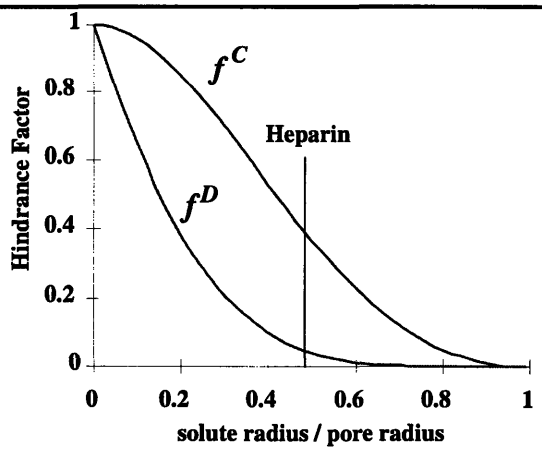

Figure 2.3 The hydrodynamic hindrance factors for diffusion (f^D) and convection (f^C) of a nonrotating uncharged sphere in a cylindrical pore, as derived by Bungay and Brenner[133] and adapted for biological membranes by Deen.[134]

2.4. Results

2.4.1. Transmural Flux in Rat Abdominal Aorta

The diffusivity of heparin in aqueous solutions at room temperature was measured to be 1.39 $x10^{-6}$ cm^2/s (R^2 = 0.996). After correction from room temperature to 37 °C using the Stokes-Einstein relation:[135] D_{aq} = $1.45x10^{-6}$ cm^2/s. The multiple linear regression (R = 0.920) of the data taken without a hydrostatic pressure gradient (Appendices 8.1 and 8.2) showed that D_{med} = 7.73 x 10^{-8} cm^2/s (P=0.03), D_{adv} = 1.21 x 10^{-7} cm^2/s (P = 0.07), and R_{end} =25,100 s/cm (P=0.004). The diffusive resistance of these three arterial layers were calculated over a range of thicknesses (Fig. 2.4).

The estimations of the Peclet numbers are shown for a range of medial thicknesses, for both native and deendothelialized arteries (Fig. 2.5). *Pe* was estimated to lie within upper and lower bounds, reflecting either no convective hindrance or alternatively, convective and diffusive hindrances that are equal. The range of *Pe* numbers is less than unity in the rat abdominal aorta, except following deendothelializing injury. An approximation for the Peclet numbers within these bounds was predicted by pore theory (Section 2.3.3) to be 0.65 for denuded arteries. Native arteries were predicted to asymptote toward this value with increasing medial thickness.

Rat abdominal aortas were perfused with and without transmural pressure gradients and direct comparison of the transmural heparin transfer from each of these sets of data would experimentally confirm the relative importance of convection and diffusion. However, under physiologic pressure the arteries are significantly thinner (Appendix 8.1) and greater in perimeter, decreasing the length over which heparin must migrate and increasing the area perpendicular to transport. Thus, any impediment to mass transfer attributable to opposing connective flows is overwhelmed by these effects.

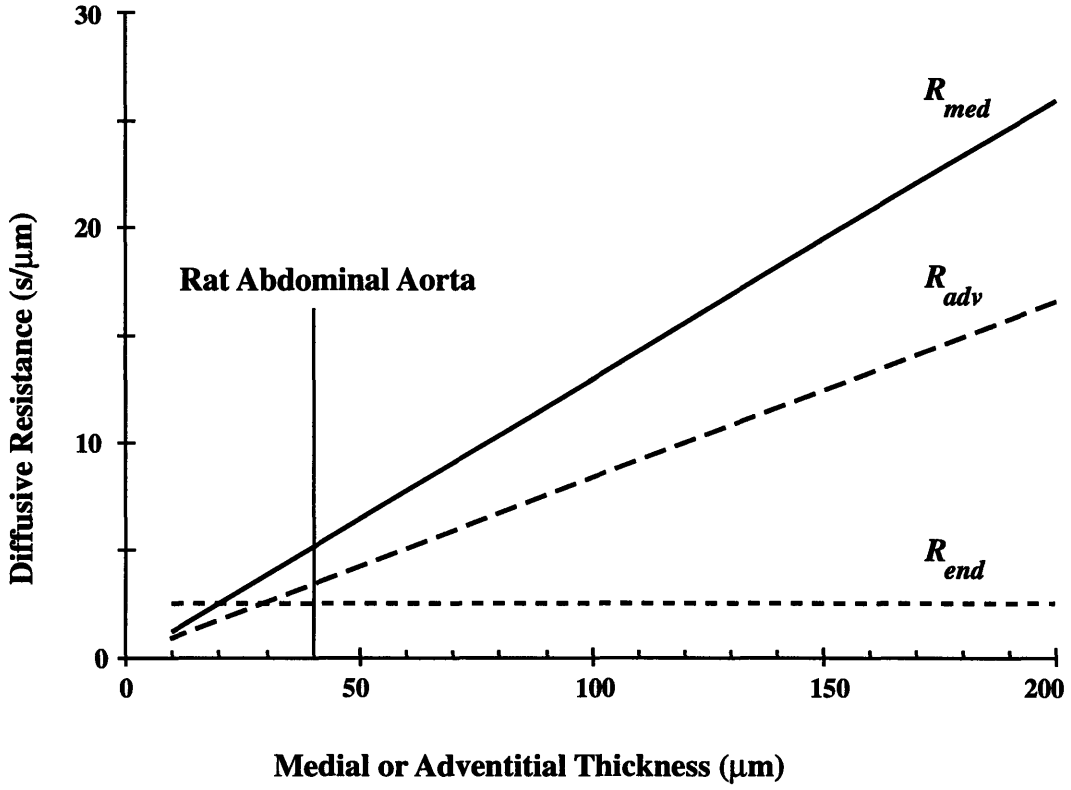

Figure 2.4. The diffusive resistance of the media and adventitia as a function of the arterial layer thickness. Note that the endothelial resistance is constant. Diffusive resistance is defined as the thickness of the arterial layer divided by the diffusivity of heparin in that layer.

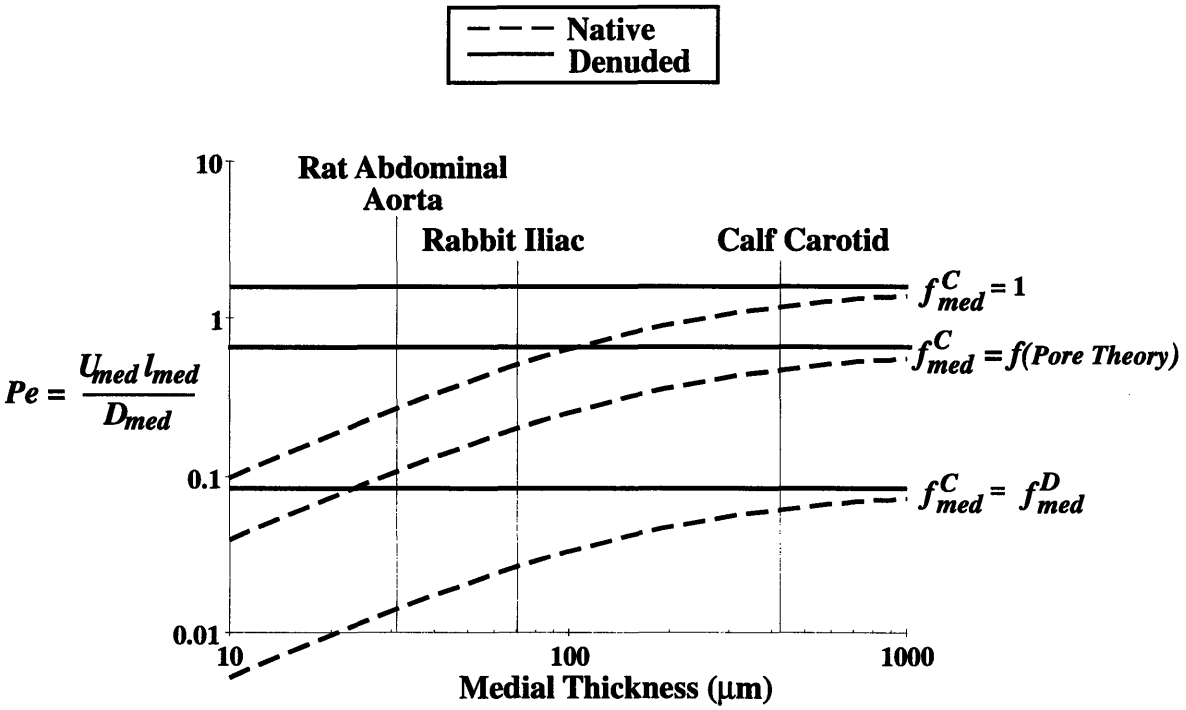

Figure 2.5. The range of Peclet numbers for both native and denuded arteries, as a function of medial thickness, computed from the measurements of the diffusivity of heparin in arterial media and published correlations of hydraulic flux. A range is shown because the convective hindrance imposed by the media has not been measured for heparin and is hypothesized to lie between one and the diffusive hindrance imposed by the media. Centerline pore theory is used to estimate the convective hindrance more precisely (Fig. 2.3).

To circumvent the artifact generated by these morphological changes, a non-dimensional parameter was defined (ψ) which evaluated how much of the observed mass transfer was due to diffusion alone. ψ equals the right-hand side of Equation 2.2 normalized by the left hand side:

$$\psi \equiv \frac{j}{\left(c_{pv} - c_{ev}\right)LP}\left(R_{adv} + R_{med} + b_{end}R_{end} + R_{bl}\right) \tag{2.16}$$

This value represents the mass transfer nondimensionalized by the diffusive driving potential and diffusive resistances. Note that this characterization only incorporates diffusive terms, and therefore if diffusion is the only driving force, ψ = 1. Conversely, if convection is the only driving force then ψ= 0 because in these perfusions the concentration gradient of heparin was directed against the hydraulic flux. Certainly, ψ should equal 1 for the experiments performed with ΔH=0. The coefficient of R_{end} (b_{end}) is 0 following a denuding injury and 1 with intact native arteries. The ψ parameter was computed for native and deendothelialized arteries, with and without a physiologic transmural pressure gradient (Fig. 2.6). ψ was approximately unity except when there was a pressure gradient and deendothelialization, where the value dropped by 20%.

2.4.2. Heparin Deposition in Calf Carotid and Rabbit Iliac Arteries

^{3}H-heparin deposition in calf carotid arteries following one hour perfusion *in vitro* is shown for both native and denuded arteries, with transmural hydrostatic pressure gradients of 0 or 100 cm H_20, and for endovascular (Fig. 2.7a) or perivascular (Fig. 2.7b) heparin administration (Appendix 8.3). In the absence of a transmural hydrostatic pressure gradient the deposition was indistinguishable whether the arteries were native or denuded or heparin was applied from the endovascular or perivascular aspect. The deposition with endovascular delivery was significantly increased 2.0 fold by the addition of 100 cm H_20 pressure gradient, and following denudation this increase was 2.5 fold. In contrast, the addition of this pressure gradient decreased the deposition significantly following perivascular delivery by 30% and 36% in native and denuded arteries, respectively. The heparin deposition in native and balloon deendothelialized rabbit iliac arteries was indistinguishable following perivascular delivery from hydrogel collars *in vivo* (Fig. 2.8, Appendix 8.4).

$$\Psi = \frac{j''\Sigma R}{c_{pv} - c_{ev}}$$

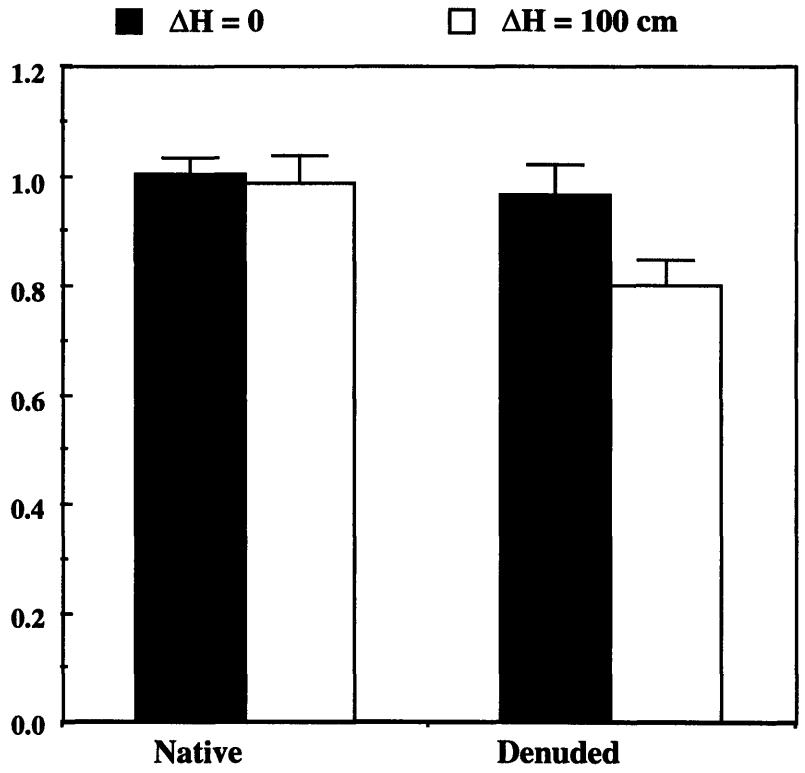

Figure 2.6. The Ψ parameter is a measure of how much of the transmural heparin transfer can be attributed to diffusion (Eq. 2.16). For these rat aorta perfusion experiments where the heparin is applied perivascularly and the convective current is directed against the concentration gradient, $\Psi = 0$ implies that heparin moves only by convection. $\Psi = 1$ implies that heparin moves only by diffusion. (average $\pm$ SEM.)

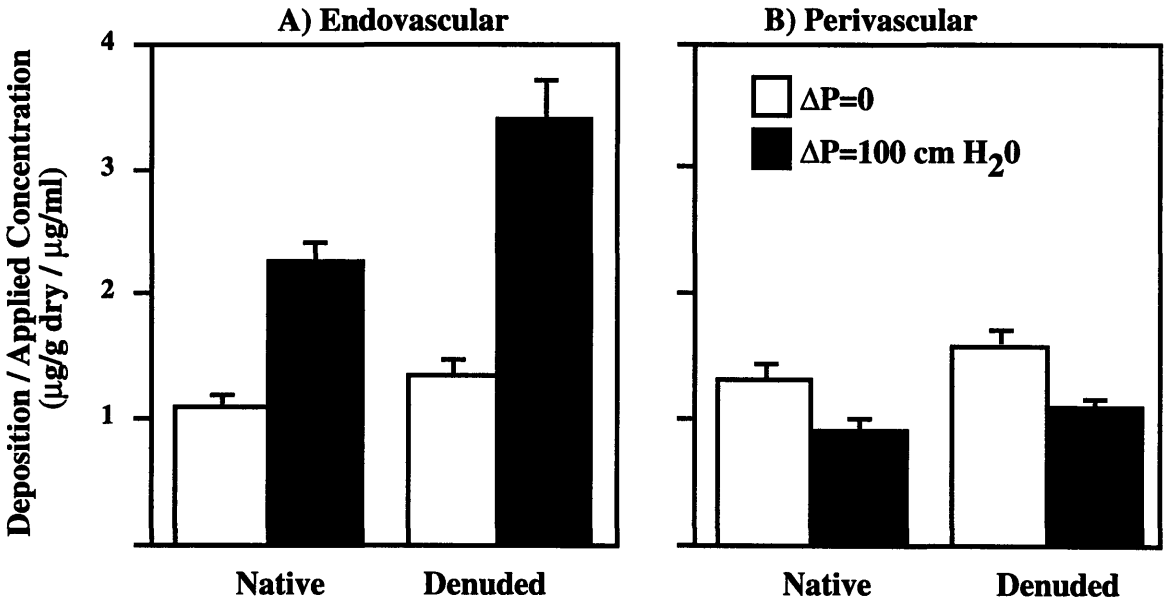

Figure 2.7. The *in vitro* heparin deposition per applied drug concentration in calf carotid arteries one hour after a) endovascular and b) perivascular application. Arteries were either left intact (native) or balloon deendothelialized (denuded), and either subjected to a physiologic or no transmural pressure gradient (ΔP). Deposition is normalized by both the dry mass of the artery and the applied heparin concentration gradient (n=12, average ± SEM).

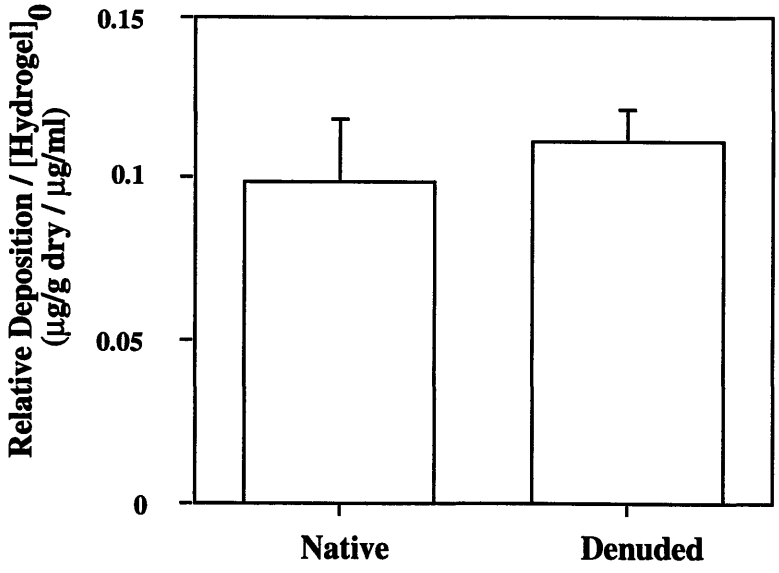

Figure 2.8. The *in vivo* heparin deposition per initial hydrogel concentration in native and denuded rabbit iliac arteries 2 hours after perivascular release from 635-μm-thick hydrogel collars (n=12, average ± SEM).

2.5. Discussion

Evaluation of the extent and processes that govern the transvascular transport of macromolecules is central to our understanding of both the accumulation of atherogenic proteins and lipids in the vessel wall, and the potential treatment of proliferative vascular diseases with exogenous vasotherapeutic compounds. These phenomena have been studied extensively in the context of the former, but have generally not been applied to the latter. Despite decades of research, controversy remains as to the importance of the role of various mechanisms of transvascular solute transport. For instance, different investigators using a variety of compounds and animal models have reported or assumed that diffusion exclusively controls transmural transport,[76,78,102,104,136] that diffusive mechanisms dominate only in healthy arteries but that convective forces become significant after endothelial injury and denudation,[79,87,93,100] or that convection is always important and may even overwhelm diffusion.[83,88,89,126,137] Although this debate may focus on a subtle pathophysiologic aspect of chronic atherosclerotic disease, these issues are essential to pharmacologic treatment of injured blood vessels. Indeed, local vascular drug delivery systems have been designed to release drug from either the endovascular or the perivascular aspect of the artery.[26,34,51,138] If convective forces are inconsequential compared to diffusive forces, then the deposition from either aspect of the artery should be similar. If convective forces are significant, however, they will be aligned with diffusive forces for endovascular but opposed for perivascular delivery, leading to potentially overwhelmingly enhanced deposition in the former over the latter (Fig. 2.9). The above example shows that it is essential to fully describe all the mechanisms of transmural solute transport in order to rationally design pharmacologic treatments.

In this chapter, an *in vitro* perfusion apparatus was used to control the environment inside the lumen and around the artery, to measure the diffusive resistance of each arterial layer, and to assess the balance between diffusive and convective mechanisms of transmural transport. In the rat abdominal aorta diffusion exclusively controls the transmural distribution of heparin under normal conditions, convective forces rise to one-quarter the magnitude of diffusive forces with extreme

endothelial disruption, the diffusive barrier to heparin posed by the endothelium is minor, and the barrier to heparin transport posed by the adventitia depends on its thickness.

All of these mechanisms together determine vascular distribution and the extent to which they individually impact deposited drug was tested in two additional animal models: the calf carotid artery *in vitro* and rabbit iliac artery *in vivo*. The effects of molecular diffusion and the intimal barrier to transport were examined *in vitro* in the absence of a transmural pressure gradient, and therefore without convective forces. The contribution of convection was then assessed when these experiments were repeated with a physiologic transmural hydrostatic pressure gradient. The potential of the endothelium to behave as a resistance to the transport of heparin was also examined *in vivo*.

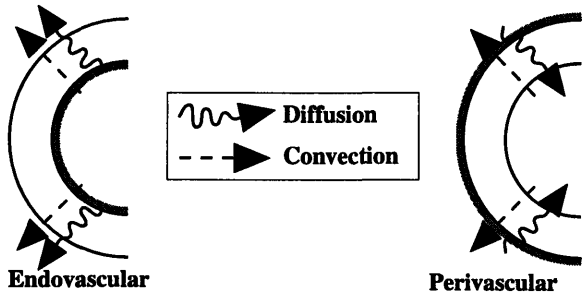

Figure 2.9. Schematic showing the directions in which diffusion and convection act in transmural transport following endovascular and perivascular drug delivery. Diffusion always moves drug away from the point of administration (shaded region) and convection, which arises from the transmural hydrostatic pressure gradient, is always directed across the arterial wall from inside to out.

2.5.1. The Role of Diffusion and Convection in Transmural Transport

2.5.1.1. Theoretical Peclet Numbers

Diffusion is an omni-directional process resulting from random molecular movements, and thus the magnitude of diffusive forces should be independent of the aspect of delivery. In contrast, convective forces are always aligned with the physiologic hydrostatic pressure gradient across the water-permeable arterial wall, and are directed from the intima towards the adventitia (Fig. 2.9). Thus, it would appear that endovascular delivery should always be superior to perivascular delivery because convective and diffusive forces appear to augment the former, while in the later

drug must diffuse in the face of an oncoming convective current. Yet, it is the balance between the diffusive and convective mechanisms that will determine the appropriateness of this interpretation. If diffusive forces are much larger than convective forces, then endovascular delivery is no more advantageous than perivascular delivery.

The balance between diffusive and convective forces in transmural transport is characterized by the Peclet number (Pe). For native uninjured rat aortas, the range of Pe was usually less than one, implying that convective effects are limited by the hydraulic resistance of the arterial media and endothelium. However, convection can play a more significant role in thicker arteries or when the endothelial barrier to convective flux is removed. In the former, Pe will increase because the diffusive resistance increases more so than the hydraulic resistance, due to the nonlinear effects of the endothelium on the overall arterial hydraulic conductivity. In the latter, Pe will increase to its theoretical maximum irrespective of medial thickness, as the endothelial monolayer can account for a large fraction of the hydraulic resistance.[132] Despite limitations in applying pore theory to transvascular heparin transport (Sec. 2.3.3), this analysis shows that diffusive hindrance always exceeds convective hindrance (Fig. 2.3), and therefore the actual Peclet number lies between the two extremes presented (Fig. 2.5). Hence, under conditions of severe endothelial injury or dysfunction, or for large healthy arteries, the transmural convective currents will reach significance where they enhance heparin distribution following endovascular delivery, and need to be considered in vascular pharmacokinetic analyses.

2.5.1.2. Empirical Verification by Transmural Heparin Flux

It is possible to verify these theoretical considerations empirically in the rat abdominal aorta by comparing transmural transport with and without adverse convective forces. The ψ parameter represents the measured mass transfer nondimensionalized by the diffusive driving potential and diffusive resistances, and it evaluates how much of the observed mass transfer arises from diffusion alone. If diffusion is the only driving force, $\psi = 1$ and if convection is the only driving force then $\psi = 0$. The data show that $\psi \approx 1$ with native intact arteries (Fig. 2.6), regardless of whether there is a transmural pressure gradient or not ($\Delta H = 0$ or 100 cm). Following a balloon

denuding injury, the introduction of a physiologic transmural pressure gradient reduced ψ from 1 to 0.8. Under these circumstances, convective forces can reduce the transmural transport of heparin following perivascular delivery, and thus endovascular delivery may lead to slightly enhanced distribution of drug.

It is possible that the applied pressure caused the tissue to compact and the transmural transport to fall, due to increased steric interactions that slow heparin diffusion. Such effects would be evident in both native and denuded arteries. ψ was decreased in denuded but not native arteries, suggesting that changes in the effective molecular diffusivity from compaction were not significant.

2.5.1.3. Empirical Verification by Heparin Deposition

Convection was shown to be an insignificant mechanism of heparin distribution in the native rat abdominal aorta (Section 2.4.2.2). In contrast, the *in vitro* perfusions of calf carotid arteries demonstrated that hydraulic convective mechanisms are significant determinants of transvascular solute transport, as heparin deposition increased two fold following endovascular administration to native arteries when subjected to a hydrostatic pressure gradient of 100 cm H_20 (Fig. 2.7a). Conversely, the addition of this pressure gradient lowered the deposition with perivascular delivery (Fig. 2.7b). In the former, hydraulic convective forces are aligned with the concentration gradient and assist drug distribution, whereas in the latter they are opposed and thus limit transmural deposition (Fig. 2.9). These data support the Peclet number predictions that convective forces are more significant in thicker vessels, as the calf carotid is 450 μm thick and the rat abdominal aorta is 40 μm thick (Fig. 2.5). Experimental evidence that the balance between diffusive and convective forces may depend on arterial thickness dates back to 1962, when Duncan, et al. reported that supraphysiologic blood pressure increased arterial uptake of intravascularly administered albumin in the thick canine ascending aorta, but that this enhancement diminished as one examined thinner arteries more distally.[83] The introduction of vascular dimension as a governing parameter might help explain some of the long running controversy over the role of convective arterial transport.

2.5.2. Endothelium Modulate Distribution

The endothelial monolayer can potentially impact the distribution of applied drug in two independent ways. First, the endothelium may impose a direct barrier to solute flux. There are several potential pathways for solute to cross the endothelium, such as intercellular diffusion and convection, and active and passive transcellular transport. All of these processes are readily characterized as a single resistance.[94,99,102,104,105] The primary resistance to transarterial transport of macromolecules such as albumin, HRP or LDL, however, is the endothelium.[63,76,94,139] The ratio of endothelial to medial diffusive resistance varies for different compounds and arteries. This value was about 10 for albumin or LDL,[63,76] but only ~0.5 for heparin in the rat abdominal aorta ($l_{med} \approx 40$ μm) used here, and ~0.1 in arteries as thick as the rabbit thoracic aortas used in the albumin studies. In addition to the four fold difference in size of heparin (12-15 kDa) and albumin (60 kDa), enhanced transendothelial heparin transport may arise from the flexibility of the linear, highly charged compound.[140,141] Phenomenon such as reptation may allow heparin to pass through far smaller pores than other compounds of similar molecular weights. Alternatively, transcytotic pathways may exist for heparin but not for albumin. This distinction in transport properties illustrates the need for in depth analysis for each compound, and the danger of extrapolating from the results of studies with one molecule to another.

The lack of transendothelial resistance to heparin was corroborated in the calf carotid artery. In the absence of a pressure gradient the deposition of endovascularly applied drug did not increase following endothelial denudation (Fig. 2.7a). The possibility exists that the endothelium is not completely intact *in vitro* and that intercellular gaps may allow solutes to pass that might be restricted *in vivo*. However, the monolayer does modulate pressure driven hydraulic currents (Figs. 2.6 and 2.7), and therefore should be largely intact, exerting much of its normal resistance to solute transport.

In vivo delivery experiments to rabbit iliac arteries support the limited role of the endothelium as a barrier to heparin transport. With perivascular delivery any potential endothelial resistance to transport would prevent the loss of drug to the lumen flow and would result in elevated deposition

in native over denuded arteries. Yet the data show that the deposition was not significantly different with and without the endothelium (Fig. 2.8). One might best appreciate these results by considering hypothetical transmural concentration profiles generated by a simple resistor model to solute transport (Fig. 2.10).

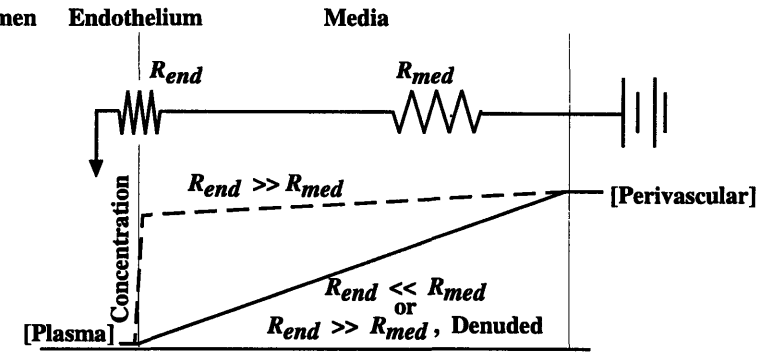

Figure 2.10. Linear resistor model of drug transport across the media and endothelium from a perivascular source, and resulting hypothetical transmural concentration profiles. Note that the thicknesses of each layer are not drawn to scale as the endothelium has virtually no thickness.

At steady-state the release device will impose a constant perivascular concentration. If the endothelium offers no resistance (*solid line*) the concentration at the lumenal edge of the media would reflect that of the plasma. Denudation could not reduce the endothelial barrier any further, the concentration at the lumen would still be that of plasma, and the concentration profile would not change. Alternatively, if the endothelial resistance to solute flux is high (*dashed line)* the concentration at the luminal side of the media would be closer to the perivascular concentration. Endothelial denudation would remove this barrier and the concentration at the lumen would fall to plasma levels, resulting in lower arterial deposition. For perivascular delivery to the rabbit iliac artery the deposition was the same in either the native or denuded case (Fig. 2.8), suggesting that the endothelial resistance to heparin transport *in vivo* is immeasurably low.

The second manner in which the endothelium impact vascular drug deposition is by imposing a barrier to transmural hydraulic flux. Convective currents within the artery are determined by the hydraulic conductivity of the arterial media and endothelial monolayer, and in a vessels the size of the rat abdominal aorta and calf carotid artery removal of the endothelium might let transmural hydraulic velocities increase by 350% and 50%, respectively (Eq. 2.13).[132] Indeed, convective

forces of heparin transport were only shown to be significant in the rat abdominal aorta after endothelial removal. Deposition of endovascularly applied heparin in the calf carotid artery with a transmural pressure gradient of 100 cm H_20 was enhanced following endothelial removal precisely through this mechanism (Fig. 2.7a). Heparin deposition with thin rabbit iliac arteries *in vivo* was unaffected by the presence of an intact endothelium after perivascular release (Fig 2.8). In the 80 μm thick rabbit iliac artery, convective forces should be less important in the native than denuded case, and thus the deposition should be lower for the latter (Fig. 2.5). However, the 635-μm-thick hydrogel release collar encircled the artery and had an unknown hydraulic conductivity, which may have impeded transmural convective flows. Convective transport may have been diminished in this arterial preparation to the point where endothelial removal could not raise it to significance. The endothelium, therefore, appears to modulate deposition by controlling hydraulic flows, rather than as a direct anatomic barrier to diffusion. One potential reconciliation for this seemingly incongruous statement may be that active transcytotic transport may negate the tight endothelial barrier to solutes, but not to solvent.

2.5.3. Resistance to Transport of the Adventitia.

The adventitial resistance to solute transport can also potentially impact the distribution of applied drug. Heparin diffuses through this layer almost twice as readily as in arterial media, perhaps owing to the loose architecture and relative acellularity of the former. The adventitial resistance increases linearly with thickness and will vary with extent of surgical manipulation (Fig. 2.4). Without a transmural pressure gradient the deposition following perivascular application to the calf carotid artery *in vitro* was not significantly different from endovascular delivery, for both native and denuded arteries (Fig. 2.7). Thus, the resistances to heparin flux at both boundaries are roughly equivalent. Since the endothelial resistance to heparin transport has been shown to be negligible *in vitro* and immeasurably small *in vivo,* the resistance of the adventitia is also small.

2.6. Chapter Summary

The quantitative methods that have been employed to examine transmural drug transport may add to the understanding of fundamental structure-function relationships within the blood vessel wall and drug-vascular tissue interactions, and provide a rational framework for the design of local vascular drug delivery systems. The diffusivity of a vasoactive compound, heparin, has been determined in arterial media and adventitia, and the transendothelial resistance to heparin transfer has been measured. The ratio of convective to diffusive forces of transmural solute transport is low in thin arteries, but becomes closer to one with thicker vessels. The endothelium and adventitia are not direct barriers to heparin diffusion, but the former does influence the magnitude of convective forces within the media. This has implications for local vascular drug delivery, as convective forces augment deposition from the endovascular aspect and inhibit deposition from the perivascular aspect.

3. TISSUE AVERAGE BINDING AND EQUILIBRIUM DISTRIBUTION

3.1. Introduction

In the preceding chapter, the mechanisms of soluble heparin transport within the blood vessel wall were examined and the diffusivity of heparin in different arterial layers was measured. Detailed descriptions of drug deposition and distribution rely to an equal extent on drug binding. For example, when exogenous drug is applied to a tissue, binding will remove drug from solution and impede net transport. In addition, soluble and bound drug function differently in tissues and therefore need to be distinguished. Soluble drug is available for redistribution and treatment of distant sites, while bound drug potentially mediates signaling events and is sequestered from or maintains increased local concentration in the vicinity of active receptors.[142,143] Soluble heparin provides some biologic function by complexing with heparin-binding growth factors, while intracellular effects of heparin on second messenger systems may require adherence or binding prior to internalization.[144,145] Finally, the elimination of drug from a tissue will depend upon the dissociation of bound drug, with multiple subsequent transport and rebinding events. Thus, the pharmacokinetic evaluation of a therapeutic strategy will be enhanced significantly by differentiation of soluble and bound drug.

While ligand binding studies almost universally are performed in cell culture and quantify binding sites and affinity of these sites, drug binding within tissues with their intact architecture is potentially far more complex. For example, heparin binding to vascular cells has been well characterized in culture.[145-148] The affinity of heparin binding to individual components of the extracellular matrix, such as fibronectin, laminin, thrombospondin and type I collagen, have been quantified as well.[149] In addition, some extracellular vascular components are not expected to be present at all in homogeneous cell cultures. The majority of drug-tissue binding interactions are potentially nonspecific without any biologic effect. The overall binding characteristics of drug within tissues includes the combined effects of all the binding sites and their respective affinities and have not been measured for any compound in any tissue, let alone heparin within arterial media

or adventitia. In this chapter, a novel approach to characterizing the binding of any solute within any tissue is derived and quantifies the drug-tissue interaction in terms of binding site density, tissue-average dissociation constant, and fractional volume of tissue in which drug can distribute. This technique quantifies both biologically active and nonspecific binding, and provides a rationale for discriminating bound from soluble fractions of drug in tissues. Though validated here with heparin, the method is applicable to many drugs and tissues.

3.2. Equilibrium Distribution Model

The equilibrium distribution technique measures the binding and distribution constants by incubating many samples of tissue in a wide range of radiolabeled drug concentrations and curve-fitting the resulting data to the following model. The model is derived in general terms and should be applicable to many compounds and tissues. The total concentration of drug observed within a volume of tissue (c_T) is considered to be the superposition of soluble (c_s) and bound (c_b) components:

(3.1) $$c_T = c_s + c_b$$

At very low drug concentrations, an increase in total concentration results in a linear increase in both soluble and bound concentrations (Fig. 3.1).

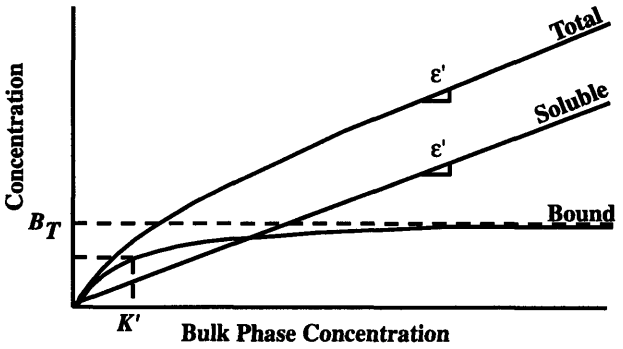

Figure 3.1. Equilibrium distribution model of compounds in tissues.

As binding sites saturate, increases in the total concentration will be solely noted as increases in the soluble concentration. In a unit volume of tissue there are regions where soluble drug is excluded by steric interactions. The fractional volume in which drug can distribute (ε) is given by:

(3.2) $$\varepsilon = \frac{V_a}{V_T}$$

where V_a is the accessible space for drug distribution and V_T is the total tissue volume. Note that the convention used in this work is that the drug concentrations c_T, c_s and c_b are defined as the moles of drug per unit *total* volume of tissue. Thus, the moles of soluble drug per unit *total* volume of tissue (c_s) is related to the moles of soluble drug per unit *accessible* volume (c_a) by the fractional volume:

(3.3) $$c_s = \varepsilon c_a$$

The law of mass action defines the dissociation constant (K_d) as the product of the drug concentration in the accessible volume and the ratio of the molar densities of free (B_f) and bound (B_b) binding sites:

(3.4) $$K_d = \frac{c_a B_f}{B_b}$$

The number of binding sites is assumed to be conserved so that the total binding site density (B_T) can be expressed as:

(3.5) $$B_T = B_f + B_b$$

Although in the context of the law of mass action these binding site densities should be defined as moles of binding sites per unit *accessible* volume, because the bound and free density are related as in Eq. 3.4, they can be and are defined per unit *total* volume. By assuming a one to one ligand to binding site ratio:

(3.6) $$c_b = B_b$$

By combining Eqs. 3.1, 3.3 - 6:

(3.7) $$c_T = \varepsilon c_a + \frac{B_T c_a}{K_d + c_a}$$

3.2.1. Equilibrium Distribution Measurements

In these equilibrium distribution measurements, the concentration of drug in the accessible volume (c_a) is established by incubating the tissues in solutions containing radiolabeled drug until equilibrium. The concentration of drug in the accessible volume (c_a), however, is not necessarily equal to the external or bulk phase concentration (c_{bulk}) because of potential charged partitioning. Thus:

(3.8) $$c_{bulk} = \kappa c_a$$

where κ is the partition coefficient of drug into the accessible volume. Thus:

(3.9) $$c_T = \frac{\varepsilon}{\kappa} c_{bulk} + \frac{c_{bulk} B_T}{\kappa K_d + c_{bulk}}$$

The dissociation constant and the partition coefficient are combined into a modified dissociation

constant reflecting binding and charged association:

(3.10) $$K' = \kappa K_d$$

Similarly, a modified fractional volume of distribution reflecting sterical and charged effects can be defined:

(3.11) $$\varepsilon' = \frac{\varepsilon}{\kappa}$$

Thus:

(3.12) $$c_T = \varepsilon' c_{bulk} + \frac{c_{bulk} B_T}{K' + c_{bulk}}$$

Thus, the total concentration is a function of the concentration outside the tissue, and the three binding and distribution constants (ε', B_T, and K'), which are specific to each drug and tissue.

3.2.2. Curve Fitting and Initial Estimates

A commercially available non-linear least squares Levenberg-Marquardt algorithm including a Pearson minimization (TableCurve 2D, Jandel Scientific) was used to fit the data and determine the binding and distribution constants (ε', B_T, and K'). Because the bulk phase concentration data must span many orders of magnitude, a fit to Eq. 3.12 would preferentially weight the data taken at the highest bulk phase concentrations. The inherent weighting can be distributed over all of the data points by fitting the logarithm of the measured total concentration (c_T) to the following equation:

(3.13) $$\ln(c_T) = \ln\left(\varepsilon' c_{bulk} + \frac{c_{bulk} B_T}{k' + c_{bulk}} \right)$$

Non-linear least squares algorithms are sensitive to the initial estimates of the unknown constants.[150] The following approximate method for determining ε', B_T, and K' from the equilibrium distribution curve is used to provide the initial estimates for the curve-fit. Consider an idealized equilibrium distribution curve that is the sum of the bound and soluble drug (Fig. 3.1). A least squares estimate of the slope (ε') at high bulk phase concentrations allows the soluble component of the data ($\varepsilon' c_{bulk}$) to be subtracted from the total concentration data, reducing Eq. 3.12 to:

(3.14) $$c_b = \frac{c_{bulk} B_T}{K' + c_{bulk}}$$

The resulting plateau can be considered equivalent to the total number of binding sites. The average dissociation constant can be estimated as the bulk phase concentration at which half of the binding sites are occupied.

The reliability of the commercial software was assessed by writing an alternative curve-fitting program utilizing a Nelder -Meade function minimization routine (Matlab, Math Works). All of the constants computed by the former algorithm differed maximally from the later by 8%, thus validating the former.

3.2.3. Bound and Soluble Fractions

The equilibrium distribution method also allows for the a total concentration measurement (c_T) to be resolved into bound and soluble components. By solving for Eqs. 3.1,3.3 and 3.7:

(3.15) $$c_s = \frac{c_T - B_T - K'\varepsilon' + \sqrt{\left(c_T - B_T - K'\varepsilon'\right)^2 + 4c_T K'\varepsilon'}}{2}$$

The distinction between bound and soluble drug is important. While soluble drug binds to active receptors and mediates extracellular signaling events, non-specific binding sites play a distinct role, as they sequester drug in the vicinity of active receptors.[142,143] Furthermore, in terms of drug distribution and pharmacokinetics, only the soluble fraction of drug is available to diffuse or convect through a tissue, while potential binding sites tend to impede the movement of drug.

3.3. Experimental Methods

The equilibrium distribution method described above was used to determine the binding and distribution constants (B_T, k' and ε') for heparin in porcine carotid media with endothelium intact and after endothelial denudation, and in the adventitia. Porcine carotid arteries were explanted and stored on ice for no more than 2 hours. The adventitia was stripped from the media, and both were temporarily stored in 2% Penicillin-Streptomycin (Gibco) in sterile phosphate buffered saline. The endothelium of some of these arteries were denuded with three passes of an inflated 3 French embolectomy catheter (Baxter).[129] Arteries were cut into 10 - 40 mg pieces and incubated in Dulbecco's Modified Eagle Media (DMEM, Gibco) with 10% Fetal Bovine Serum (Gibco) and 2% Penicillin-Streptomycin, with ^{3}H-heparin (Dupont-NEN) concentrations ranging from approximately 100 pM to 0.2 mM. All incubations were performed in 2 ml of culture media and were carried out until equilibrium, which was achieved when the time rate of increase of drug concentration in the tissue reached zero. Following incubation, the arterial specimens were blotted on dry towels, weighed wet, solubilized and scintillation counted. At least four pieces of each type of tissue were incubated at each bulk phase concentration (c_{bulk}). Bulk phase heparin concentration measurements were made at the end of the incubations and were the average of three 50 µl samples from each culture well. These equilibrium distribution measurements were repeated twice for each tissue type, using different batches of reagents. Histologic frozen sections were taken from representative arteries for morphologic evaluation.

Prior to the above experiments, the time course of heparin equilibration was quantified in samples of porcine carotid media with endothelium by incubating in a bulk phase concentration of 0.15 mg/ml (Fig. 3.2). Although vascular cells and interstitial molecules may continue to exchange drug with the bulk phase, these data show that heparin reaches equilibrium with the tissue as a whole well within 24 hours. All subsequent incubations were therefore carried out for this duration. In separate experiments, the density of fresh porcine carotid media was measured using a micro-graduated cylinder and an analytical balance. The resulting density of 0.983±.024 g/ml (n=5, ± standard deviation) was used to convert wet weight to volume for calculations of total

drug concentration in tissue.

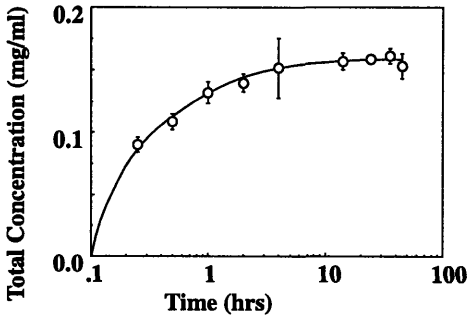

Figure 3.2. Total concentration of porcine carotid media over time when incubated in 0.15 mg/ml of heparin (average ± SEM , n = 4).

3.4. Verification of the Equilibrium Distribution Method

Equilibrium distribution data are shown for arterial media with intact and denuded endothelium and adventitia (Fig. 3.3, Appendix 8.5). Each point shown represents the average of at least four total concentration measurements on samples of tissue from the same culture well and three measurements of the bulk phase concentration in that well. Note that the error bars are present but unappreciable on the logarithmic scale. For each tissue type, initial estimates of the fractional volume of tissue in which drug can distribute (ε') were determined through linear regression of the high bulk phase concentration data ($c_{bulk} > 10^{-5}$ M, Table 3.1). Figure 3.4 shows all of these data following the subtraction of the soluble fraction of drug ($\varepsilon' c_{bulk}$). For arterial media with intact and denuded endothelium, initial estimates of the binding site density (B_T) were estimated as the plateau of these curves. The dissociation constant of the average binding site (K') was estimated as the bulk phase concentration where half of the binding sites were saturated. The Levenberg-Marquardt curve-fit algorithm converged to the solutions shown (Table 3.2) using the initial estimates (Table 3.1), and when these initial estimates were perturbed up or down by two orders of magnitude for B_T and K', and by 0.2 for ε'. This curve-fit software also calculated standard errors for each binding and distribution constant. These curve-fits were further assessed by computing best-fit curves for the experimental data and the computed bound concentrations using Eqs. 3.12 and 3.14, respectively (solid lines, Figs. 3.3 and 3.4). It was not possible to obtain initial estimates of B_T and K' for the adventitia, because the bound concentration spread about zero following the subtraction of the linear soluble component (Fig. 3.4c). This indicated that the binding site density in this tissue was lower than the scatter in the data at high bulk phase concentrations. Despite this, the curve-fit algorithm converged on binding constants for the adventitia (Table 3.2) that were consistent over a wide range of assumed initial estimates.

Table 3.1. Sample binding and distribution constants determined by 1) finding the slope (ε') of the equilibrium distribution data (Fig. 3.3) for $c_{bulk} > 10^{-5}$ M, 2) subtracting $\varepsilon' c_{bulk}$ from the data and replotting (Fig. 3.4). 3) B_T is approximated as the plateau of the subsequent data, and 4) K' is approximated as c_{bulk} at $B_T/2$.

	ε'	B_T(μM)	K'(μM)
Arterial Media with Intact Endothelium	**0.60**	**4**	**12**
Arterial Media with Denuded Endothelium	**0.63**	**8**	**10**
Adventitia	**0.78**	-	-

Table 3.2. Sample binding and distribution constants determined with a non-linear least-squares Levenberg - Marquardt algorithm (values ± SEM).

	ε'	B_T	K'
Arterial Media with Intact Endothelium	**0.61±*0.03***	**4.2±*1.7*** (μM)	**6.8±*2.5*** (μM)
Arterial Media with Denuded Endothelium	**0.70±*0.03***	**2.5±*1.1*** (μM)	**5.0±*2.1*** (μM)
Adventitia	**0.87±*0.02***	**2.2±*1.3*** (nM)	**8.1±*5.7*** (nM)

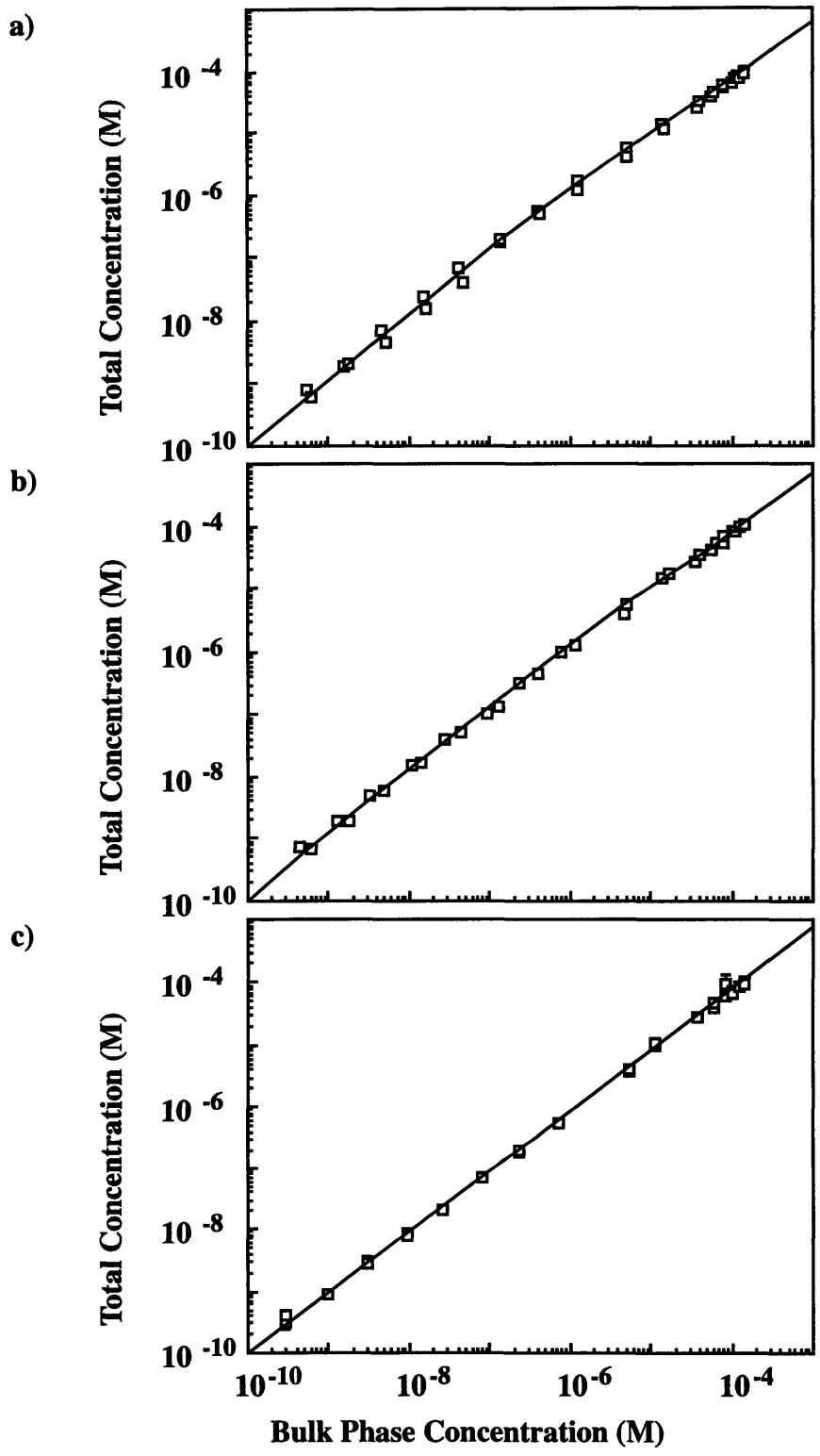

Figure 3.3. Measured equilibrium distribution curves for heparin within a) arterial media with endothelium, b) denuded media, and c) adventitia (average ± SEM, n > 4). Solid lines are generated from Eq. 3.12 and the curvefit binding and distribution constants (ε', B_T and K') shown in Table 3.2.

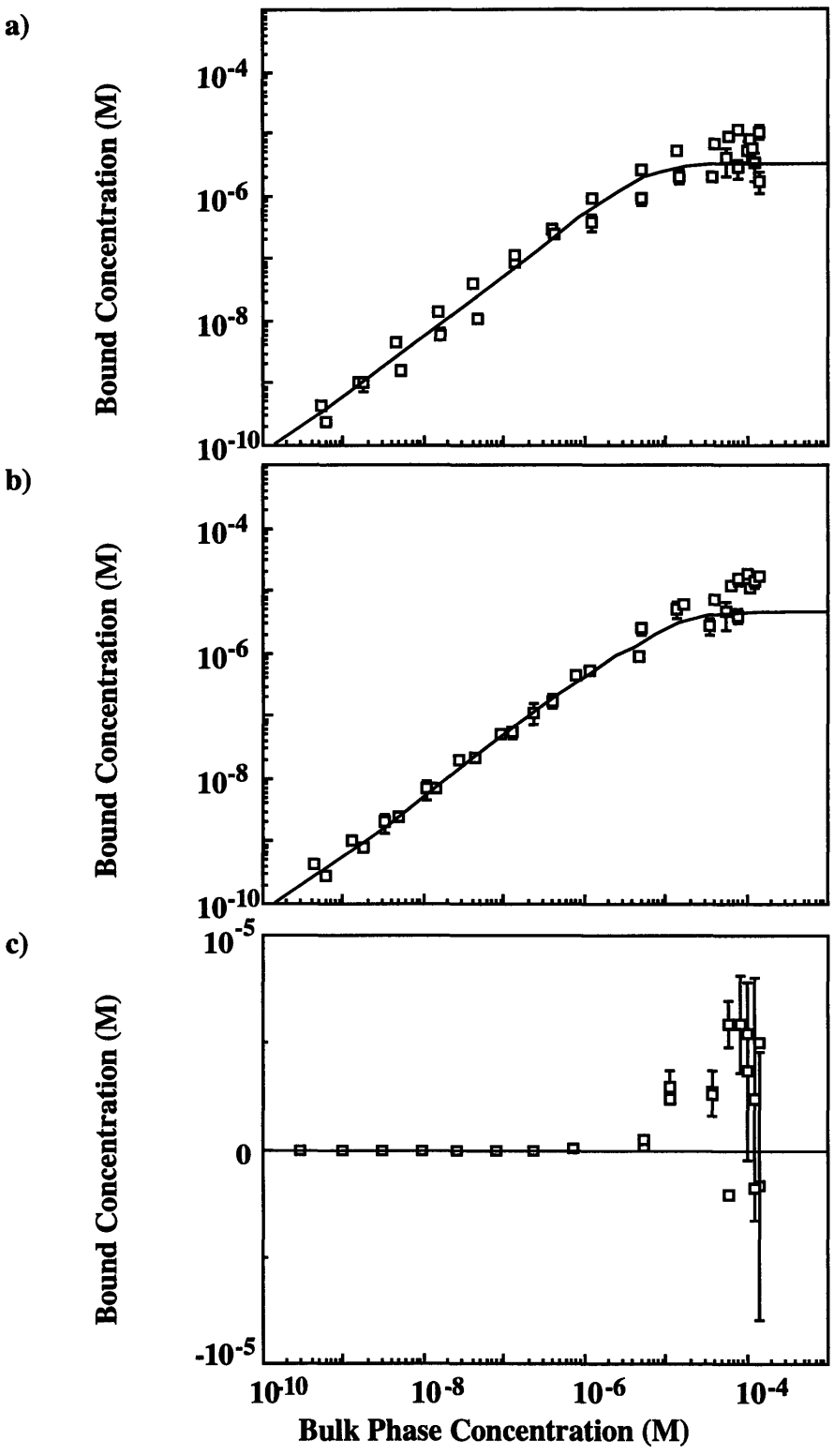

Figure 3.4. Bound concentration of drug in the tissue (c_b) for a) arterial media with endothelium, b) denuded media, and c) adventitia, determined by subtracting the linear soluble (c_s) fraction from the total concentration (c_T, average ± SEM, n > 4). The plateau corresponds to the binding site density (B_T). Note that low signal:noise ratios prevented the demonstration of the binding site density in the adventitia. Solid lines are generated from the curvefit binding constants (B_T and K') and Eq. 3.14.

The equilibrium distribution analysis for heparin within arterial tissues predicts observed heparin-vascular tissue interactions. The fractional volume of tissue in which a drug can distribute (ε') is highest in the adventitia and increases in the arterial media following balloon denuding injury (Table 3.2), reflecting the loose architecture and high content of connective tissues of the former, and the role of structural damage and edematous changes in the latter.[151,152] The analysis also showed that the concentration of heparin binding sites (B_T) in the arterial wall is larger with intact endothelium, consistent with many reports that this monolayer binds heparin.[146-148,153-155] Cultured endothelial cells posses nearly 100 fold more heparin binding sites than cultured vascular smooth muscle cells.[145,147] The binding site density measured for heparin in arterial media without the endothelium was 2.5 μM. If the volume of a smooth muscle cell can be approximated by a cylinder that is 10 μm long and 3 μm in diameter, the number of binding sites per cell is approximately 100,000, which is the density previously measured in culture.[145] The dissociation constant of the average binding site (K') of the arterial media, assuming a partition coefficient of one, is three orders of magnitude higher than for growth arrested cultured smooth muscle cells and basic fibroblast growth factor and about one to two orders of magnitude higher than laminin, fibronectin, and type I collagen, indicating that much of the binding is to arterial elements with even lower affinity.[145,149] The dissociation constant of the arterial media is much higher than that of the adventitia, indicating that although there are far fewer binding sites in the latter, they are of much higher affinity. This may be explained by the large concentration of type I collagen in the latter, whose affinity for heparin is about the same as the values reported here for the adventitia, and the relative scarcity of cells and associated potential binding sites.[149,151,152] These trends are consistent with known properties of the heparin-arterial tissue interaction and help validate the equilibrium distribution technique.

3.5. Discussion

A quantitative description of how drugs distribute and bind to intact tissues was sought, with the hope of incorporating these findings into detailed pharmacokinetic models. The equilibrium distribution analysis described in this chapter quantifies drug binding to all the potential binding sites and distinguishes soluble from bound components. The technique involves incubating many samples of tissue in solutions containing a wide range of drug concentrations, measuring the corresponding tissue concentrations, and computationally fitting these data to a model of drug distribution and binding. Through these steps, the binding site density, dissociation constant of the average binding site, and fractional volume of drug distribution were measured for heparin in arterial tissues and these results were used to validate the technique.

Two methods of determining the binding and distribution constants (ε', B_T, and K') from an equilibrium distribution curve have been described. The first requires a linear regression of the data, algebraic manipulation of these data, and visual inspection of resulting curves. While this method is relatively simple, it affords no assessment of the "goodness of fit" or statistical measure of accuracy. In addition, errors in estimating ε' are carried through to B_T and K'. The second curve-fitting technique requires the use of more sophisticated computational algorithms to arrive at estimations of the binding and distribution constants. A commercially available software package is used which computes the standard error for each measured constant. The former method, however, provides the required initial estimates used in the latter method.

Although the tissue concentration data are repeatable (Fig. 3.3), some of the standard errors are relatively high (Table 3.2). This results in part from the dependence of these particular constants on the subtle convexity of the equilibrium distribution curve, so that small concentration measurement errors create uncertainty. Furthermore, if the scatter in the data is greater than the binding site density, as was encountered with the adventitia, following the subtraction of the soluble component the bound concentration data spreads about zero (Fig. 3.4c). Thus, a low signal to noise ratio limits the accuracy of the technique to drug-tissue interactions with relatively large number of binding sites.

The derivation of the equilibrium distribution method assumed that there was a one-to-one stochiometric relationship between binding sites and drug. While this may be valid for many drugs, for some compounds a single ligand may be able to simultaneously bind several sites, thus limiting the applicability of the law of mass action. This phenomenon may occur in some of the heparin binding sites in arterial tissues. In addition, the partition coefficient (κ) remains unquantified as it is difficult to measure in complicated structures such as arterial tissues, however, it is expected to be about one for hydrophilic compounds such as heparin. Despite these possible sources of artifact, these binding constants empirically reflect the drug-tissue interaction and allow for the realistic distinction between bound and soluble drug.

3.6. Chapter Summary

The equilibrium distribution measurements and subsequent numerical analysis are a useful method of describing the binding of compounds to tissues, not just individual binding sites. Each set of measurements simultaneously determines the fractional volume of tissue available for drug distribution, binding site density, and affinity of the average binding site. These constants allow the determination of the bound and soluble fraction of drug from tissue concentration measurements. This information not only describes the physical interaction between the compound and tissue quantitatively, but also is an integral part of vascular pharmacokinetics as it characterizes how soluble drug distributed across an artery deposits. Although demonstrated here with heparin in vascular tissues, this technique is applicable to many compounds and tissues.

4. DRUG TRANSPORT IN THE LOCAL ARTERIAL ENVIRONMENT

4.1. Introduction

The complete vascular pharmacokinetic description includes intramural mechanisms of solute transport, the interaction of soluble drug with potential intra-arterial binding sites, and the movement of drug from the point of administration to the blood vessel wall. The former two have been quantified in the preceding chapters and the latter can be thought of as providing boundary conditions for quantitative intramural analysis of solute deposition and distribution. The pathways by which drug released in the local arterial environment both enters the arterial wall and is siphoned away to the rest of the organism has been characterized through the following local drug delivery experiments using inulin and heparin:

I Routes of drug clearance from the perivascular space.

II Routes from the perivascular space to the blood vessel wall.

III Drug losses from the endovascular and perivascular spaces.

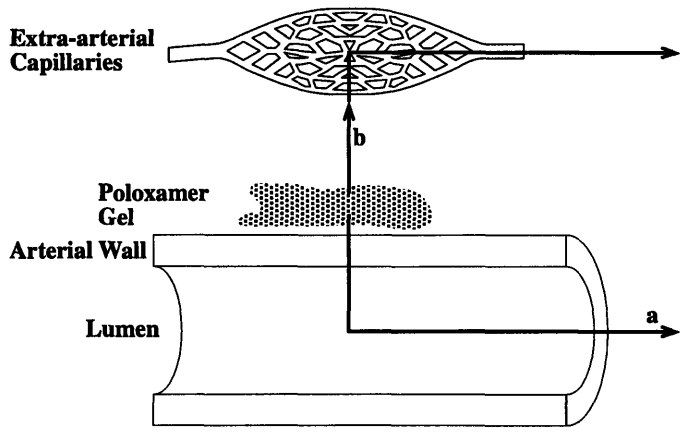

Figure 4.1. a) Routes of clearance from the perivascular space include transarterial transport with entry into the lumen flow (pathway a) and absorption by extra-arterial capillaries (pathway b).

4.1.1. Routes Of Drug Clearance From The Perivascular Space

Drug can be cleared from the perivascular space by transmural diffusion (*pathway a*, Fig. 4.1), or absorption by extra-arterial micro-vessels (*pathway b*). The relative importance of these pathways was determined by measuring the urinary excretion rate of perivascularly released inulin as each route was systematically eliminated. Urinary inulin excretion can be used as a proxy for

drug entry into the general circulation as this polysaccharide is eliminated from plasma through the renal glomerulus without metabolism, secretion or tubular reabsorption.[156] Initial results showed that the overwhelming majority of adventitially released inulin is cleared from the perivascular environment through the extra-arterial capillaries.

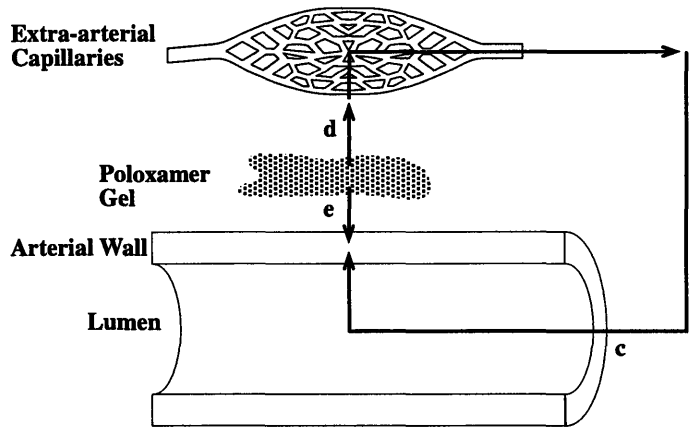

Figure 4.2 Routes of entry to the blood vessel wall from the perivascular space include endovascular administration from the systemic circulation (pathway c) following absorption by extra-arterial capillaries (pathway d) and direct diffusion (pathway e).

4.1.2. Routes from the Perivascular Space to the Blood Vessel Wall

It is reasonable then to suspect that drug absorbed by these capillaries could join the systemic circulation and enter the vessel wall from its endovascular aspect. This possibility, as well as the potential for drug to diffuse in directly from the perivascular aspect, was tested by following the deposition of heparin released from outside the blood vessel. Heparin deposition was measured in the native unmanipulated state and after elimination of pathways that could lead to: endovascular administration from the systemic circulation (*pathway c*, Fig. 4.2), extra-arterial capillary uptake (*pathway d*, Fig. 4.2), or direct diffusion from the perivascular space (*pathway e*, Fig. 4.2). These data showed that the majority of drug released in the perivascular space is absorbed by the extra-arterial capillaries, yet virtually all of the drug deposited in the artery arrives directly from its adventitial aspect.

4.1.3. Drug Losses to the Endovascular and Perivascular Spaces

The above experiments demonstrate overwhelming loss of drug to the perivascular extra-arterial capillaries. The extent to which drug is lost from the artery to either the rapid lumen flow on the endovascular aspect or these extra-arterial micro-vessels on the perivascular aspect was compared by placing equivalent polymeric controlled heparin releasing devices on either of these surfaces and comparing arterial deposition. The results in Chapter 2 suggested that there were no anatomic barriers to solute entry from either surface, and therefore in this preparation the deposition with each mode of delivery was considered inversely proportional to the loss of drug to that aspect. For example, if heparin deposition following endovascular delivery exceeds that from perivascular administration, then the loss of drug to the perivascular microvessels exceeds the loss to the lumen flow.

4.2. Materials And Methods

4.2.1. Drug Release from Poloxamer

Drug was released *in vivo* from 28% (wt./vol) gels of Poloxamer copolymer (poly(oxyethylene)-poly(oxypropylene) [Pluronic 407, BASF Wyandotte Corp. and Anti-adhesion 28, MDV Technologies]). Poloxamer 407 solutions undergo reverse phase gelation, remaining as a free flowing liquid until the ambient temperature is raised above the critical threshold of 15 °C, well below room and body temperature. Above this temperature, the viscosity increases markedly and the gel solidifies into a solid mass. Erosion of, and subsequent release from, such a gel is then prolonged enabling use as drug depots.

4.2.2. Routes Of Clearance From The Perivascular Space

Sprague Dawley female rats (275-325 g) were anesthetized with an intraperitoneal injection of ketamine (50 mg/kg) and xylazine (10 mg/kg). The bladder, exposed after a midline abdominal incision, was cannulated with an 8 inch polyethylene tube (ID 0.58 mm, Clay Adams) and secured with a purse string suture. Urinary inulin excretion was monitored continuously through this catheter. Incisions were closed and supplementary anesthesia with ketamine (12.5 mg/kg) and xylazine (2.5 mg/kg) was administered as necessary.

The left common carotid artery was exposed and cleaned of excess fat and fascia. In one experimental group, a 100-µl-dose of ^{14}C-inulin (0.35 µCi, 0.14 mg, NEN-Dupont) in 28% (wt/vol) Poloxamer solution kept on ice (3-5°C) was injected into the perivascular space. The gel, which had remained fluid while cool, gelled immediately upon contact with the artery at 37°C, conforming to the irregular surface of the vessel.[39] Urinary flow through the bladder cannula was collected in a clean scintillation vial which was changed every 15 minutes for the first hour, and every half hour for the next three hours. In the second experimental group, the potential for transarterial inulin clearance was eliminated by ligating arteries at proximal and distal sites spaced 1 cm apart (*blocking pathway a*, Fig. 4.1). Any inulin that traversed the wall was then trapped within the occluded segment and could not mix with systemic circulation for excretion. In the third

experimental group, the Poloxamer gel and the artery were separated from the extra-arterial capillary beds by a Silastic sheath (ID 3.18 mm) whose ends and seam were plugged with a silicon glue (Type A Medical Adhesive, Dow Corning). The Poloxamer solution was injected only into the space within the sheath, retaining arterial contact with the gel but eliminating possible capillary bed absorption of inulin (*blocking pathway b*, Fig. 4.1). Following all of these experiments the ^{14}C-inulin content within each urine sample was determined by liquid scintillation spectroscopy (1214 RackBeta, LKB-Wallac). In a fourth experimental group the integrity of the Silastic wrap was determined. Each of the manipulations described for the previous two groups were employed and both transmural and extra-arterial capillary clearance were eliminated (*blocking pathways a and b*, Fig. 4.1). Four rats were examined in each of the four experimental groups. To visualize potential leaks from the seam or plugs at the ends of the Silastic barrier, Evan's Blue Dye (Sigma) was mixed into the Poloxamer solution (25 mg/ml), and then injected into a wrapped artery of an additional animal.

4.2.3. Routes from the Perivascular Space to the Blood Vessel Wall.

In a similar fashion, drug entry and deposition into the arterial wall was characterized with Heparin-releasing Poloxamer gels fabricated as described above. Female Sprague Dawley (275-325 g) rats were anesthetized and their left carotid arteries isolated as above. Four animals were examined in each experimental group. One hundred-µl of ^{3}H-heparin (1.0 µCi, 1.4 µg, NEN-Dupont) in 28% Poloxamer solution kept on ice (3-5°C) was injected into the perivascular space of the left carotid artery. The Poloxamer 407 solution gelled immediately upon contact with the artery. One hour after administration of the heparin-gel, the left carotid artery was excised, blotted to remove excess fluid, and dipped into 100% ethanol to dissolve adhering Poloxamer gel. The artery was dehydrated, weighed, solubilized with 0.5 ml of Soluene-350 (Packard) and counted by liquid scintillation spectrometry for ^{3}H-heparin deposition. In addition, 10 - 60 mg tissue samples from the abdominal aorta, iliac, and femoral arteries, and liver were harvested, dehydrated, weighed, solubilized, and counted. The liver was assayed in particular because its high density of endothelial cells created a large potential source for heparin binding.[146,154] Liver samples were

bleached to reduce color quenching of tritium by adding 0.5 ml of hydrogen peroxide prior to scintillation counting.

In a second experimental group the possibility that heparin could be deposited from blood flowing in the lumen was eliminated by occluding the artery with proximal and distal ligatures (*blocking pathway c*, Fig. 4.2). Any heparin detected in the wall could have only arrived directly from the perivascular space . In a third group of animals the possibility that heparin might enter the systemic circulation following extra-arterial capillary drug absorption was prevented with a Silastic wrap. The heparin-Poloxamer solution was injected around the artery but inside a silicon glue sealed Silastic sheath (*blocking pathway d*, Fig. 4.2). In the fourth experimental group heparin deposition in the carotid artery was quantified after the Poloxamer solution was injected into the highly vascularized peritoneal cavity (*blocking pathway e*, Fig. 4.2). The contribution of direct diffusion from the perivascular space could then be determined by comparison to data obtained after local arterial delivery. In this group, care was taken to remove liver samples that were not in contact with any injected Poloxamer gel.

4.2.4. Drug Losses to the Endovascular and Perivascular Spaces

Heparin deposition was compared 90 minutes after endovascular and perivascular administration to the rabbit iliac artery *in vivo*, through hydrogel drug delivery devices of similar composition and geometry and therefore release rates. Perivascular hydrogel release devices were formed in molds and wrapped around isolated arteries, and endovascular devices were formed *in situ*. The hydrogel prepolymer formulation and crosslinking protocol were described in Section 2.2.3.

4.2.4.1. Perivascular Administration

The iliac arteries of New Zealand White rabbits were isolated as described in Section 2.2.3.2. Eosin Y (20 μg/ml, Sigma) was added to heparin containing prepolymer solutions and this mixture was injected into 70 μm thick planar glass molds where it was photopolymerized with an argon laser (488-514 nm, 70 mW/cm^2, American Laser). The resulting films were cut into strips

approximately 7 mm wide and two were folded over adjacent segments of each iliac artery. The abdomen was sutured closed for the 90 minute drug deposition experiment and the arteries were harvested and assayed for heparin deposition in the same manner as described in Section Sec. 2.2.3.2.

4.2.4.2. Endovascular Administration

Rabbits were anesthetized and maintained on inhaled halothane (1 - 3% in oxygen) anesthesia throughout the procedure. A specialized double balloon hydrogel delivery catheter (Focal, Inc.) was inserted through a carotid arteriotomy and advanced to the iliac arteries under fluoroscopic guidance.[157] Once in the iliac artery, the catheter was advanced so that both the proximal and distal balloons were beyond the aortic bifurcation. The endothelium was removed by inflating the distal balloon and withdrawing the catheter 35 mm towards the aortic bifurcation a total of 3 times. Following denudation the catheter was repositioned and the balloons inflated, isolating a 25 mm segment of the artery within the de-endothelialized zone. This vascular segment was subject to sequential 3 ml flushes of saline, initiator solution (eosin Y, 20 μg/ml), saline, and the liquid prepolymer solution. At the conclusion of the injection sequence a fiber optic element within the catheter delivered laser light (514 nm, American Laser) to the endoluminal surface, forming a 70 μm thick layer of heparin-containing hydrogel on the vessel wall. Following the deposition procedure the balloons were deflated, the catheter withdrawn, and the procedure repeated in the contralateral iliac artery. Endovascular hydrogels were formed on both iliac arteries within five minutes of each other. Shortly before excision, the abdomen was opened and the iliac arteries were isolated, removed, and assayed for heparin deposition as described in Section 2.2.3.2.

4.3. Results

4.3.1. Routes Of Clearance From The Perivascular Space

Inulin was administered from Poloxamer 407 gels into the perivascular space of unmanipulated native arteries, or ligature occluded arteries whose transarterial pathways to the systemic circulation were removed (Fig. 4.1). Rates of inulin clearance from the perivascular space of these two vessels, native and occluded, were statistically indistinguishable, implying that drug released into the perivascular space was cleared exclusively through the extra-arterial capillaries and not through the wall of the carotid artery into the lumen (Fig. 4.3a, Appendix 8.6). These observations are further supported by tracking inulin excretion rates when the polysaccharide was released from the perivascular space of wrapped arteries. The wraps served as an impermeable barrier preventing drug from clearing through the extra-arterial capillaries. Inulin excretion rates from wrapped arteries were far lower than for native or occluded arteries, but indistinguishable from that observed in arteries that were both occluded and wrapped (Fig. 4.3b). Thus, the minimal amount of inulin excretion detected with wrapped arteries reflects leakage through imperfections in the Silastic barrier rather than transmural clearance. The presence of barrier leaks was detected visually when Evan's Blue Dye delivered from Poloxamer 407 gel extravasated from the ends of the wrap and migrated along the artery, ultimately spreading to the capillaries in the perivascular space.

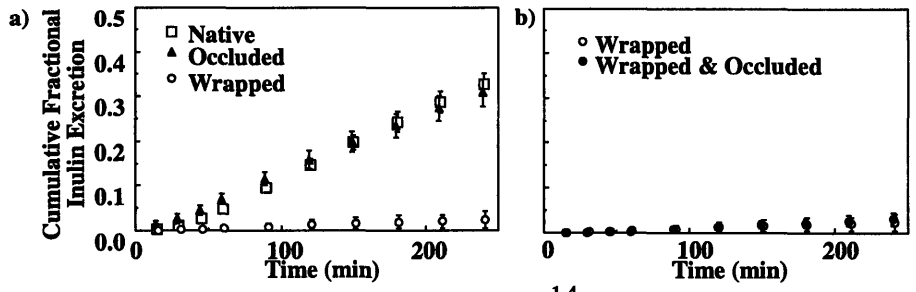

Figure 4.3. a) Cumulative urinary excretion of ^{14}C-inulin per amount administered following pericarotid delivery to native arteries, occluded arteries, and arteries wrapped to shield the extra-arterial capillaries from the drug. b) Cumulative urinary excretion of ^{14}C-inulin per amount administered following pericarotid delivery with wrapped arteries, and both wrapped and occluded arteries, reflects the leak from the wrap (average ± SEM, n = 4).

4.3.2. Routes from the Perivascular Space to the Blood Vessel Wall.

Deposition of heparin released into the perivascular space was followed as each potential pathway from release device to the tissue, extra-arterial capillary absorption, delivery from the general circulation, and direct diffusion was systematically eliminated (Fig. 4.2). Following one hour of release, the amount of heparin in the carotid artery was much higher than in distant arteries or the liver, and was not statistically altered by ligature occlusion of the blood vessel (Fig. 4.4, Appendix 8.7). Following the intraperitoneal application of the heparin-Poloxamer gel, drug deposition in the carotid artery was similar to other tissues and was 500 fold lower than with perivascular delivery to native arteries. Drug delivery from inside a wrap surrounding the carotid did not result in a statistically significant increase local arterial concentrations. In addition, concentrations in distant structures were not diminished, apparently because the wrap failed to completely eliminate extra-arterial capillary absorption.

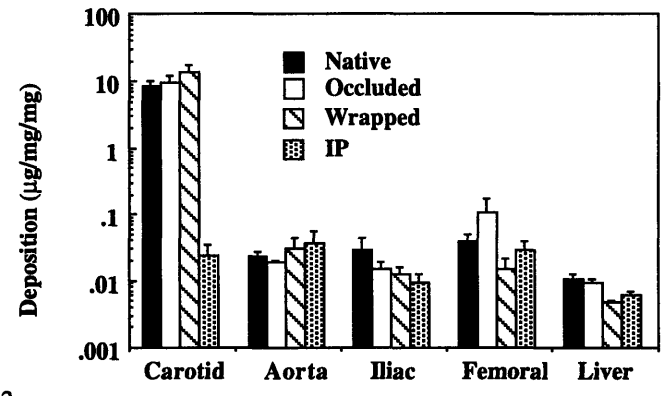

Figure 4.4. ^{3}H-Heparin deposition (µg of heparin per mg administered per mg dry tissue) following one hour release. Poloxamer containing heparin was injected into the perivascular space of carotid arteries that were native, occluded or wrapped, or was given through an intraperitoneal (IP) injection (average ± SEM, n=4).

4.3.4. Drug Losses to the Endovascular and Perivascular Spaces

Deposition of ^{3}H-heparin in rabbit iliac arteries from an interfacially formed 70-μm thick endovascular hydrogel was 7.7 times higher than that observed for the same release device placed as a perivascular wrap (Fig. 4.5, Appendix 8.8).

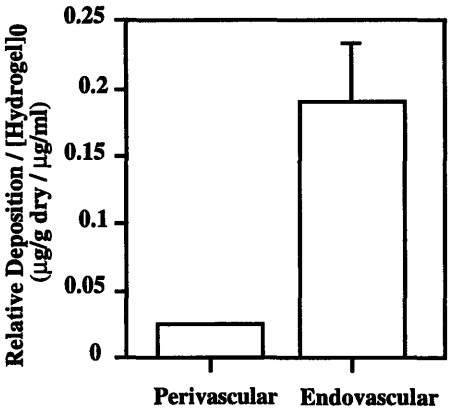

Figure 4.5. The *in vivo* heparin deposition per initial hydrogel concentration in rabbit iliac arteries ninety minutes after either perivascular or endovascular deployment from 70-μm-thick hydrogels (n=12, average ± SEM).

4.4. Discussion

Precise elucidation of the pharmacokinetics not only requires quantitative evaluation of the forces that govern transport and binding within arterial tissues but also a description of how drug arrives at the boundary of the blood vessel wall. In the previous chapters, transport and binding constants were evaluated for a model vasotherapeutic compound, heparin, in vascular tissues, however, the boundary conditions remain obscure. Controversy exists as to whether drug released into the perivascular space diffuses directly to the artery or whether drug is absorbed by capillaries outside the artery, mixed with the systemic circulation and only then returned to the endovascular aspect. Furthermore, it has been assumed that locally applied drug is more likely to be lost to the rapid lumen flow rather than to these extra-arterial structures. Countless studies have exhaustively characterized both the mechanisms and kinetics of drug release from polymeric systems, and devices can now be fabricated to deliver virtually any pattern of release. There is, however, a dearth of information regarding the fate of drug once freed. In this chapter the local pharmacokinetic administration of drug to the blood vessel wall has been characterized through experiments that elucidated the pathways of drug clearance from the perivascular space, illustrated the routes by which locally applied drug enters the blood vessel wall, and directly compared the potential for drug to be lost to the lumen flow and the extra-arterial capillaries.

4.4.1. Model Pathways from the Perivascular Space to the Arterial Wall

The present studies determined the relative importance of each of the pathways by which drug leaves the perivascular space, and by which pathways it enters the blood vessel wall. Model drugs, inulin and heparin, were delivered perivascularly and the urinary excretion and arterial deposition were monitored as the pathways of vessel wall clearance and entry were systematically eliminated, respectively. The potential routes of drug clearance from the perivascular space are absorption by extra-arterial micro-vessels or transarterial diffusion directly into the circulation (Fig. 4.1), while the pathways to the arterial wall are endovascular application from the circulation or direct diffusion through the adventitial aspect (Fig. 4.2). Ligature occlusion of the blood vessel

lumen did not decrease inulin excretion (Fig. 4.3a) nor decrease heparin deposition (Fig. 4.4). Extravascular wraps designed to prevent exposure of the extra-arterial capillaries to drug reduced inulin excretion but left heparin deposition unchanged. The carotid deposition of heparin following perivascular delivery, however, was much higher than for intraperitoneal administration. The combination of these analyses reveals that the overwhelming amount of perivascularly released drug is absorbed by the extra-arterial capillaries, yet virtually all the drug found in the artery diffuses directly from the device through the perivascular space and into the arterial wall.

These seemingly contrary processes are neither paradoxical nor mutually exclusive. The surface area for absorption of the extra-arterial capillaries is very large compared to that of the carotid artery. Moreover, the transmural diffusive resistance of the artery is much greater than that of an individual capillary simply because it is much thicker (Sec. 2.3.1). Both of these effects cause the vast majority of drug to be cleared by the extra-arterial capillaries. That all of the drug deposited in the arterial wall comes from the perivascular space, and not from the circulation, reflects systemic dilution far below the drug concentration in the perivascular interstitial fluids. Therefore, there is a large transmural concentration gradient forcing drug into the vessel wall from the perivascular space. Although inulin and heparin are physically and chemically distinct polysaccharides and may diffuse through and bind to tissues differentially, these two results have been combined to provide a unified qualitative model of how drug is handled by vascular tissues and their typical local environments.

4.4.2. Drug Losses to the Endovascular and Perivascular Spaces

The former analyses showed how drug arrives at the blood vessel and the following data address how drug is likely to leave the arterial wall. Heparin deposition following endovascular administration to the rabbit iliac artery from a 70 μm thick sheet of hydrogel was 7.7 fold higher than following perivascular delivery from an equivalent device (Fig. 4.5). Since, the experiments in Chapter 2 demonstrated that there are few anatomic barriers to heparin distribution, and since the hydrogels decrease overall arterial hydraulic conductivity to an unknown extent, the deposition *in vivo* in the rabbit iliac artery mostly reflects the conditions surrounding the applied drug delivery

device. For example, the endovascular hydrogel was tightly adherent to the blood vessel wall, but was subject to losses to rapid flow in the lumen. On the other hand, the perivascular hydrogels were exposed to interstitial fluids which provided a low resistance pathway away from the artery. These data suggest that the losses from perivascular dilution and clearance outweighed the losses from the lumen flow (Fig. 4.5). Tightly adhering perivascular release devices may have negated some of the difference in deposition. The resistance of heparin transport from the vessel wall to the lumen flow has been shown through mass transfer boundary layer analysis to be small relative to the resistance of traversing the arterial media.[105] The current results imply that the perivascular resistance to drug loss provided by extra-arterial capillaries is even smaller than the endovascular resistance provided by the mass transfer boundary layer. These arguments will be used to justify zero resistance boundary conditions in subsequent computational modeling of vascular drug distribution (Chap. 5).

4.4.3. Is There a Need to Wrap both the Device and Artery?

These experiments characterize the local administration of drug to the blood vessel wall, which is one of the determining principles of vascular pharmacokinetics. The potential loss of drug to extra-arterial capillaries has prompted some to advocate that perivascular drug delivery might be more efficient if the artery and release device are wrap-isolated with impermeable barriers.[138,158] These data show that inulin can still leak out of wrapped spaces, even after the ends were plugged (Fig. 4.3b). It is possible that the continuity of the artery through the plug and beyond support a continuous aqueous layer on the adventitial surface that provides a low resistance pathway for drug to escape from within the wrap. This leak was noted visually by administering Evan's Blue Dye in Poloxamer gel from within a wrap around the carotid and observing the diffusion along the arterial surface. Although more heparin was deposited in the carotid artery when wrapped, this increase was not statistically significant (Fig. 4.4). Likewise, the arterial wrap did not decrease deposition in distant structures. Thus, the wrap failed to completely eliminate extra-arterial capillary absorption. The rush to wrap arteries and release devices should be tempered, therefore, especially in light of evidence that wrapping arteries can impose deleterious ischemic and proliferative

injury.[159,160] Although the wrap did not increase deposited drug, it did slow the rate of drug release from the Poloxamer gel and would presumably extend the duration of elevated local arterial concentrations (Fig. 4.3).

4.5. Chapter Summary

Drug has been released into the perivascular space *in vivo* in an attempt to settle a long running debate as to how drug moves from local release devices to the blood vessel wall. These studies have shown that the overwhelming majority of drug leaves the perivascular space through the extra-arterial microcirculation, and yet little enters the vessel wall from the endovascular aspect. All of the small fraction of drug that enters the blood vessel wall arrives by direct diffusion from the perivascular space. The potential for drug to be lost to the lumen flow was found to be smaller than the loss to the extra-arterial capillaries. These experiments characterize the local administration and the movement of drug in the arterial environment, which is a fundamental component of vascular pharmacokinetics.

5. COMPUTATIONAL SIMULATIONS OF VASCULAR HEPARIN DEPOSITION AND DISTRIBUTION

5.1. Introduction

The preceding chapters described how all of the relevant vascular transport and binding parameters were measured in isolation. They also discussed mechanisms of drug administration, distribution and clearance to, through and from the arterial wall. All of these works have been incorporated into a series of mathematical pharmacokinetic models of heparin distribution. This chapter illustrates the derivation of these computational models and their utility in interpreting and designing local drug delivery systems. These simulations predict that heparin will be rapidly cleared from the arterial wall, implying that sustained modes of delivery will be needed to treat vascular disease with these and similar soluble compounds. The models have been validated by comparison to local drug delivery data from a novel endovascular hydrogel delivery system. As a consequence, the simulations added unanticipated insight into these data and the function of this drug delivery system. In general the pharmacokinetic models derived here have spatial resolution that far exceeds that of radiolabeled drug deposition studies, and demonstrate the kinetic movement of drug that could only be elucidated with countless animal experiments. In addition, these mathematical simulations distinguish soluble, reversibly bound and internalized drug, which helps discriminate between committed biologically inactive drug from potentially useful drug. These models are essential for the rational design of vascular pharmacotherapies.

5.2 General Model Construction

A series of generalized one-dimensional models of drug deposition and distribution across multi-layered tissues have been written in Matlab (Mathworks) using a forward-difference algorithm (Appendix 8.9). Each distinct tissue layer is divided into N consecutive elements each with a computational node at its center. The drug can be in one of three phases or compartments: soluble, bound (reversibly) and internalized (or irreversibly bound or metabolized), whose concentrations are defined per unit tissue volume and are considered homogeneous throughout

each element. For each step in time (Δt) the diffusive transport of the soluble compound into and out of each element is computed (Fig. 5.1a). The diffusive and convective flux of soluble drug (j'') is determined through Fick's first law:

$$j'' = Uc_s - D\frac{\partial c_s}{\partial x} = Uc_s - D\frac{\Delta c_s}{\Delta x} \tag{5.1}$$

where c_s is the concentration of soluble drug in an element, Δx is the internodal distance, D is the effective molecular diffusivity of the compound in the tissue layer, and U is the convective solute velocity. From a mass balance on an element, the rate of change of soluble drug is equivalent to the net vectorial flux of drug across each of its faces in a time interval (Δt):

$$\Delta x\frac{c_{s_{n,t+\Delta t}} - c_{s_{n,t}}}{\Delta t} = j''_{n-} - j''_{n+} = Uc_{s_{n-1,t}} + D\frac{c_{s_{n-1,t}} - c_{s_{n,t}}}{\Delta x} - Uc_{s_{n,t}} - D\frac{c_{s_{n,t}} - c_{s_{n+1,t}}}{\Delta x} \tag{5.2}$$

The subscript n denotes the computational element. Thus, the concentration of soluble drug in an element depends on its prior concentration and those of its neighbors:

$$c_{s_{n,t+\Delta t}} = c_{s_{n,t}} + \frac{D\Delta t}{\Delta x^2}\left(c_{s_{n+1,t}} + c_{s_{n-1,t}} - 2c_{s_{n,t}}\right) + \frac{U\Delta t}{\Delta x}\left(c_{s_{n-1,t}} - c_{s_{n,t}}\right) \tag{5.3}$$

Eq. 5.3 allows the soluble concentration of drug to be computed at each of the interior elements, 2 through N-1, in a tissue layer. The elements at the ends, 1 and N, require special boundary conditions that are specific for the particular application of the model.

5.2.1 Incorporation of Binding into Distribution Models

In between each step in time, after the new soluble concentrations are determined, the amount of soluble drug that binds and the amount of reversibly bound drug that dissociates is determined by invoking an assumption of local equilibrium within each element (Fig. 5.1a). The total noninternalized drug concentration (c_T) is equal to the old reversibly bound and the new soluble drug:[53]

$$c_{T_{n,t+\Delta t}} = c_{s_{n,t+\Delta t}} + c_{b_{n,t}} \tag{5.4}$$

The soluble and reversibly bound concentrations (c_b) are then redistributed based solely upon the newly computed total noninternalized concentration within each element and the density of specific and nonspecific binding sites (B_T), the fractional volume in which drug can distribute (ε') and the dissociation constant of the average binding site (K', Eq. 3.15):

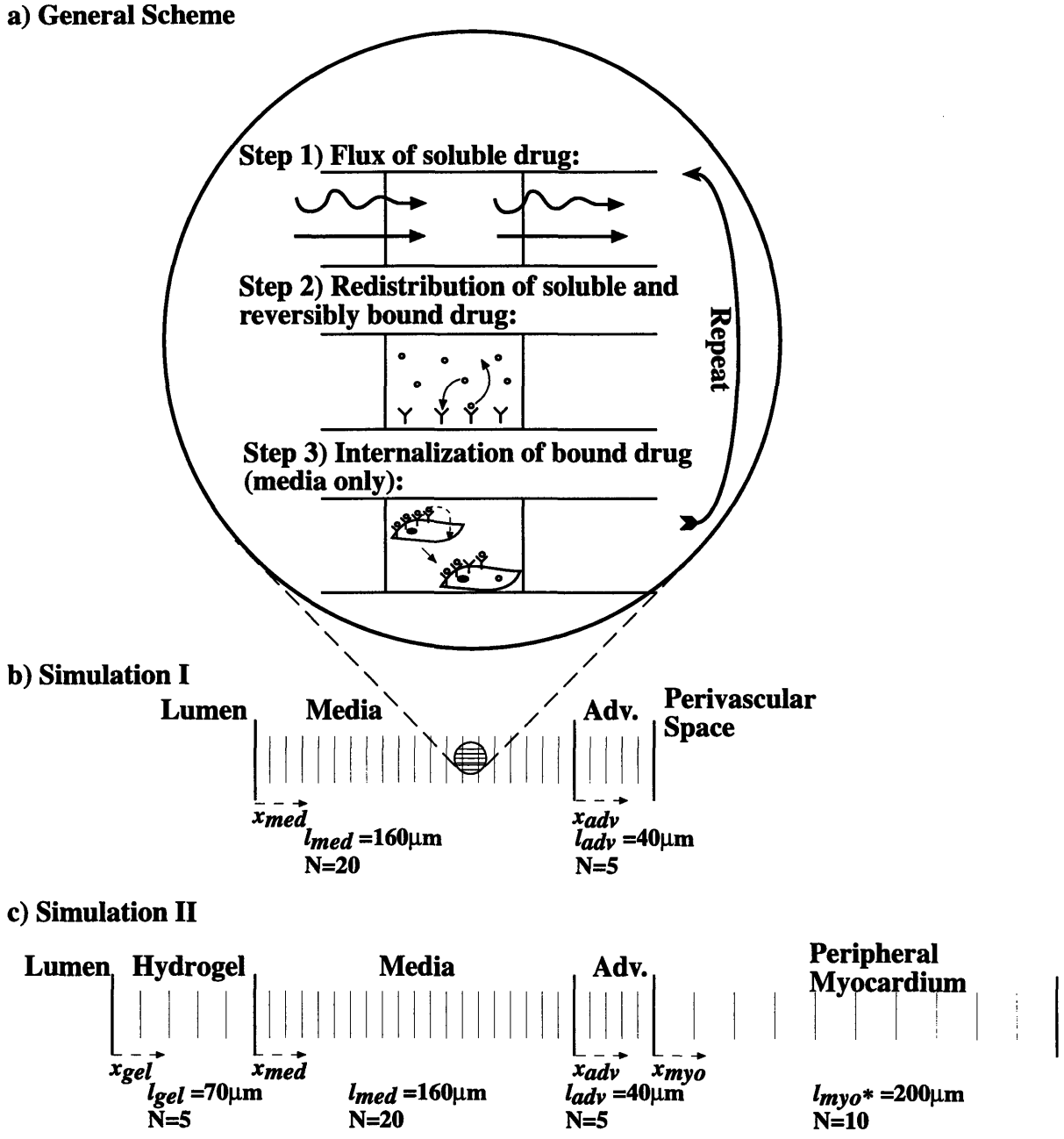

Figure 5.1. Outline of the general scheme used in the model of vascular drug deposition and distribution (a) and one dimensional computational grid used in the simulations of arteries uniformly loaded with heparin (b, simulation I) and of the endovascular hydrogel drug delivery system to the coronary artery (c, simulation II).

$$\hat{c}_{s_{n,t+\Delta t}} = \frac{c_{T_{n,t+\Delta t}} - B_T - K'\varepsilon' + \sqrt{\left(c_{T_{n,t+\Delta t}} - B_T - K'\varepsilon'\right)^2 + 4c_{T_{n,t+\Delta t}} K'\varepsilon'}}{2} \tag{5.5}$$

The ^ marker on the soluble concentration denotes that drug has already been redistributed between the soluble and the reversibly bound components according to local equilibrium. The reversibly bound fraction in each element can now be computed as the total noninternalized concentration less the redistributed soluble concentration defined by Eq. 5.5. Thus, static binding constants are used to incorporate the dynamic effects of binding and dissociation on the deposition and distribution of compounds.

5.2.2. Justification of Local Equilibrium Assumption

The complete partial differential equation of soluble drug transport that allows for drug binding is as follows:

$$\frac{\partial c_s}{\partial t} = -Uc_s + D\frac{\partial^2 c_s}{\partial x^2} - k_{on}c_s B_f + k_{off}c_b \tag{5.6}$$

where k_{on} is the rate of heparin association to the average binding site, k_{off} is the rate of heparin dissociation, and B_f is the molar density of free binding sites. By assuming quasi-steady transport and most binding sites to be free, the local equilibrium assumption can be justified by scaling the diffusive and associative binding terms, thus defining the Damkohler number:

$$Da = \frac{k_{on}l^2 B_f}{D} \tag{5.7}$$

Because heparin binds to many potential binding sites in the heterogeneous arterial wall,[53,149] and the rates of association potentially vary among the sites, a conservatively low estimate of k_{on} can be estimated from structurally homologous molecules. k_{on} for heparan sulfate binding to basic fibroblast growth factor (bFGF) is 0.9×10^8 min^{-1} M^{-1}.[143] Note that heparin and heparan sulfate are similar in composition, and that the heparin binding domains on many proteins are conserved.[161] Therefore, the above k_{on} may be applicable as a lower bound since it reflects the mechanical coupling to complicated structures and much of the binding in arterial tissues is probably loosely charged associations that should act even faster. The Damkohler number in

arterial media will be about 10 for length scales (l) about 4 μm, indicating that the rate of binding will exceed the rate of diffusive transport of soluble drug over this distance. Thus, equilibrium can be assumed at each instant for elements of this length scale or longer. Note that the rate of association, however, is also proportional to the number of free binding sites. As these sites saturate, the Damkohler number falls, and the local equilibrium assumption may require reevaluation. Because k_{on} and k_{off} are not quantified in the heterogeneous arterial tissues, Eq. 5.6 can not be solved explicitly. Rather, the forward-difference scheme outlined above, including the local equilibrium assumption, was used to incorporate the effects of binding and dissociation (Fig. 5.1a). To describe the following simulations in the most concise notation, the governing equations and boundary conditions of soluble drug transport were written in differential notation. Note that although these equations do not explicitly include such terms, drug binding and internalization were determined after each time step, the former according to local equilibrium and the latter as described below (Fig. 5.1a).

5.2.3. Estimation of the Rate Of Heparin Internalization

Approximately 10% of the heparin bound to smooth muscle cells in culture has been shown to be internalized with a $t^{1/2}$ of 15 to 20 minutes and an additional 10% of the bound heparin is endocytosed at a much slower, but unquantified rate.[145] In these simulations, 5% of the bound drug in arterial media was assumed to be on the smooth muscle cell surface, 20% of which was assumed internalized with a $t^{1/2}$ of 15 minutes. Internalization of heparin in the adventitia was neglected since the cell density is much lower than in the media and the kinetics of heparin internalization into fibroblasts and adipocytes are unknown. Internalized heparin has been shown to be metabolized to smaller fragments,[162] and was therefore subtracted from the reversibly bound concentration, defined by Eq. 5.6, after each time step (Fig. 5.1a).

5.3. Applications of the Model

The generalized model presented above has been applied to the transarterial distribution and deposition of heparin.

5.3.1. Simulation I. Artery Uniformly Loaded With Heparin

The deposition and distribution of heparin throughout the media (*med*) and adventitia (*adv*) was simulated using the following differential form of Eq. 5.3 and the above forward-difference scheme (Fig. 5.1a):

$$\frac{\partial c_{i,s}}{\partial t} = -U_i c_{i,s} + D_i \frac{\partial^2 c_{i,s}}{\partial x_i^2}; \qquad 0 \le x_i \le l_i \text{ where } i = med \text{ and } adv \tag{5.8}$$

The initial soluble concentration was assumed to be uniform throughout the media and adventitia:

$$c_{i,s}(x_i) = c_{init}; \qquad t=0 \tag{5.9}$$

The intimal boundary condition was derived from a mass balance across the endothelial monolayer:[99,102]

$$U_{med} c_{med,s} - D_{med} \frac{\partial c_{med,s}}{\partial x_{med}} = \frac{1}{R_{end}} \left(C_{plasma} - \frac{c_{med,s}}{\varepsilon'_{med}} \right); \qquad x_{med} = 0 \tag{5.10}$$

The fluxes and the soluble concentrations in the available spaces was considered continuous across the medial/adventitial interface:[95]

$$U_{med} c_{med,s} - D_{med} \frac{\partial c_{med,s}}{\partial x_{med}} = U_{adv} c_{adv,s} - D_{adv} \frac{\partial c_{adv,s}}{\partial x_{adv}}; \qquad x_{med} = l_{med},\ x_{adv} = 0 \tag{5.11}$$

$$\frac{c_{med,s}}{\varepsilon'_{med}} = \frac{c_{adv,s}}{\varepsilon'_{adv}}; \qquad x_{med} = l_{med},\ x_{adv} = 0 \tag{5.12}$$

A zero resistance boundary condition was assumed at the outer edge of the adventitia as suggested by earlier data (Sec. 4.4.3):

$$c_{med,s} = \varepsilon'_{med} C_{pv}; \qquad x_{adv} = l_{adv} \tag{5.13}$$

Recall that after each time step the soluble and reversibly bound drug were redistributed according to local equilibrium and the amount internalized by medial cells determined (Fig. 5.1a). These simulations were carried out with an initial heparin loading (c_{init}) of 1 μM, and dimensions representative of human coronary arteries, including a 160-μm-thick media and a 40-μm-thick

adventitia (simulation Ia, Table 5.1; Fig. 5.1b). To investigate the effects of drug saturation of the binding sites on the clearance, the simulation was repeated with an initial loading (c_{init}) of 1 mM (simulation Ib). To investigate the effects of arterial thickness and to compare the simulations to heparin deposition data collected in our laboratory using rabbit iliac arteries, the simulations were repeated with half the medial (80 μm) and adventitial (20 μm) thicknesses used above (simulation Ic). The diffusion and binding properties of heparin in arterial media and adventitia have been measured in Chapters 2 and 3 and are summarized in Table 5.2. The convective solute velocity was calculated from the hydraulic velocity (Eq. 2.13) and on the convective hindrance of the arterial media as suggested by pore theory (Section 2.3.3). As an approximation, the convective hindrance in the adventitia is assumed to be the same as in the media and therefore the solute velocities are the same in these layers. The transendothelial resistance to heparin (R_{end}) has been measured in an *in vitro* perfusion preparation to be 2.5 s/μm (Sec. 2.4.1). The boundary layer resistance to heparin transport in the lumen flow has been shown to be negligible compared to the diffusive resistance of the endothelium or media.[105] The concentration of heparin in plasma (c_{plasma}) and in the perivascular space (c_{pv}) were considered to be zero throughout this simulation.[95,99]

Table 5.1. Summary of Simulations

Simulation I. Artery Uniformly Loaded With Heparin

	Medial Thickness (μm)	Adventitial Thickness (μm)	Initial Loading (c_{init})
Simulation Ia	160	40	1 μM
Simulation Ib	160	40	1 mM
Simulation Ic	80	20	1 μM

Simulation II. Endovascular Hydrogel Heparin Delivery to Porcine Coronaries

	Endovascular hydrogel?	Initial Heparin Concentration in Endovascular Hydrogel	Myocardium Loaded Initially with Intracoronary Bolus?
Simulation IIa	Y	0.33 mg/ml	Y
Simulation IIb	Y	0	Y
Simulation IIc	N	-	Y

Table 5.2. Physical constants for heparin in the hydrogel and arterial tissues.

	Hydrogel	Media	Adventitia	Myocardium
Effective Diffusivity ($\mu m^2/s$)	24	7.7	12	7.7
Fractional Space	1	0.61	0.85	0.61
Binding Site Density (μM)	-	2.5	0.0022	2.5
Average Dissociation Constant (μM)	-	5.0	0.0081	5.0

5.3.2. Simulation II. Endovascular Hydrogel Heparin Delivery

In a series of *in vivo* experiments described elsewhere, a photopolymerizable hydrogel drug delivery system was used to deliver heparin to the endovascular aspect of the left anterior descending (LAD) branch of porcine coronary arteries.[163] A bolus of heparin mixed with hydrogel prepolymer was delivered to balloon denuded, isolated segments of artery through a double balloon catheter that was described earlier (Sec. 4.2.4.2) The hydrogel was then photopolymerized *in situ* resulting in an approximately 70-μm-thick interfacial sheet formed on the intimal surface. Approximately 1% of the delivered volume of drug and hydrogel prepolymer were incorporated into this endovascular sheet. The remaining drug and hydrogel prepolymer flowed downstream, some deposited in the myocardium and the rest entered the systemic circulation. In separate experiments, "ungelled control" animals received the same intracoronary bolus of heparin and hydrogel prepolymer without photopolymerization and subsequent endovascular sheet formation.

The heparin deposition in the LAD 48 hours after photopolymerization was greater than that observed in the corresponding ungelled control. This implied that the presence of a formed 70-μm-thick endovascular hydrogel led to increased deposition in the LAD, presumably because it was able to provide a sustained release of drug over this duration. Subsequent to these findings, the *in vitro* release kinetics (*See* Sec. 5.3.2.2) showed that a thicker sheet of the same hydrogel releases its contents entirely in less than a half hour (Fig. 5.2). Thus, it seemed unlikely that the endovascular hydrogel was releasing heparin *in vivo* at 48 hours and it must therefore have increased deposition over controls by some other mechanism.

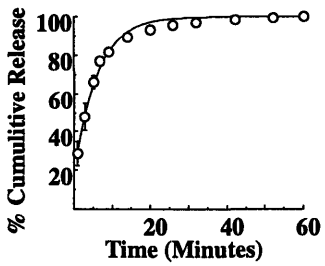

Figure 5.2. *In vitro* bi-directional release of heparin from a uniformly loaded 300-μm-thick hydrogel sheet(average ± SEM, n=3). A numerical curvefit of this data to a theoretical release profile for this geometry (Eq. 5.28) determined the effective diffusivity of heparin in the hydrogel to be 24 $\mu m^2/s$ (Solid line).

As a consequence of the endovascular hydrogel deployment process, following photopolymerization the remaining 99% of the hydrogel prepolymer and heparin that was not incorporated into the endovascular sheet was washed into the myocardium and systemic circulation. At every time of sacrifice after endovascular hydrogel deployment, the deposition of heparin in the myocardium and in the LAD were similar. This led to the hypothesis that the LAD and myocardium were continuously exchanging drug and that the endovascular hydrogel, in addition to delivering heparin to the arterial wall, also served as a barrier to limit the loss of drug diffusing from the myocardium. This hypothesis was tested with computational simulations that assessed the extent to which the endovascular hydrogel behaved as a drug delivery device or alternatively as a diffusion barrier. Because the myocardium has many sources of perfusion, the heparin clearance was assumed independent of events in the LAD. A single exponential was fit to the myocardial deposition data obtained during these porcine coronary experiments (R = 0.62):[163]

(5.14) $$c_{myo}(t) = 0.17\mu M \cdot e^{-t/40.5hrs}$$

The concentration within the peripheral myocardium was allowed to vary to a penetration depth (l_{myo*}) of 200 μm. This length scale roughly corresponds to half the distance into the myocardium in which histologic sections showed other smaller blood vessels, which were considered independent sources of clearance. Beyond this depth the myocardium was considered well mixed and followed Eq. 5.14. Although the transport and binding of heparin in epicardium and myocardium have not been characterized, as a first order approximation the peripheral myocardium was assumed homogeneous and to resemble arterial media.

The physical constants used in this model are summarized in Table 5.2. The soluble concentration of drug throughout the geometry was determined by applying Eq. 5.8 to each of the following four layers: the endovascular hydrogel (*gel*), arterial media (*med*), adventitia (*adv*), and peripheral myocardium (*myo*). Note that because the hydraulic conductivities of the endovascular hydrogel and myocardium are unknown, the solute convective velocities (U) in Simulation II were assumed to be zero. Initially, the hydrogel was considered uniformly loaded, and the artery and peripheral myocardium were devoid of drug:

(5.15) $$c_{gel}\left(x_{gel}\right) = c_{init}; \qquad t = 0$$

(5.16) $$c_{i,s}\left(x_i\right) = 0; \qquad t = 0 \quad \text{where } i = \textit{med, adv,} \text{ and } \textit{myo}$$

The boundary layer resistance to heparin transport in the arterial lumen has been shown to be negligible and therefore a zero resistance boundary condition is applied:[105]

(5.17) $$c_{gel} = \varepsilon'_{gel} C_{plasma}; \qquad x_{gel} = 0$$

Note that as the endovascular hydrogel deployment requires endothelial denudation, the diffusive resistance imposed by the endothelium was removed from these simulations. Although studies have shown that the fractional space for heparin can increase slightly following balloon denudation,[53] this parameter was not adjusted in these simulations. Again, the fluxes and the soluble concentrations in the available spaces must be continuous across each interface:[95]

(5.18) $$D_{gel}\frac{\partial c_{gel}}{\partial x_{gel}} = D_{med}\frac{\partial c_{med,s}}{\partial x_{med}}; \qquad x_{gel} = l_{gel},\ x_{med} = 0$$

(5.19) $$\frac{c_{gel,s}}{\varepsilon'_{gel}} = \frac{c_{med,s}}{\varepsilon'_{med}}; \qquad x_{gel} = l_{gel},\ x_{med} = 0$$

(5.20) $$D_{med}\frac{\partial c_{med,s}}{\partial x_{med}} = D_{adv}\frac{\partial c_{adv,s}}{\partial x_{adv}}; \qquad x_{med} = l_{med},\ x_{adv} = 0$$

(5.21) $$\frac{c_{med,s}}{\varepsilon'_{med}} = \frac{c_{adv,s}}{\varepsilon'_{adv}}; \qquad x_{med} = l_{med},\ x_{adv} = 0$$

(5.22) $$D_{adv}\frac{\partial c_{adv,s}}{\partial x_{adv}} = D_{myo}\frac{\partial c_{myo,s}}{\partial x_{myo}}; \qquad x_{adv} = l_{adv},\ x_{myo} = 0$$

(5.23) $$\frac{c_{adv,s}}{\varepsilon'_{adv}} = \frac{c_{myo,s}}{\varepsilon'_{myo}}; \qquad x_{adv} = l_{adv},\ x_{myo} = 0$$

Again, the concentration within the bulk of the myocardium is assumed to follow Eq. 5.14:

(5.24) $c_{myo,s} = c_{myo}(t); \qquad x_{myo} = l_{myo*}$

Recall that after each time step in the forward-difference scheme, the soluble and reversibly bound drug were redistributed according to local equilibrium and the amount internalized by medial cells determined (Fig. 5.1a). The plasma concentration was assumed to be zero and the initial heparin concentration in the endovascular hydrogel (c_{init}) was 0.33 mg/ml, as was used in the corresponding *in vivo* studies.[163] The thickness of each arterial layer and the number of computational elements to which each was divided into are shown (Fig. 5.1c).

5.3.2.1. Permutations on the Porcine Coronary Simulations

The simulations were also carried out with the following permutations (Table 5.1). Simulation IIa models the heparin delivery experiments performed on porcine LADs, where heparin was mixed in with hydrogel prepolymer, a 70-μm-thick endovascular hydrogel was formed, and the myocardium was loaded from the intracoronary bolus. In simulation IIb the myocardium was assumed to be loaded by the same initial intracoronary bolus of drug and hydrogel prepolymer, however, the endovascular hydrogel formed initially contained no drug. In this simulation the following initial condition replaced Eq. 5.15:

(5.25) $c_{gel}(x_{gel}) = 0; \qquad t = 0$

This represents a case where an unloaded endovascular hydrogel was formed and then heparin was administered to the myocardium by an initial intracoronary bolus. In simulation IIc the myocardium was assumed loaded with the same initial intracoronary bolus of drug and hydrogel prepolymer, but there was no endovascular hydrogel formation at all. In this simulation the following boundary condition replace Eqs. 5.17-19:

(5.26) $c_{med,s} = \varepsilon'_{med} C_{plasma}; \qquad x_{med} = 0$

This simulated the ungelled control experiments performed *in vivo*, where the heparin and hydrogel prepolymer were introduced to the LAD but were not photopolymerized.

5.3.2.2 *In Vitro* Release Kinetics

Flat 300-μm-thick sheets were formed between two glass slides from the same hydrogel prepolymer containing an identical concentration of ^{3}H-heparin (NEN Dupont) as in the porcine coronary experiments. These sheets were placed in 2 ml of phosphate buffered saline at 37°C, which was replaced periodically. The *in vitro* release data (Fig. 5.2) were used to estimate the effective diffusivity of ^{3}H-heparin within the hydrogel. The concentration of drug at each face was considered zero, so that the following equation describes the dynamic concentration profiles:[164]

$$c(x,t) = \frac{4c_{init}}{\pi} \sum_{j=1,3,5...}^{\infty} \frac{e^{-D_{gel}t[j\pi/l]^2}}{j} \sin\left(\frac{j\pi x}{l}\right) \tag{5.27}$$

where x is the spatial coordinate across the thickness (l). Integration across the thickness resulted in a relation that was used to numerically curve-fit (TableCurve 2D, Jandel Scientific) the *in vitro* release data:

$$\%cumulative\ release = 1 - \frac{\bar{c}(t)}{c_{init}} = 1 - \frac{8}{\pi^2} \sum_{j=1,3,5...}^{\infty} \frac{e^{-D_{gel}t[j\pi/l]^2}}{j^2} \tag{5.28}$$

The effective diffusivity of heparin in the hydrogel was thus determined to be 24 μm^2/s. Note that this method of measuring the effective diffusivity of heparin incorporates potential binding and therefore only the total concentration in the hydrogel was computed in the simulations.

5.4. Findings from the Simulations

5.4.1. Simulation I. Artery Uniformly Loaded With Heparin

The predicted heparin concentration profiles for the case of a uniformly loaded arterial cross section are shown (Fig. 5.3). At 4 minutes there was significant loss of drug at the periphery of the artery. At 15 minutes the average medial concentration was about 25% and by one hour the concentration was about 2% of the original concentration. At four hours the heparin in the blood vessel wall was 4 orders of magnitude lower than what it had been initially, and was entirely in the internalized fraction. The clearance of heparin from the blood vessel wall was even more rapid for higher initial loadings (Fig. 5.3b) and for thinner vessels (Fig. 5.3c). These results strongly suggest that soluble drugs such as heparin must be continuously supplied to the vessel wall in order to maintain therapeutic levels.

5.4.2. Simulation II. Endovascular Hydrogel Heparin Delivery

Simulated soluble and total transmural concentration profiles following endovascular hydrogel heparin delivery are shown at 3 minutes, 10 minutes, and 3 hours (Fig. 5.4). Within 3 minutes, much of the heparin initially in the endovascular hydrogel was lost to the lumen flow, and the peak concentration was 14% of the initial hydrogel concentration located at the interface with the media. At 10 minutes the peak concentration was in the media and was about 4% of the initial hydrogel concentration. There were gradients from the media both toward the myocardium as well as the lumen, implying that at this early time, drug released from the media was loading the adventitia and myocardium. A concentration gradient was also evident from the myocardium towards the adventitia, indicating that drug entered the artery from the external aspect. At 3 hours the only existing concentration gradients came from the myocardium, and the peak medial concentration was about 0.6% of the initial hydrogel concentration. Note that all of the drug in the adventitia was in the soluble phase indicating that these binding sites were saturated. Conversely, the binding sites in the media and myocardium did not appear to be filled.

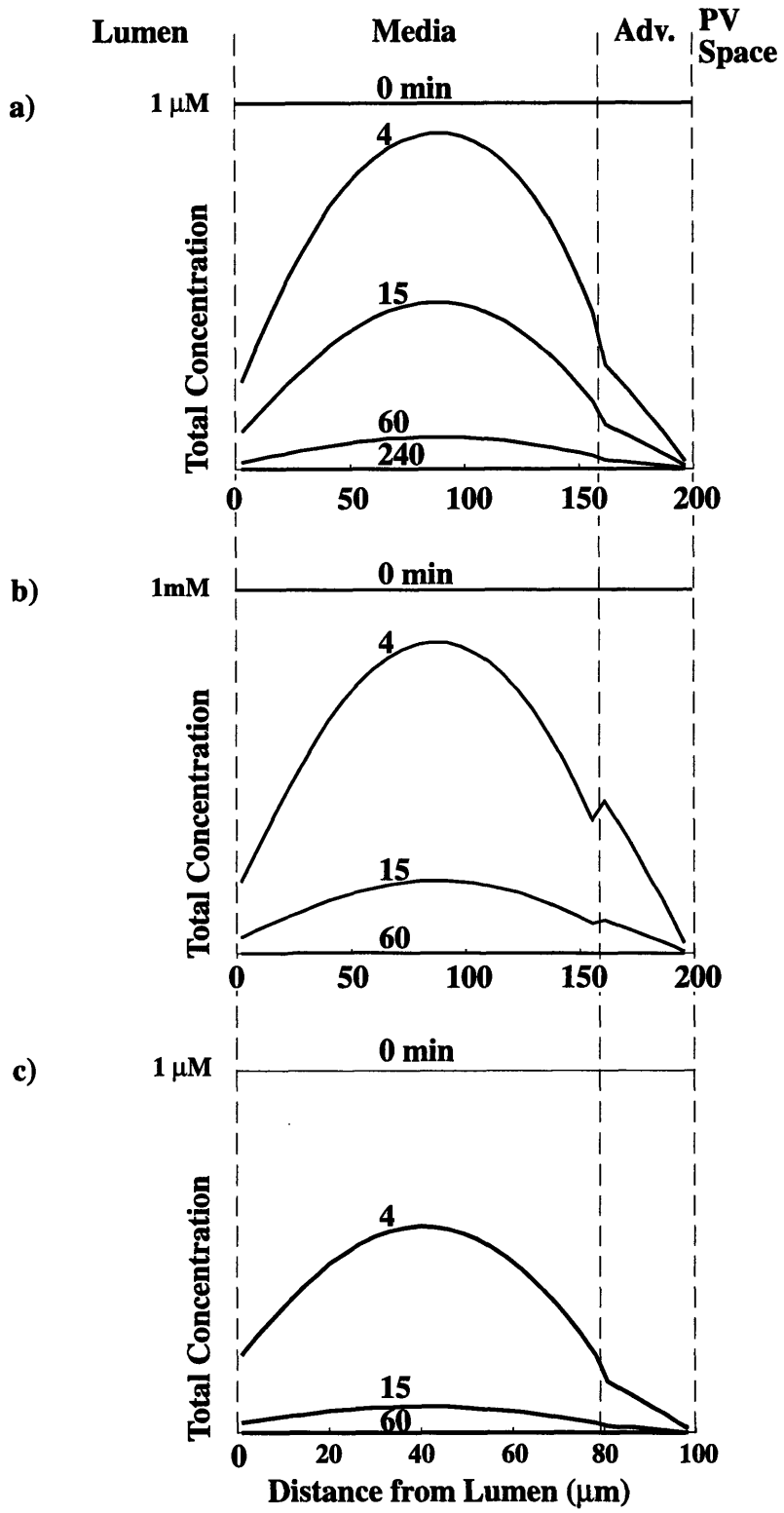

Figure 5.3. Predicted heparin concentration profiles for a uniformly loaded artery at 0, 4, 15, 60, and 240 minutes showing the effects of arterial thickness and initial drug loading. The ordinate is the total concentration of drug and the abscissa is the distance from the lumen. Dashed lines denote the boundaries of each tissue layer. a) Simulation Ia: medial thickness of 160 μm, adventitial thickness of 40 μm, and initial concentration of 1 μM. b) Simulation Ib: medial thickness of 160 μm, adventitial thickness of 40 μm, and initial concentration of 1 mM. c) Simulation Ic: medial thickness of 80 μm, adventitial thickness of 20 μm, and initial concentration of 1 μM.

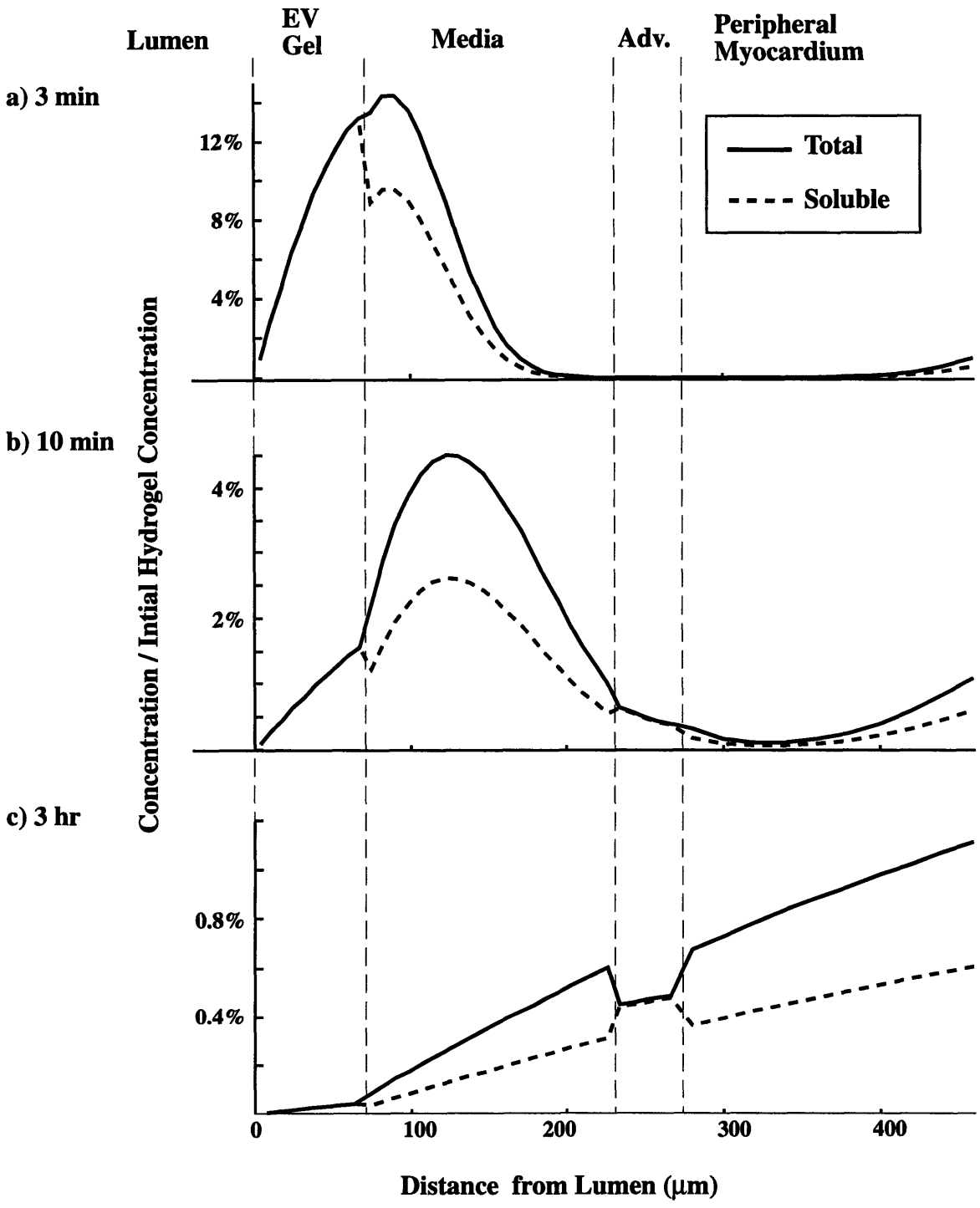

Figure 5.4. Predicted total and soluble transmural concentration profiles from endovascular hydrogel heparin delivery to porcine coronary arteries (simulation IIa). Heparin profiles across the endovascular hydrogel, media, adventitia, and peripheral myocardium are shown at a) 3 minutes, b) 10 minutes and c) 3 hours. Concentrations are expressed as a percentage of the initial concentration of the endovascular hydrogel.

In addition to the above simulation where the endovascular hydrogel initially was loaded with heparin (simulation IIa), simulations were also carried out in which the endovascular hydrogel initially contained no heparin (simulation IIb), and alternatively when there was no endovascular hydrogel formed (simulation IIc). The average concentration of heparin in the arterial media from all three of these simulations are shown normalized by the initial heparin concentration in the hydrogel (Fig. 5.5). In all of these permutations the myocardium was considered to be initially loaded to the same level and cleared at the same rate, according to Eq. 5.14. Note that the average heparin concentrations include soluble, reversibly bound and internalized drug. Including drug initially in the endovascular hydrogel resulted in the highest average medial concentration at all times, and having no endovascular hydrogel resulted in the lowest average medial concentration.

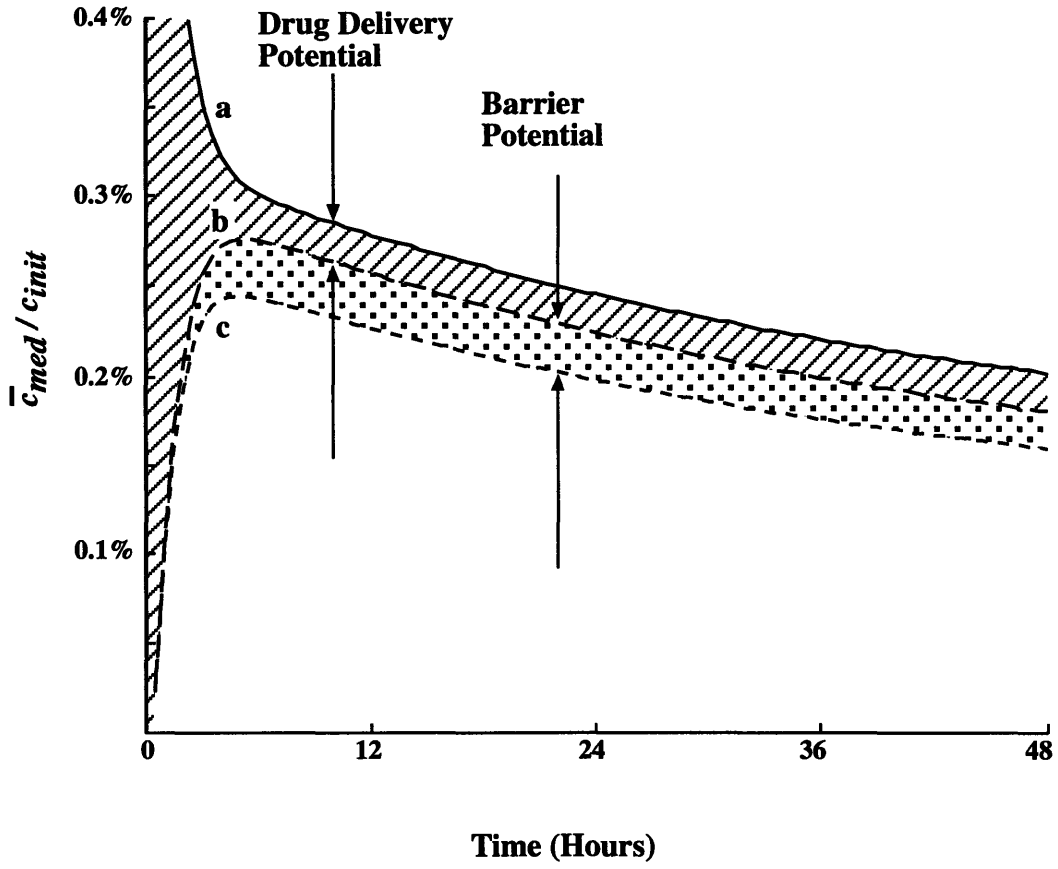

Figure 5.5. Simulated average medial total (soluble, reversibly bound and internalized) heparin concentration following endovascular hydrogel delivery to porcine coronaries as a function of time, expressed as a percentage of the initial concentration in the hydrogel (if formed and initially loaded with heparin). Simulations are performed with a) heparin delivered in the endovascular hydrogel, b) no heparin initially in the endovascular hydrogel, and c) no endovascular hydrogel formed. The drug delivery potential (cross-hatched) of the endovascular hydrogel is defined as the difference between tracings (a) and (b). The barrier potential (stippled) is defined as the difference between tracings (b) and (c).

5.5. Discussion

More often than not, proposed pharmacologic therapies that show promise *in vitro* do not succeed in animals or humans. It is just as often not clear whether this arises from biologic or pharmacologic etiologies. In other words, whether the drug is impotent in the disease is a question of whether drug deposition and distribution within tissues is ultimately inadequate. Detailed quantitative pharmacokinetic analyses are required to differentiate between these failure modes, and future study designs must include such analyses to ensure that costly animal experiments and clinical trials are not doomed by limited deposition and distribution of drug. These issues are especially acute with local modes of vascular therapy, which by its nature imparts large concentration gradients across tissues with potentially chaotic kinetics. Local delivery has been studied to date phenomenologically, mostly through radiolabeled drug deposition studies. In this chapter, generalized models of drug deposition and distribution were applied to local heparin delivery data using quantitative analyses of the transport and binding within arterial tissues (Chapters 2 - 4). These models have spatial resolution that far exceed that of radiolabeled drug deposition studies, and they demonstrate the kinetic movement of drug that could only be elucidated with tremendous numbers of animal experiments. In addition, these mathematical simulations distinguish soluble, reversibly bound and internalized drug, which helps discriminate between committed biologically inactive drug from potentially useful drug. Such distinctions could never be determined in drug deposition experiments *in vivo*. This modeling approach describes the net effects of diffusive and convective transport, binding, dissociation and cellular internalization. Many physiologic, pathologic, and therapeutic processes that involve intracellular signaling through soluble mediators are dependent upon and are potentially dampened by these physical interactions. Similar models to the one described here, with the incorporation of appropriate transport and binding properties, can be used to augment biological studies of these processes.

5.5.1. Simulation I. Artery Uniformly Loaded With Heparin

The predicted heparin transmural concentration profiles for the case of a uniformly loaded artery (simulation Ia) show extremely rapid clearance (Fig. 5.3), as a result of the relatively high diffusivity and the weakness of the overall binding. Increasing the initial loading (Fig. 5.3b, *simulation Ib*) has the effect of filling more binding sites, forcing a greater fraction of drug into the soluble phase, which results in even faster clearance. Simulations were performed on arterial thicknesses representative of human coronary (200 μm) and rabbit iliac arteries (100 μm). The clearance was much more rapid for thinner vessels (Fig. 5.3c, *simulation Ic*) because the diffusive resistance of the artery is proportional to its thickness (Sec. 2.3.1). This rapid clearance has been noted with other compounds delivered from porous balloon catheters.[23,165] The rapid loss of drug from the blood vessel wall bodes poorly for the clinical application of soluble compounds such as heparin from catheter-based bolus delivery systems. No matter how well an endovascular catheter loads the arterial wall, drug will rapidly diffuse back into the lumen and to the extravascular microcirculation. This implies that soluble compounds such as heparin must be deployed from locally implanted continuous-release systems in order to sustain adequate levels of drug to treat vascular diseases.

These simulations predict that a small percentage ($< 0.01\%$) of drug initially in the artery is internalized before it clears, implying that this fraction may be detectable following bolus delivery if the infusion concentrations are very high. This early internalization helps explain how some have observed drug within the arterial wall days after bolus endovascular delivery.[46] Unfortunately, experimental studies using fluorescent tracers are inherently unquantitative due to arterial autofluorescence and limitations in cryo-sectioning.

5.5.2. Simulation II. Endovascular Hydrogel Heparin Delivery

In the porcine coronary experiments, the deposition was greater when the hydrogel prepolymer was photopolymerized than when it was not, indicating that the endovascular sheet delivered drug. Simulations of both of these scenarios and an intermediate condition where an endovascular

hydrogel was formed but initially devoid of drug showed that this system influences arterial drug concentration through more subtle mechanisms.

The difference in average medial concentration when heparin was initially incorporated into the endovascular hydrogel (simulation IIa) from when the hydrogel initially contained no drug (simulation IIb) was considered to be the drug delivery potential (Fig. 5.5, *cross-hatched*). The presence of the initially unloaded endovascular hydrogel (simulation IIb) caused a higher average medial concentration than when the endovascular hydrogel was not formed (simulation IIc). This difference was considered to be the barrier potential of the endovascular hydrogel (Fig. 5.5, *stippled)*, as it apparently slowed the loss of drug from the myocardium to the lumen flow. The average medial *noninternalized* (soluble and reversibly bound) concentrations are shown for these three simulations (Fig. 5.6). After the first few hours the initial inclusion of heparin into the endovascular hydrogel did not lead to any more medial noninternalized drug than when the endovascular hydrogel initially contained no drug. Thus, with respect to noninternalized heparin, the drug delivery potential rapidly falls to zero. The presence of the endovascular hydrogel, however, still leads to more medial noninternalized drug then when it was not formed, and thus it still behaves as a barrier for noninternalized drug that diffuses from the myocardium. Appreciation of these important functions *in vivo* would require countless animal experiments with many endpoints and controls.

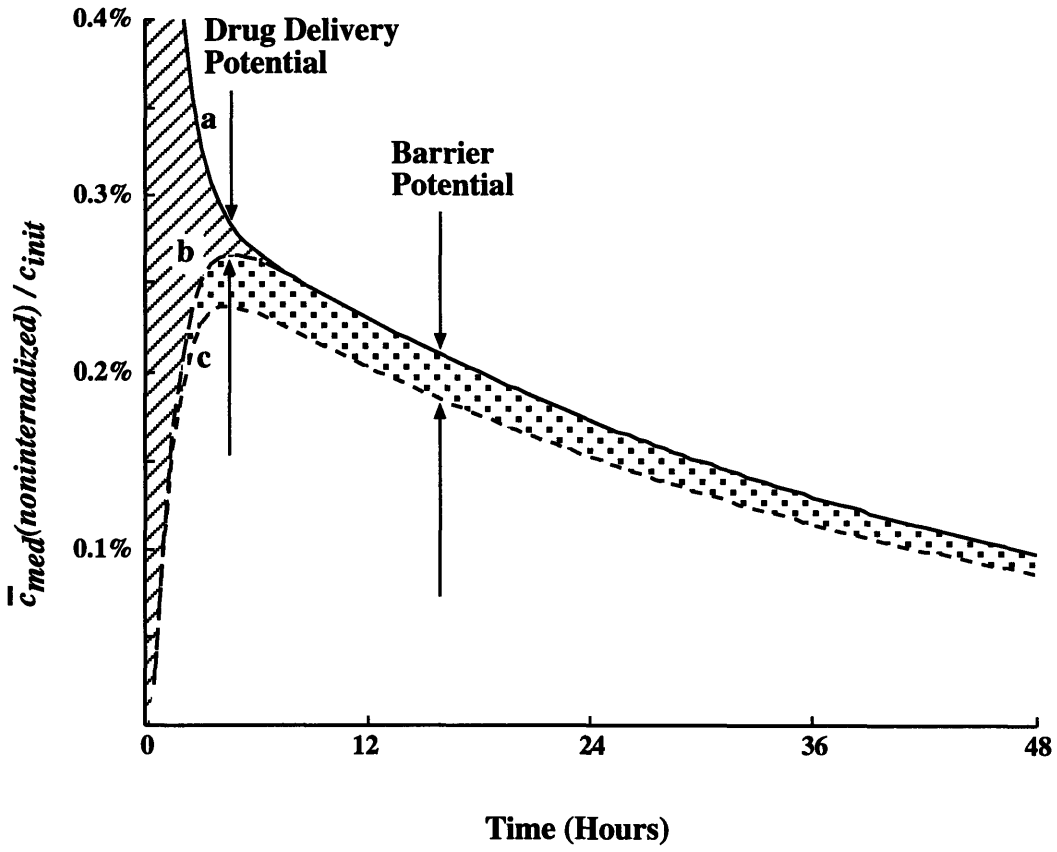

Figure 5.6. Simulated average medial noninternalized (soluble and reversibly bound) heparin concentration (soluble and bound) following endovascular hydrogel delivery to porcine coronaries as a function of time, expressed as a percentage of the initial concentration in the hydrogel (if formed and initially loaded with heparin). Simulations are performed with a) heparin delivered in the endovascular hydrogel, b) no heparin initially in the endovascular hydrogel, and c) no endovascular hydrogel formed. The drug delivery and barrier potentials are defined as in the caption of Figure 5.5.

5.5.3. Empirical Verification

The simulations of the endovascular hydrogel delivery system to porcine LADs, and the model in general, were verified by comparing the predicted average medial concentrations to the deposition measured experimentally.[163] The experimental deposition at 4 hours, 48 hours and 6 days is compared to both the predicted (simulation IIa) average medial noninternalized and total concentrations (Fig. 5.7). For all times, the experimental deposition was below the predicted total and above the noninternalized concentration. As time progresses these discrepancies grow. A possible explanation for this trend is that either the rate of cellular internalization or the fraction of total binding sites residing on cell surfaces were over estimated in the model. Another is that some of the internalized drug may be eliminated from the cells and artery, possibly as metabolites.[162]

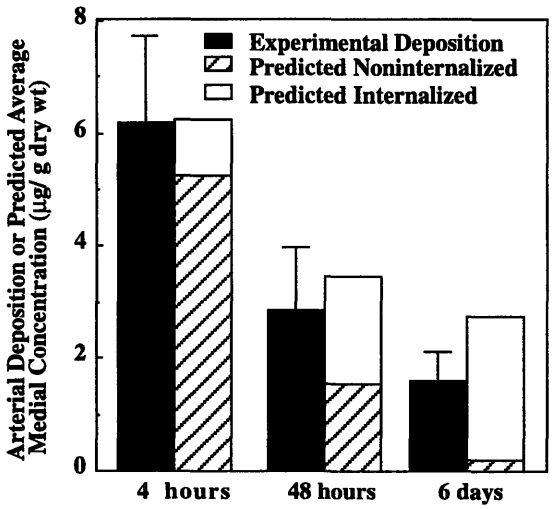

Figure 5.7. Comparison of model predictions (simulation IIa) of average medial concentrations following endovascular hydrogel heparin delivery to experimental deposition in porcine coronaries at 4 hours, 48 hours, and 6 days. Internalized concentrations (open) are superimposed on noninternalized concentrations (cross-hatched). Computational predictions were converted to deposition per dry tissue mass by assuming a wet:dry mass ratio of 5. Experimental heparin deposition (closed) from is the average ± SD.[163]

5.5.4. Advantages of Augmenting Experiments with Simulations

These simulations discriminate soluble, bound, and internalized drug; an impossible feat to perform experimentally *in vivo*. These distinctions can lead to markedly different interpretations of deposition data. For example, examination of the total amount of drug indicates that the

endovascular hydrogel drug delivery system indeed had drug delivery potential for all times (Fig. 5.5), while examination of the noninternalized fraction showed that there is no drug delivery potential past the first few hours (Fig. 5.6). The goal of a controlled-release drug delivery system is to continually provide *new* drug, and these simulations suggest that the endovascular hydrogel delivery system used in the porcine LAD experiments did not do so after a few hours. Thus, some of the drug found in the LAD *in vivo* after a few days must have been internalized earlier within cells. This fraction of drug is committed to the cell it is internalized within and may not be available to exert a biologic effect. In fact, one potential mechanism for heparin's antiproliferative effects is that it binds and inactivates extracellular mitogenic stimuli.[166,167] *In vivo* drug deposition experiments almost universally utilize radiolabeled drug, and unfortunately this assay determines the fate of the label and not that of the drug. Of a radiolabel signal observed in a tissue, it is unknown how much is extracellular viable drug and how much represents internalized, committed drug or metabolites. The estimates of heparin internalization in these models provides a valuable feel for the elimination of biologically potent drug and the persistence of misleading radiolabel signal.

The aforementioned traditional radiolabeled drug deposition experiments lack spatial resolution. The assays employed in vascular pharmacokinetic studies almost universally consist of removing the entire artery at sequential sacrifice times and quantifying deposition in the entire organ. In such experiments, there is no means to discriminate deposition in the media or adventitia. Since vascular pharmacotherapies target medial smooth muscle cells, it is of critical importance to resolve the concentration gradients across the artery imposed by local delivery strategies. These computational simulations can quantify transmural concentration gradients and can assess whether drug reaches target tissues (Fig. 5.4).

5.6. Chapter Summary

These simulations have provided valuable insights into local vascular drug delivery systems. They have shown that regardless of the method of applying soluble drugs to arteries, their rapid clearance mandates sustained modes of delivery. In addition, many of the deficits of the standard

labeled-drug assays can be overcome by augmenting experimental work with numerical models. These simulations provide spatial resolution, elucidate the kinetic nature of local vascular distribution without numerous costly animal experiments, and help discriminate biologically active drug from label signal. An example has been illustrated where the implications of experimental local heparin delivery data were reinterpreted following computational simulation. This modeling approach also serves as a paradigm for studying the physical interactions between tissues and chemical signals that modulate many physiologic and pathologic phenomenon.

6. NEXT STEPS

The work presented in this thesis has attempted to describe the physical interaction between vasoactive drugs and arterial tissues. The deposition and distribution of heparin following any mode of vascular administration can now be predicted. However, there are several avenues that remain unexplored. The following analyses will broaden the applicability of the models to other compounds and states of arterial injury, will improve the accuracy by refining some of the measurements and assumptions, and will further demonstrate the utility of pharmacokinetic modeling by allowing dose response experiments *in vivo* that were formerly only achievable in cell culture:

I. Extension of pharmacokinetic modeling to other compounds.

II. Extension to more complete models of vascular pathology.

III. Measurement of the average rate of drug internalization.

IV. Measurement of transendothelial resistance *in vivo.*

V. Dose response of intimal hyperplasia in injured arteries to heparin.

6.1. Extension of Pharmacokinetic Modeling to Other Compounds

Several of the analyses in this work show that heparin differs from standard tracer molecules in terms of fundamental transport and binding properties in vascular tissues, such as effective molecular diffusivity in arterial media, convective hindrance coefficients, transendothelial diffusive resistance, fractional tissue volume, nonspecific binding site density and average binding affinity. These transport and binding properties are in part a function of solute molecular characteristics. For example albumin is a 65 kD globular protein and heparin is a linear, flexible glycosaminoglycan of dispersed molecular weights between 6 and 20 kD. These two compounds should move through and interact with arterial tissues differently. Unfortunately, endogenous growth regulators and potential pharmacologic agents exhibit broad ranges of chemical properties, including molecular weight, charge density, and three-dimensional conformation. Rather than measure the arterial transport and binding properties of every potential therapeutic compound,

principles by which each of them vary with solute chemical properties will be established. For example, the impact of solute molecular weight on effective molecular diffusivity in arterial media will be determined by measuring this transport property for families of dextrans that vary only in molecular weight. Similarly, these compounds will be used to correlate solute weight with all other transport and binding properties. The effects of solute charge and solubility will be determined with dextrans, dextran sulfates of varying charge density, and hydrophobic carbohydrate polymers. The effects of geometrical conformation will be examined by comparing albumin to dextran sulfates of comparable molecular weight or effective molecular radius. These series of measurements will allow the estimation of the transport and binding properties and therefore prediction of vascular deposition and distribution of any vasoactive drug or compound by simply knowing standard solute chemical properties.

6.2. Extension to More Complete Models of Vascular Pathology

All of the analyses in this work have used normal healthy or balloon deendothelialized arteries. The transport and binding properties will be assessed in more complicated and complete forms of acute and chronic vascular injury. Acute injuries can be caused by mechanical revascularizations including balloon angioplasty, and synthetic and venous interposition grafts. Endovascular stents are wire mesh devices that can be expanded within arteries to remain in place for the lifetime of the recipient and impose both acute and chronic forms of injury. Other chronic conditions arise more slowly from years of subacute arterial insult, such as atherosclerotic arteries with calcified plaques. Drug deposition and distribution through these chronically diseased vessels will be studied *in vivo* with Watanabe heritable hyperlipidemic rabbits, and *in vitro* with adult porcine carotid and coronary arteries which are known to have pathologies similar to human vascular lesions.[168,169] All of these forms of arterial injury carry a unique set of hemodynamic and cell/tissue reactions and are expected to impact drug transport and binding properties in distinct manners. These studies will help elucidate how the arterial wall may potentially modulate transport and binding, either to help assist in repair or alternatively to further exacerbate vascular pathology.

6.3. Measurement of the Average Rate of Drug Internalization

The internalization of heparin by smooth muscle cells was shown to be crucial in terms of drug deposition and the interpretation of experimental data (Chap. 5). The rate of heparin internalization used in the current pharmacokinetic analyses has been measured in cell culture but not the intact three-dimensional arterial architecture.[145,170] It is possible that isolated cells may not exhibit the same internalization characteristics as organized tissues. For example, the free and matrix exposed surface binding site densities of sparse cells in culture may be dramatically different and also distinct from cells in a three dimensional hierarchy. The rate of vesicular formation and endocytosis may also be regulated in a manner that is effected by three-dimensional cell-to-cell contact. Therefore, in order to better predict vascular drug distribution and to add insight into fundamental biological phenomenon, the rate of cellular internalization of radiolabeled compounds will be studied in organ-culture-uptake studies and interpreted through mathematical analysis of the data.

Drug will be administered to arterial segments in their native tube configuration so that the *in vivo* cell architecture is preserved and that transport is essentially one-dimensional. The segments will be exposed to drug at a fixed concentration (c_{bulk}) and the tissue average concentration will be measured as a function of time. The following set of differential equations and boundary conditions describes the transmural diffusion and first order internalization of soluble drug.

$$\frac{\partial c_{ec}}{\partial t} = D_{art}\frac{\partial^2 c_{ec}}{\partial x^2} - r_i c_{ec} \tag{6.1}$$

$$c_{ec}(0) = c_{ec}(l) = \varepsilon' c_{bulk} \tag{6.2}$$

$$\frac{\partial c_{ic}}{\partial t} = r_i c_{ec} \tag{6.3}$$

where c_{ec} is the extracellular drug concentration, c_{ic} is the intracellular concentration, r_i is the first order internalization rate constant. Initially c_{ec} and c_{ic} are zero. The analytic solutions to these equations can be integrated across the wall of the artery to describe the space-average concentrations as a function of time. The total concentration of drug (c_T) is the sum of the internalized and extracellular concentrations, and is represented by the following analytic solution:

(6.4) $$\frac{\bar{c}_T(t)}{\varepsilon' c_{bulk}} = \frac{\bar{c}_s(t) + \bar{c}_{ic}(t)}{\varepsilon' c_{bulk}} = r_i t + 1 - \sum_{j=1,3,5\ldots}^{\infty} \frac{8}{j^2\pi^2} \frac{D_{art}[j\pi/l]^2 e^{-t\left(D_{art}[j\pi/l]^2 - r_i\right)} + r_i}{\left(D_{art}[j\pi/l]^2 - r_i\right)}$$

The arterial drug uptake profiles will be measured at 4°C, where the internalization rate constant will be assumed zero. The resulting time-varying deposition data will be fit to the analytic solution to establish the diffusivity of drug in the interstitium of the artery (D_{art}). The measurements will be repeated at 37°C and will be fit to the full solution to determine the internalization rate constant. The measured rate of drug internalization will be incorporated into computational simulations of drug transport and will also be contrasted to rates obtained in cell culture models, thus potentially illustrating the advantage of preserving arterial architecture when quantitatively studying this process.

6.4. Measurement of Transendothelial Resistance *In Vivo*

The endothelial resistance to heparin measured *in vitro* was several orders of magnitude lower than values predicted from *in vivo* studies of other macromolecules (Chap. 2). The resistance to transport imposed by the endothelium may for many compounds depend upon tight intracellular junctions, and slight changes in these gaps caused by moving this organ to culture may have lead to significant artifact. The endothelial barrier to transport will be examined *in vivo* by measuring the difference in deposition between both wire deendothelialized and unmanipulated native arteries. The former procedure has been shown to remove the endothelial monolayer with minimal subsequent damage to the underlying arterial media.[171] Drug will be given in an intravenous bolus and the resulting increase in deposition in deendothelialized over native arteries will correlate with the transendothelial resistance to solute transport. More precise definition of this property will be provided by augmenting this data with computational simulations of transmural drug deposition and distribution. These simulations will be repeated by adjusting the endothelial resistance to transport until the hypothetical removal of this resistance in the model yields the same increment in deposition observed in the rat carotid artery experiments. The endothelial resistance measurements will be repeated for molecules that vary in chemical characteristics such as molecular weight,

charge density, and three dimensional conformation (Sec. 6.1). The quantitative determination of the barrier function of the endothelium to these molecules may help rigorously explain the observation that this organ acts as a barrier to plasma proteins such as albumin but not to endogenous vascular regulators that are secreted by endothelial cells to act on vascular smooth muscle, such as heparin.

6.5. Dose Response of Intimal Hyperplasia in Injured Arteries to Heparin

Although *in vivo* experiments have shown that heparin prevents intimal hyperplasia during experimental models of arterial injury,[10,13,26,127] the concentration of heparin in the pericellular environment needed to achieve these effects are unknown. Dose response analyses are readily performed in cell culture as there are no limitations of drug distribution. These goals, however, are difficult to achieve in isolated organs *in vivo* because the correlation between the administered dose and the organ concentration varies from one mode of drug delivery to another. For example, drug delivered systemically will produce much lower arterial levels than drug released perivascularly. Thus, a method of determining local arterial drug requirements that is independent of the mode of administration is desired. This goal will be achieved through a combination of perivascular heparin delivery and computational modeling of vascular drug distribution. Heparin eluting ethylvinyl acetate copolymer matrices that circumferentially wrap around arteries will be coated with an impermeable material so that release is constrained towards the artery. Rat common carotid arteries will be balloon denuded and the matrices will be placed around the injured segment. Two weeks after injury the tissue will be harvested, sectioned, stained for proliferative indices and the intima:media ratios measured. The delivered dose will be varied by substituting a fraction of the heparin loaded into the matrices with bovine serum albumin. The computational models will predict the heparin concentration in the pericellular milieu, and thus the relationship between local concentration and neointimal thickening will be determined independent of the drug delivery vehicle.

7. CONCLUDING REMARKS

This work has attempted to illustrate how vascular pharmacokinetics should be assessed for any mode of delivery of any solute. The administration, distribution, and elimination of compounds have been evaluated by quantifying the mechanisms of intramural soluble drug transport, the sequestration and potential binding to biologically active and nonspecific sites, and the movement of drug in the perivascular and endovascular extramural spaces. Almost all of these phenomena have been elucidated with novel *in vitro* and *in vivo* and techniques. It has been shown that many of these properties are markedly different for vasoactive drugs than standard tracer compounds. Therefore, these measurements have been illustrated with a potentially vasotherapeutic agent, heparin. The results have been assembled into computational models of drug deposition and distribution that provide insights that could not be appreciated from *in vivo* studies. They provide spatial resolution, elucidate the kinetic nature of local vascular distribution without numerous costly animal experiments, and help discriminate biologically active drug from label signal. In addition, these models have already been used extensively to assist experimental drug delivery protocol design. It is hoped that such analyses will be routine in formulating actual pharmacologic therapies to be used in the clinic, and that trials of novel compounds and drug delivery devices will not be attempted until they are shown in simulations to provide adequate drug concentrations for sufficient periods of time.

Although the preceding analyses have been motivated by arterial diseases and a desire to treat them, the techniques used could easily be adapted to study the physical interaction between any compound in and around any tissue. Transport and binding characteristics are important in many physiological, pathophysiological, and therapeutic scenarios where cells communicate through soluble mediators. Similar models to the ones described here, with the incorporation of appropriate transport and binding properties, can be used to augment biological studies of these processes.

8. APPENDICES

8.1. Rat Perfusion Morphometry

Native, ΔH=0 section	IEL (cm)	EEL (cm)	Lumen Area (cm^2)	Medial Area (cm^2)	Adventitial Area (cm^2)	Medial Thickness (cm)	Adventitial Thickness (cm)
p31-1	0.350	0.375	0.00451	0.00170	0.00221	0.00468	0.00588
p31-3	0.365	0.397	0.00682	0.00174	0.00205	0.00457	0.00515
p31-5	0.377	0.407	0.00856	0.00204	0.00258	0.00521	0.00633
p31-7	0.365	0.392	0.00518	0.00190	0.00170	0.00502	0.00435
p31-9	0.317	0.351	0.00334	0.00163	0.00134	0.00488	0.00380
p31-11	0.359	0.396	0.00663	0.00210	0.00185	0.00555	0.00468
p31-12	0.367	0.404	0.00844	0.00231	0.00200	0.00599	0.00496
average	**0.357**	**0.389**	**0.00621**			**0.00513**	**0.00502**
p32-1	0.341	0.384	0.00222	0.00243	0.00200	0.00670	0.00520
p32-3	0.344	0.387	0.00225	0.00250	0.00226	0.00684	0.00584
p32-5	0.341	0.379	0.00185	0.00228	0.00169	0.00635	0.00445
p32-7	0.313	0.351	0.00148	0.00196	0.00190	0.00591	0.00543
p32-9	0.317	0.351	0.00202	0.00210	0.00220	0.00629	0.00627
p32-11	0.315	0.354	0.00394	0.00186	0.00278	0.00629	0.00627
average	**0.329**	**0.368**	**0.00229**			**0.00642**	**0.00544**
p33-1	0.333	0.374	0.00736	0.00250	0.00162	0.00706	0.00433
p33-3	0.346	0.385	0.00602	0.00235	0.00223	0.00644	0.00580
p33-5	0.323	0.382	0.00330	0.00242	0.00278	0.00687	0.00728
p33-7	0.307	0.351	0.00263	0.00223	0.00180	0.00678	0.00513
p33-9	0.344	0.382	0.00210	0.00228	0.00163	0.00629	0.00426
p33-11	0.338	0.375	0.00393	0.00215	0.00113	0.00602	0.00300
average	**0.332**	**0.375**	**0.00422**			**0.00657**	**0.00497**
p34-1	0.319	0.348	0.00551	0.00163	0.00209	0.00487	0.00599
p34-2	0.307	0.341	0.00379	0.00170	0.00133	0.00525	0.00390
p34-7	0.327	0.359	0.00060	0.00187	0.00115	0.00546	0.00321
p34-10	0.315	0.362	0.00045	0.00184	0.00162	0.00543	0.00447
p34-13	0.334	0.370	0.00292	0.00197	0.00187	0.00559	0.00505
p34-15	0.328	0.369	0.00616	0.00211	0.00241	0.00604	0.00652
average	**0.322**	**0.358**	**0.00324**			**0.00544**	**0.00486**
p35-1	0.300	0.333	0.00558	0.00175	0.00144	0.00551	0.00431
p35-4	0.300	0.329	0.00145	0.00163	0.00220	0.00517	0.00667
p35-7	0.319	0.351	0.00093	0.00153	0.00168	0.00456	0.00480
p35-10	0.342	0.381	0.00256	0.00227	0.00166	0.00629	0.00437
p35-12	0.373	0.411	0.00740	0.00225	0.00310	0.00574	0.00755
average	**0.327**	**0.361**	**0.00359**			**0.00546**	**0.00554**

Rat Perfusion Morphometry (con't)

Denuded, ΔH=0 section	IEL (cm)	EEL (cm)	Lumen Area (cm^2)	Medial Area (cm^2)	Adventitial Area (cm^2)	Medial Thickness (cm)	Adventitial Thickness (cm)
p36-3	0.287	0.317	0.00262	0.00145	0.00035	0.00481	0.00109
p36-5	0.275	0.309	0.00125	0.00147	0.00051	0.00502	0.00165
p36-7	0.311	0.334	0.00114	0.00158	0.00083	0.00491	0.00248
p36-9	0.297	0.338	0.00075	0.00160	0.00084	0.00505	0.00248
p36-11	0.277	0.309	0.00051	0.00131	0.00075	0.00446	0.00243
p36-13	0.274	0.307	0.00042	0.00139	0.00054	0.00477	0.00178
p36-15	0.300	0.323	0.00219	0.00159	0.00057	0.00512	0.00175
average	**0.289**	**0.320**	**0.00127**			**0.00488**	**0.00195**
p37-1	0.294	0.341	0.00570	0.00220	0.00480	0.00692	0.01408
p37-4	0.305	0.338	0.00112	0.00176	0.00195	0.00547	0.00577
p37-7	0.309	0.343	0.00066	0.00163	0.00234	0.00500	0.00682
p37-10	0.317	0.349	0.00176	0.00157	0.00190	0.00471	0.00543
p37-12	0.313	0.339	0.00483	0.00183	0.00160	0.00560	0.00471
p37-13	0.341	0.380	0.00769	0.00200	0.00179	0.00556	0.00471
average	**0.313**	**0.348**	**0.00363**			**0.00554**	**0.00692**
p38-10	0.290	0.325	0.00090	0.00157	0.00178	0.00509	0.00548
p38-13	0.303	0.342	0.00115	0.00165	0.00139	0.00512	0.00407
p38-4	0.304	0.341	0.00059	0.00175	0.00209	0.00541	0.00614
p38-7	0.287	0.319	0.00066	0.00158	0.00295	0.00521	0.00924
p38-15	0.335	0.374	0.00140	0.00237	0.00278	0.00669	0.00743
p38-2	0.319	0.353	0.00201	0.00189	0.00189	0.00563	0.00535
average	**0.306**	**0.342**	**0.00112**			**0.00552**	**0.00628**
p40-1	0.303	0.347	0.00409	0.00226	0.00193	0.00695	0.00558
p40-3	0.284	0.327	0.00106	0.00175	0.00125	0.00574	0.00383
p40-11	0.279	0.302	0.00051	0.00138	0.00159	0.00477	0.00527
p40-13	0.264	0.311	0.00124	0.00174	0.00213	0.00607	0.00684
p40-5	0.280	0.309	0.00047	0.00140	0.00148	0.00477	0.00478
p40-7	0.270	0.305	0.00046	0.00145	0.00120	0.00503	0.00392
p40-9	0.274	0.304	0.00052	0.00138	0.00162	0.00478	0.00531
average	**0.279**	**0.315**	**0.00119**			**0.00544**	**0.00508**

Rat Perfusion Morphometry (con't)

Native, ΔH=100 cm section	IEL (cm)	EEL (cm)	Lumen Area (cm^2)	Medial Area (cm^2)	Adventitial Area (cm^2)	Medial Thickness (cm)	Adventitial Thickness (cm)
p50-1	0.433	0.433	0.01433	0.00235	0.00235	0.00778	0.01023
p50-7	0.461	0.461	0.01507	0.00298	0.00298	0.00638	0.00188
p50-3	0.432	0.432	0.01213	0.00196	0.00027	0.00454	0.00062
p50-5	0.420	0.481	0.01080	0.00199	0.00048	0.00475	0.00100
average	**0.437**	**0.457**	**0.01308**			**0.00464**	**0.00081**
p51-1	0.381	0.433	0.00991	0.00096	0.00038	0.00252	0.00101
p51-10	0.396	0.430	0.00973	0.00180	0.00180	0.00454	0.00420
p51-3	0.393	0.393	0.00948	0.00155	0.00154	0.00395	0.00392
p51-5	0.402	0.422	0.00871	0.00156	0.00074	0.00386	0.00176
average	**0.393**	**0.415**	**0.00946**			**0.00372**	**0.00272**
p52-13	0.455	0.499	0.01379	0.00209	0.00082	0.00460	0.00164
p52-10	0.469	0.487	0.01523	0.00190	0.00105	0.00404	0.00214
p52-7	0.410		0.00000	0.00133	0.00102	0.00324	0.00249
p52-1	0.405	0.485	0.00000	0.00196	0.00119	0.00484	0.00244
average	**0.435**	**0.490**	**0.00726**			**0.00418**	**0.00218**
						0.00035	0.00020
p53-0	0.439	0.471	0.01389	0.00207	0.00212	0.00470	0.00450
p53-2.5	0.452	0.482	0.01209	0.00151	0.00152	0.00334	0.00316
p53-4	0.397	0.428	0.00872	0.00132	0.00132	0.00333	0.00308
p53-6	0.476	0.513	0.01588	0.00233	0.00099	0.00489	0.00193
p53-8	0.485	0.510	0.01416	0.00184	0.00147	0.00378	0.00289
p53-10	0.465	0.493	0.01474	0.00178	0.00112	0.00383	0.00227
average	**0.452**	**0.483**	**0.01325**			**0.00396**	**0.00254**
p54-1	0.421	0.434	0.00757	0.00234	0.00164	0.00556	0.00379
p54-3	0.413	0.433	0.00877	0.00157	0.00087	0.00379	0.00201
p54-5	0.402	0.431	0.00962	0.00170	0.00066	0.00422	0.00153
p54-9	0.380	0.406	0.00804	0.00143	0.00071	0.00376	0.00176
p54-12	0.358	0.393	0.00725	0.00167	0.00081	0.00466	0.00205
average	**0.395**	**0.419**	**0.00825**			**0.00411**	**0.00184**

Rat Perfusion Morphometry (con't)

Denuded, ΔH=100 cm section	IEL (cm)	EEL (cm)	Lumen Area (cm^2)	Medial Area (cm^2)	Adventitial Area (cm^2)	Medial Thickness (cm)	Adventitial Thickness (cm)
p55-1	0.427	0.444	0.00949	0.00163	0.00186	0.00381	0.00418
p55-4	0.456	0.490	0.01490	0.00188	0.00156	0.00412	0.00318
p55-7	0.459	0.484	0.01323	0.00174	0.00179	0.00379	0.00370
p55-11	0.431	0.457	0.01225	0.00176	0.00279	0.00408	0.00610
p55-14	0.441	0.469	0.01065	0.00168	0.00106	0.00382	0.00225
p55-16	0.424	0.444	0.01163	0.00151	0.00143	0.00355	0.00323
average	**0.440**	**0.464**	**0.01203**			**0.00386**	**0.00377**
p56-1	0.457	0.476	0.01517	0.00161	0.00156	0.00352	0.00327
p56-3	0.422	0.440	0.01235	0.00113	0.00113	0.00268	0.00256
p56-5	0.464	0.492	0.01367	0.00153	0.00165	0.00330	0.00337
p56-7	0.424	0.455	0.01268	0.00138	0.00139	0.00326	0.00306
p56-11	0.433	0.466	0.01336	0.00163	0.00165	0.00377	0.00354
average	**0.440**	**0.466**	**0.01345**			**0.00331**	**0.00316**
p57-4	0.373	0.398	0.01033	0.00127	0.00136	0.00341	0.00341
p57-7	0.393	0.416	0.01172	0.00135	0.00164	0.00344	0.00394
p57-10	0.408	0.435	0.01175	0.00158	0.00181	0.00389	0.00416
p57-13.5	0.397	0.416	0.00945	0.00126	0.00198	0.00318	0.00476
p57-14.5	0.423	0.449	0.01384	0.00170	0.00211	0.00401	0.00470
average	**0.399**	**0.423**	**0.01142**			**0.00358**	**0.00419**
p58-1	0.418	0.445	0.01137	0.00149	0.00254	0.00356	0.00571
p58-4	0.377	0.399	0.01016	0.00160	0.00244	0.00423	0.00613
p58-7	0.415	0.444	0.01136	0.00178	0.00215	0.00430	0.00484
p58-10	0.435	0.467	0.01447	0.00216	0.00286	0.00496	0.00611
p58-13	0.447	0.485	0.01500	0.00238	0.00320	0.00533	0.00660
average	**0.418**	**0.448**	**0.01247**			**0.00448**	**0.00588**

8.2. Rat Abdominal Aorta Perfusion Summary

Native, ΔH=0						
Rat #		p31	p32	p33	p34	p35
Heparin Transport (j)	(mg/s)	1.02E-05	9.77E-06	1.13E-05	1.21E-05	7.94E-06
Length	cm	0.89	0.99	1.18	1.09	1.05
Perimeter (IEL)	cm	0.357	0.329	0.332	0.322	0.327
Concentration Difference	mg/ml	3.69	4.05	3.68	4.53	2.61
Volume Flow Rate	ml/s	0.0064	0.0060	0.0078	0.0101	0.0061
Hydraulic Diameter	cm	0.0688	0.0280	0.0507	0.0402	0.0430
Lumen Area	sq. cm	0.0062	0.0023	0.0042	0.0032	0.0036
Average Lumen Velocity	cm/s	1.14	2.86	2.22	6.1342	2.9957
Re (d)		8.26	8.39	10.79	14.35	8.59
Sh(d) developing		26.76	18.93	23.94	25.06	21.73
Boundary Layer Resistance	s/cm	1,776	1,022	1,460	1,108	1,365
ψ		1.00	0.99	1.05	0.90	1.07

Denuded, ΔH=0						
Rat #		p36	p37	p38	p39	p40
Heparin Transport (j)	(mg/s)	1.31E-05	1.22E-05	1.09E-05	1.71E-05	1.25E-05
Length	cm	1.14	0.95	1.21	0.98	1.00
Perimeter (IEL)	cm	0.289	0.313	0.306	0.302	0.279
Concentration Difference	mg/ml	3.12	3.19	3.06	4.69	4.75
Volume Flow Rate	ml/s	0.0049	0.0130	0.0068	0.0103	0.0029
Hydraulic Diameter	cm	0.0175	0.0458	0.0144	0.0402	0.0166
Lumen Area	sq. cm	0.0013	0.0036	0.0011	0.0030	0.0012
Average Lumen Velocity	cm/s	5.68	7.53	7.23	3.59	4.19
Re (d)		7.79	19.10	10.20	15.72	4.75
Sh(d) developing		14.73	30.24	14.86	26.84	12.62
Boundary Layer Resistance	s/cm	819	1,045	670	1,033	908
ψ		1.02	1.22	0.91	1.09	0.84

Rat Abdominal Aorta Perfusion Summary (con't)

Native, ΔH=100 cm							
Rat #		p50	p51	p52	p53	p54	p60
Heparin Transport (j)	(mg/s)	1.20E-05	1.43E-05	1.81E-05	1.56E-05	1.04E-05	1.23E-05
Length	cm	0.66	0.95	0.88	0.95	0.88	0.90
Perimeter (IEL)	cm	0.457	0.415	0.490	0.483	0.419	0.431
Concentration Difference	mg/ml	3.87	2.82	3.58	3.64	2.81	3.06
Volume Flow Rate	ml/s	0.0033	0.0027	0.0063	0.0047	0.0063	0.0033
Hydraulic Diameter	cm	0.1075	0.0964	0.1256	0.1162	0.0866	0.1080
Lumen Area	sq. cm	0.0131	0.0095	0.0073	0.0132	0.0083	0.0112
Average Lumen Velocity	cm/s	0.2927	0.2858	0.4384	0.3729	0.7618	0.3015
Re (d)		3.61	3.16	6.32	4.79	7.54	3.70
Sh(d) developing		25.99	21.04	30.10	25.94	28.18	23.58
Boundary Layer Resistance	s/cm	2,855	3,162	2,880	3,092	2,121	3,162
ψ		0.98	1.16	1.11	0.86	0.93	0.86

Denuded, ΔH=100 cm						
Rat #		p55	p56	p57	p59	p58
Heparin Transport (j)	(mg/s)	2.38E-05	1.36E-05	1.42E-05	1.85E-05	1.27E-05
Length	cm	1.1557	0.8128	0.9906	1.2446	0.9398
Perimeter (IEL)	cm	0.464	0.466	0.423	0.425	0.448
Concentration Difference	mg/ml	3.43	2.89	2.48	3.09	2.87
Volume Flow Rate	ml/s	0.0058	0.0054	0.0020	0.0057	0.0118
Hydraulic Diameter	cm	0.1092	0.1221	0.1143	0.1016	0.1187
Lumen Area	sq. cm	0.0120	0.0134	0.0114	0.0102	0.0125
Average Lumen Velocity	cm/s	0.4910	0.4054	0.1777	0.5896	0.1636
Re (d)		6.05	5.67	2.30	6.59	2.20
Sh(d) developing		25.75	29.49	19.71	25.21	20.02
Boundary Layer Resistance	s/cm	2,926	2,857	4,001	2,781	4,091
ψ		0.85	0.71	0.89	0.68	0.87

8.3. Heparin Deposition in Calf Carotid Arteries *In Vitro*

Artery #	Start EV DPM	Start PV DPM	End EV DPM	End PV DPM	Artery Dry (mg)	Artery DPM	Deposition μg/g/(μg/ml)
Native, Perivascular Administration, ΔH = 100 cm							
pc37	11786.4	52.7	10575.9	38.4	7.3	1119.9	0.656
	11622.5	46.5	11041.1	26.3	2.9	402.9	0.553
	11999.5	54.3	10769.5	50.0	3.9	682.6	0.730
pc39	7990.1	46.3	7111.6	50.5	8.4	1071.7	0.798
	8975.5	36.2	6425.9	44.5	10.7	1114.0	0.653
	8755.3	54.9	7088.1	74.7	7.3	915.8	0.780
pc41	12065.5	60.3	10999.4	48.3	10.0	3748.4	1.590
	11954.0	46.8	11594.9	74.3	126.6	6699.7	0.226
	12045.9	56.9	11555.2	52.5	11.3	3437.5	1.289
pc43	10425.4	96.1	10179.2	53.8	8.0	2399.3	1.398
	10845.2	61.9	10448.0	85.2	6.4	1612.7	1.164
	11149.2	78.9	10489.3	60.1	8.2	2252.8	1.279
Denuded, Perivascular Administration, ΔH = 100 cm							
pc38	10575.9	38.4	7990.1	46.3	6.8	823.1	0.596
	11041.1	26.3	8975.5	36.2	4.0	595.3	0.718
	10769.5	50.0	8755.3	54.9	4.9	1117.9	1.139
pc40	11744.3	54.5	12065.5	60.3	9.8	2632.5	1.096
	10326.3	38.5	11954.0	46.8	5.2	1283.6	0.990
	14499.4	30.1	12045.9	56.9	11.8	3575.5	1.242
pc42	10999.4	48.3	10425.4	96.1	9.3	2163.7	1.033
	11594.9	74.3	10845.2	61.9	14.0	3675.0	1.175
	11555.2	52.5	11149.2	78.9	9.4	4056.1	1.933
pc44	10179.2	53.8	9473.1	88.6	9.6	2427.9	1.244
	10448.0	85.2	9292.2	88.4	8.2	1747.2	1.041
	10489.3	60.1	10343.5	57.8	6.5	1478.8	1.106

Heparin Deposition in Calf Carotid Arteries *In Vitro* (con't)

Artery #	Start EV DPM	Start PV DPM	End EV DPM	End PV DPM	Artery Dry (mg)	Artery DPM	Deposition μg/g/(μg/ml)
Native Endovascular Administration, ΔH = 100 cm							
pc45	11233.1	63.8	11336.9	71.7	9.6	2655.9	1.181
	11518.3	56.0	11945.2	58.4	10.8	2604.0	1.029
	11837.4	30.3	11665.3	64.5	10.9	3187.9	1.252
pc47	11031.5	**63.8**	11036.2	207.0	11.3	**7287.2**	2.824
	11450.5	56.0	11909.9	226.0	12.2	7823.7	2.809
	11389.7	30.3	11649.4	223.0	8.5	6048.3	3.112
pc49	226.0	63.8	11683.3	342.1	11.5	5314.8	2.936
	223.0	56.0	11789.7	385.6	12.8	4492.6	2.226
	11538.3	30.3	11746.6	441.1	12.4	4370.5	2.235
pc51	385.6	63.8	11247.2	243.3	9.8	3765.1	2.447
	441.1	56.0	11233.7	208.6	12.3	4473.0	2.320
	11796.8	30.3	11841.0	251.7	7.6	3190.4	2.668
Denuded, Endovascular Administration, ΔH = 100 cm							
pc46	11336.9	63.8	11031.5	209.6	14.2	9738.4	2.992
	11945.2	56.0	11450.5	224.1	17.7	12897.7	3.182
	11665.3	30.3	11389.7	225.2	17.6	7840.5	1.941
pc48	11036.2	63.8	11229.0	198.9	12.3	7695.3	2.763
	11909.9	56.0	10555.1	289.8	13.5	7312.1	2.391
	11649.4	30.3	11538.3	261.5	12.2	5292.2	1.911
pc50	289.8	63.8	11012.7	405.5	17.6	17401.7	6.356
	261.5	56.0	11781.2	361.5	12.6	8053.5	4.098
	11746.6	30.3	11796.8	367.6	15.9	9780.7	3.948
			11796.8		10.9	7119.4	4.185
pc52	361.5	63.8	11374.3	242.0	13.8	6367.1	2.882
	367.6	56.0	11699.3	222.0	9.8	5673.2	3.613
	11841.0	30.3	12419.4	206.8	7.7	5015.2	4.061

Heparin Deposition in Calf Carotid Arteries *In Vitro* (con't)

Artery #	Start EV DPM	Start PV DPM	End EV DPM	End PV DPM	Artery Dry (mg)	Artery DPM	Deposition μg/g/(μg/ml)
Native, Perivascular Administration, ΔH = 0							
pc53	54.9	11717.7	36.3	11682.6	12.6	4823.0	1.578
	56.2	12403.4	44.3	11757.2	13.0	4346.2	1.376
	42.6	12250.1	48.0	11639.5	12.4	3945.8	1.308
pc55	59.5	11361.1	66.1	12313.6	7.3	2498.2	1.394
	86.3	12171.2	54.1	12465.0	8.1	2702.5	1.362
	68.8	12102.6	103.1	12444.4	7.0	2540.2	1.479
pc57	66.1	12016.5	111.5	11628.7	8.4	2278.6	1.103
	66.2	12310.0	78.4	12511.9	12.4	3868.2	1.282
	78.4	12548.9	66.4	12821.1	9.2	2694.0	1.195
pc59	58.7	11893.4	79.7	10982.0	10.6	3224.9	1.246
	66.4	12188.5	78.1	12182.6	9.4	2640.6	1.146
	107.2	12474.6	87.1	12342.3	10.4	3722.8	1.470
Denuded, Perivascular Administration, ΔH = 0							
pc54	36.3	11682.6	59.5	11361.1	8.2	3498.8	1.751
	44.3	11757.2	86.3	12171.2	6.6	2564.4	1.584
	48.0	11639.5	68.8	12102.6	7.0	2892.0	1.689
pc56	66.1	12313.6	66.1	11185.1	7.5	4086.1	2.241
	54.1	12465.0	66.2	12341.6	7.5	4386.2	2.408
	103.1	12444.4	78.4	12057.6	9.7	5050.5	2.148
pc58	111.5	11628.7	58.7	11893.4	11.0	3959.5	1.480
	78.4	12511.9	66.4	12188.5	16.1	5376.5	1.381
	66.4	12821.1	107.2	12474.6	12.5	4896.3	1.615
pc60	79.7	10982.0	70.3	10633.5	14.6	5025.3	1.420
	78.1	12182.6	92.6	11913.3	14.0	5341.5	1.575
	87.1	12342.3	76.4	12440.9	17.4	6413.6	1.524

Heparin Deposition in Calf Carotid Arteries *In Vitro* (con't)

Artery #	Start EV DPM	Start PV DPM	End EV DPM	End PV DPM	Artery Dry (mg)	Artery DPM	Deposition µg/g/(µg/ml)
Native, Endovascular Administration, ΔH = 0							
pc61	15404.4	58.1	15404.5	57.6	11.9	3592.0	0.948
	16242.2	36.1	16357.9	49.8	16.5	5510.9	1.053
	15978.5	52.1	16384.7	44.5	17.3	6807.6	1.243
pc63	15513.9	58.1	15404.5	57.6	8.6	1967.7	0.711
	15538.3	36.1	16357.9	49.8	9.1	2624.2	0.901
	16309.9	52.1	16384.7	44.5	9.1	1573.4	0.535
pc65	15513.9	58.1	15404.5	57.6	6.9	2293.5	1.037
	15538.3	36.1	16357.9	49.8	5.3	1976.7	1.160
	16309.9	52.1	16384.7	44.5	5.8	4304.4	2.335
pc67	15513.9	58.1	15335.4	66.5	10.4	3987.6	1.205
	15538.3	36.1	15788.9	76.5	17.3	6002.9	1.095
	16309.9	52.1	15907.3	48.3	17.5	6492.3	1.171
Denuded, Endovascular Administration, ΔH = 0							
pc62	15404.5	58.1	15513.9	64.7	7.4	2894.4	1.225
	16357.9	36.1	15538.3	46.3	9.4	3482.0	1.163
	16384.7	52.1	16309.9	44.2	9.7	2654.5	0.856
pc64	15404.5	58.1	15513.9	64.7	7.8	3341.0	1.344
	16357.9	36.1	15538.3	46.3	7.4	2972.7	1.258
	16384.7	52.1	16309.9	44.2	7.0	2610.1	1.166
pc66	15404.5	58.1	15513.9	64.7	8.4	2127.3	0.789
	16357.9	36.1	15538.3	46.3	6.9	5398.4	2.466
	16384.7	52.1	16309.9	44.2	7.9	4330.5	1.725
pc68	15404.5	58.1	15394.1	36.1	12.4	4760.7	1.209
	16357.9	36.1	15850.3	52.3	8.8	4607.8	1.648
	16384.7	52.1	16075.1	46.3	10.2	5006.9	1.546

8.4. Deposition in Rabbit Iliac Arteries from Perivascular Collars

		<------Artery------>		<--------	Initial Gel	-------->	Deposition / [Gel]o
		dry mass		mass		activity	
Rabbit #	Artery #	(mg)	DPM	(mg)	DPM	(DPM/mg)	DPM/mg / (DPM / mg)
Native							
fr12	6	1.5	7,607	100	7,163,792	71638	0.08274
fr21	8	1.5	1,132	130.9	7,649,169	60941	0.01393
fr21	9	0.8	2,906	118.4	7,519,592	60941	0.06892
fr22	7	2.0	4,027	100	6,087,959	60941	0.03839
fr23	7	1.8	10,984	100	5,843,483	60941	0.11726
fr30	8	1.3	16,204	100	6,350,965	70570	0.20715
fr30	9	0.9	8,343	100	7,362,166	70570	0.15361
fr30	10	1.6	8,581	100	7,067,632	70570	0.08888
fr30	11	0.9	6,389			70570	0.11741
Denuded							
fr12	7	2.4	9,358	100	7,163,792	71638	0.06369
fr21	7	1.8	10,003	75	4,566,019	60941	0.10675
fr22	8	2.1	8,349	100	6,087,959	60941	0.07630
fr22	9	1.2	10,551	100	5,843,483	60941	0.16894
fr23	8	1.1	7,673	100	6,350,965	60941	0.13378
fr23	9	0.8	5,403			60941	0.12918
fr29	8	1.8	12,501	100	6,741,333	70570	0.11531
fr29	9	1.2	6,906	100	7,362,166	70570	0.09525
fr29	10	1.3	10,076	100	7,067,632	70570	0.12857
fr29	11	1.3	6,427			70570	0.09930

8.5. Equilibrium Distribution Data

Arterial Media with Intact Endothelium I

C_{bulk} (M)	Tissue wet wt (mg)	Tissue DPM	C_T (M)	C_b (M)	C_{bulk} (M)	Tissue wet wt (mg)	Tissue DPM	C_T (M)	C_b (M)
6.83E-11	12.4	76.4	1.08E-10	6.62E-11	4.10E-07	18.8	233776	6.21E-07	3.69E-07
6.83E-11	19.7	109.8	1.50E-10	1.08E-10	4.10E-07	30	333110	5.46E-07	2.93E-07
6.83E-11	16.5	210.8	4.77E-10	4.35E-10	4.10E-07	30.3	361011	5.85E-07	3.33E-07
6.83E-11	13.9	90.6	1.45E-10	1.03E-10	1.24E-06	28.5	1031769	1.79E-06	1.02E-06
6.83E-11	6.9	92.2	3.04E-10	2.62E-10	1.24E-06	35	1048493	1.48E-06	7.17E-07
6.83E-11	13.4	85.2	1.30E-10	8.78E-11	1.24E-06	26.9	734256	1.35E-06	5.88E-07
5.38E-10	9.8	234.7	9.29E-10	5.97E-10	1.24E-06	14.6	567017	1.91E-06	1.14E-06
5.38E-10	15.7	312.1	8.27E-10	4.96E-10	5.00E-06	23.5	3786.4	5.60E-06	2.52E-06
5.38E-10	19.3	346.1	7.55E-10	4.24E-10	5.00E-06	27.1	4530.7	5.86E-06	2.78E-06
5.38E-10	21.1	375.9	7.53E-10	4.22E-10	5.00E-06	25.7	3993.3	5.36E-06	2.28E-06
5.38E-10	19.7	338.4	7.17E-10	3.86E-10	5.00E-06	16.7	2675	5.44E-06	2.37E-06
5.38E-10	21.7	334.3	6.45E-10	3.14E-10	1.43E-05	34	12784.1	1.32E-05	4.37E-06
1.54E-09	25.1	936.9	1.74E-09	7.97E-10	1.43E-05	25.3	10305.3	1.43E-05	5.53E-06
1.54E-09	10.2	410.9	1.74E-09	7.94E-10	1.43E-05	12.5	4861.9	1.35E-05	4.70E-06
1.54E-09	13.1	514.5	1.74E-09	7.97E-10	3.91E-05	27.1	24699.8	3.21E-05	8.06E-06
1.54E-09	15.3	526.3	1.54E-09	5.94E-10	3.91E-05	25.4	20934.3	2.90E-05	4.99E-06
1.54E-09	14.5	826.2	2.67E-09	1.72E-09	3.91E-05	24.3	19947.8	2.87E-05	4.64E-06
1.54E-09	14.4	602.4	1.89E-09	9.39E-10	5.88E-05	20.7	25533.1	4.31E-05	6.94E-06
1.54E-09	25.3	1287.3	2.40E-09	1.46E-09	5.88E-05	34	41131.1	4.23E-05	6.14E-06
1.54E-09	12	575.4	2.15E-09	1.21E-09	5.88E-05	21.9	27629.5	4.45E-05	8.33E-06
4.51E-09	15.3	2857.6	9.08E-09	6.30E-09	5.88E-05	6.1	7986.3	4.56E-05	9.39E-06
4.51E-09	14.3	1738.3	5.80E-09	3.03E-09	8.11E-05	31.9	53263.1	5.90E-05	9.08E-06
4.51E-09	26.1	3084.5	5.74E-09	2.96E-09	8.11E-05	35.6	62347.6	6.15E-05	1.16E-05
4.51E-09	20.1	3594.3	8.84E-09	6.06E-09	8.11E-05	24.8	42135.2	5.97E-05	9.78E-06
4.51E-09	22.3	2957	6.41E-09	3.63E-09	8.11E-05	15.6	25233.8	5.69E-05	7.00E-06
1.47E-08	35.4	17564	2.45E-08	1.54E-08	1.07E-04	27.3	54397.9	7.00E-05	4.04E-06
1.47E-08	24.1	10647.1	2.22E-08	1.31E-08	1.07E-04	20.2	41309.4	7.19E-05	5.95E-06
1.47E-08	38.9	18312	2.27E-08	1.36E-08	1.07E-04	37.5	77315.2	7.22E-05	6.22E-06
4.25E-08	32.6	38618.5	5.92E-08	3.31E-08	1.07E-04	23.5	49766.7	7.38E-05	7.84E-06
4.25E-08	33.6	45042.8	6.58E-08	3.97E-08	1.22E-04	36.8	80293	7.66E-05	1.80E-06
4.25E-08	51.9	70274.1	6.60E-08	3.99E-08	1.22E-04	31.7	71613.3	7.91E-05	4.29E-06
1.38E-07	32.2	130150	2.00E-07	1.15E-07	1.22E-04	34.7	76515.9	7.70E-05	2.18E-06
1.38E-07	23.7	100253	2.07E-07	1.22E-07	1.22E-04	26.5	60888.5	8.04E-05	5.63E-06
1.38E-07	24.6	84458.4	1.70E-07	8.48E-08	1.43E-04	32	84756	9.28E-05	4.85E-06
1.38E-07	21.4	82762.3	1.90E-07	1.05E-07	1.43E-04	27.7	78447.8	1.01E-04	1.27E-05
4.10E-07	24.4	207436	4.19E-07	1.67E-07	1.43E-04	29.5	79008.4	9.38E-05	5.88E-06

Equilibrium Distribution Data (con't)

Arterial Media with Intact Endothelium II

C_{bulk} (M)	Tissue wet wt (mg)	Tissue DPM	C_T (M)	C_b (M)	C_{bulk} (M)	Tissue wet wt (mg)	Tissue DPM	C_T (M)	C_b (M)
6.29E-10	13.3	199.9	5.51E-10	1.86E-10	1.27E-06	6.8	144525	1.05E-06	3.17E-07
6.29E-10	11.3	196	6.32E-10	2.66E-10	5.11E-06	8.5	995.5	4.28E-06	1.30E-06
6.29E-10	10.4	186.9	6.43E-10	2.77E-10	5.11E-06	15.9	1649.7	3.83E-06	8.53E-07
6.29E-10	8.1	155.4	6.33E-10	2.67E-10	5.11E-06	9	1067.4	4.30E-06	1.32E-06
1.78E-09	17.2	828.8	2.27E-09	1.23E-09	5.11E-06	10.2	989.1	3.50E-06	5.24E-07
1.78E-09	9.3	559.3	2.62E-09	1.59E-09	1.48E-05	17.1	4900	1.09E-05	2.32E-06
1.78E-09	8	295.7	1.51E-09	4.77E-10	1.48E-05	11.9	3124.2	9.83E-06	1.23E-06
1.78E-09	6.5	298	1.88E-09	8.44E-10	1.48E-05	7	1960.1	1.04E-05	1.78E-06
5.25E-09	14.2	1292.3	4.34E-09	1.28E-09	1.48E-05	12.6	4168	1.24E-05	3.84E-06
5.25E-09	10.9	1206.3	5.26E-09	2.20E-09	3.65E-05	19.6	12282.8	2.39E-05	2.64E-06
5.25E-09	15.7	1468.1	4.48E-09	1.42E-09	3.65E-05	10	6360.1	2.40E-05	2.78E-06
5.25E-09	9.3	969.5	4.79E-09	1.74E-09	3.65E-05	15.3	9223	2.28E-05	1.58E-06
1.57E-08	9.1	3267.5	1.77E-08	8.60E-09	3.65E-05	6.9	4480	2.44E-05	3.19E-06
1.57E-08	10.3	2695.8	1.27E-08	3.60E-09	5.73E-05	5.3	4962.2	3.53E-05	1.95E-06
1.57E-08	8.3	2352	1.38E-08	4.62E-09	5.73E-05	10.7	11260.6	3.99E-05	6.56E-06
1.57E-08	3.6	1304.4	1.78E-08	8.62E-09	5.73E-05	11.7	10614.2	3.47E-05	1.34E-06
4.64E-08	13.8	11582.9	4.18E-08	1.48E-08	5.73E-05	25.1	28026.4	4.25E-05	9.12E-06
4.64E-08	8.7	6217.6	3.52E-08	8.17E-09	8.03E-05	18.1	23217	4.88E-05	2.07E-06
4.64E-08	11.9	9571.3	3.97E-08	1.27E-08	8.03E-05	16.5	22478.6	5.09E-05	4.16E-06
4.64E-08	12.3	9834.6	3.95E-08	1.25E-08	8.03E-05	18.5	25993.1	5.34E-05	6.73E-06
1.36E-07	7.4	25371.3	1.72E-07	9.31E-08	8.03E-05	8.7	11532.7	5.03E-05	3.58E-06
1.36E-07	12.5	52947.9	2.10E-07	1.31E-07	1.01E-04	11.2	19941.1	6.76E-05	8.98E-06
1.36E-07	10.5	34200.7	1.61E-07	8.23E-08	1.01E-04	14.8	24089.2	6.19E-05	3.20E-06
1.36E-07	6.2	16864.8	1.28E-07	4.93E-08	1.01E-04	7.7	13708.5	6.76E-05	8.89E-06
4.17E-07	10.4	105678	5.04E-07	2.62E-07	1.25E-04	11.1	22270.7	7.63E-05	3.81E-06
4.17E-07	7.5	86829.5	5.74E-07	3.32E-07	1.25E-04	14.9	29816.9	7.61E-05	3.66E-06
4.17E-07	8.5	64035	3.74E-07	1.31E-07	1.25E-04	7.4	15791	8.10E-05	8.58E-06
4.17E-07	10.3	114354	5.51E-07	3.09E-07	1.43E-04	15.7	34980.5	8.47E-05	1.38E-06
1.27E-06	16.2	485040	1.49E-06	7.48E-07	1.43E-04	11.2	25490.4	8.81E-05	4.73E-06
1.27E-06	10.5	218033	1.03E-06	2.93E-07	1.43E-04	19.6	44782.3	8.69E-05	3.57E-06
1.27E-06	4.4	86561.4	9.76E-07	2.38E-07					

Equilibrium Distribution Data (con't)

Arterial Media with Denuded Endothelium I

C_{bulk} (M)	Tissue wet wt (mg)	Tissue DPM	C_T (M)	C_b (M)	C_{bulk} (M)	Tissue wet wt (mg)	Tissue DPM	C_T (M)	C_b (M)
1.82E-11	12.6	56.8	1.49E-11	1.76E-12	7.83E-07	19	417441	1.04E-06	4.78E-07
1.82E-11	16.1	58	1.55E-11	2.30E-12	7.83E-07	23.7	469765	9.93E-07	4.28E-07
1.82E-11	18.4	67.4	3.88E-11	2.57E-11	7.83E-07	59.3	948879	8.08E-07	2.43E-07
1.82E-11	14.6	60.2	2.41E-11	1.10E-11	5.03E-06	14.5	1172.2	4.17E-06	5.44E-07
4.31E-10	19.9	317.7	6.51E-10	3.41E-10	5.03E-06	13.2	1511.5	5.97E-06	2.34E-06
4.31E-10	17.8	294.1	6.70E-10	3.59E-10	5.03E-06	11.8	1502.8	6.75E-06	3.13E-06
4.31E-10	18.7	328.1	7.16E-10	4.06E-10	5.03E-06	12.3	1403.9	5.98E-06	2.36E-06
4.31E-10	8	178.6	8.17E-10	5.07E-10	1.73E-05	26	8293.6	1.72E-05	4.74E-06
1.26E-09	20.9	818.9	1.81E-09	9.02E-10	1.73E-05	27.3	8755.9	1.72E-05	4.78E-06
1.26E-09	20.8	790.2	1.75E-09	8.42E-10	1.73E-05	13.6	4037	1.58E-05	3.38E-06
1.26E-09	22.5	940.5	1.95E-09	1.04E-09	1.73E-05	23	7088.5	1.66E-05	4.15E-06
1.26E-09	11.2	463.6	1.80E-09	8.86E-10	4.15E-05	25.4	15472.4	3.31E-05	3.18E-06
3.16E-09	18.1	1832.7	4.89E-09	2.61E-09	4.15E-05	19.6	12026.2	3.30E-05	3.12E-06
3.16E-09	19.2	1806.1	4.52E-09	2.24E-09	4.15E-05	33.8	21100.3	3.39E-05	4.06E-06
3.16E-09	29.7	3025.5	4.95E-09	2.67E-09	6.34E-05	13.4	12879.1	5.13E-05	5.66E-06
1.05E-08	15.8	4839.3	1.42E-08	6.62E-09	6.34E-05	26.6	25560.3	5.22E-05	6.53E-06
1.05E-08	22.8	6710.7	1.46E-08	7.08E-09	6.34E-05	18.6	18191.6	5.27E-05	7.02E-06
1.05E-08	15.1	5709.9	1.85E-08	1.10E-08	8.07E-05	22.5	25593.6	6.16E-05	3.42E-06
2.85E-08	16.9	12101.7	3.53E-08	1.48E-08	8.07E-05	25.2	30870.9	6.66E-05	8.42E-06
2.85E-08	15.3	10524.7	3.41E-08	1.36E-08	8.07E-05	12.6	14488.3	6.19E-05	3.72E-06
2.85E-08	14	11832.6	4.16E-08	2.11E-08	8.07E-05	16.9	22652	7.58E-05	1.77E-05
2.85E-08	14.5	11975.1	4.07E-08	2.02E-08	1.08E-04	17.5	27278.8	7.83E-05	3.85E-07
8.88E-08	22.9	48031.6	1.04E-07	3.96E-08	1.08E-04	26.7	40272.2	8.14E-05	3.53E-06
8.88E-08	13.7	36325	1.31E-07	6.69E-08	1.29E-04	11.1	20708.7	1.01E-04	7.84E-06
8.88E-08	12.5	25271.8	9.98E-08	3.58E-08	1.29E-04	15.1	28329.5	1.01E-04	8.47E-06
8.88E-08	14.7	27384.4	9.20E-08	2.79E-08	1.43E-04	11.7	26343.7	1.21E-04	1.84E-05
2.41E-07	37	258546	3.47E-07	1.73E-07	1.43E-04	21.3	42378.7	1.07E-04	4.39E-06
2.41E-07	18.6	100530	2.70E-07	9.66E-08	1.43E-04	11.6	24529.9	1.14E-04	1.10E-05
2.41E-07	21.8	129321	2.92E-07	1.18E-07	1.43E-04	13.2	25890.2	1.06E-04	2.78E-06
7.83E-07	27.2	515601	9.45E-07	3.80E-07					

Equilibrium Distribution Data (con't)

Arterial Media with Denuded Endothelium II

C_{bulk} (M)	Tissue wet wt (mg)	Tissue DPM	C_T (M)	C_b (M)	C_{bulk} (M)	Tissue wet wt (mg)	Tissue DPM	C_T (M)	C_b (M)
6.11E-11	6.7	66.8	1.08E-10	7.70E-11	1.19E-06	10	231028	1.16E-06	5.50E-07
6.11E-11	10	70.7	9.28E-11	6.16E-11	1.19E-06	19.2	441990	1.14E-06	5.28E-07
6.11E-11	5.9	65.6	1.13E-10	8.16E-11	1.19E-06	13.4	354672	1.33E-06	7.25E-07
6.11E-11	5.4	58.6	5.78E-11	2.66E-11	4.74E-06	10.7	1065.2	3.71E-06	1.29E-06
5.94E-10	15.4	291.6	7.72E-10	4.69E-10	4.74E-06	18.5	1920.6	3.85E-06	1.43E-06
5.94E-10	21.5	328.7	6.38E-10	3.35E-10	4.74E-06	16	1610.9	3.71E-06	1.29E-06
5.94E-10	14.6	230.3	6.06E-10	3.03E-10	4.74E-06	7	816.3	4.16E-06	1.74E-06
5.94E-10	8.9	166.6	6.38E-10	3.35E-10	1.40E-05	9.5	3178.5	1.25E-05	5.41E-06
1.78E-09	10.8	399	1.59E-09	6.88E-10	1.40E-05	13.8	4486.7	1.21E-05	4.94E-06
1.78E-09	11.1	473.4	1.88E-09	9.78E-10	1.40E-05	10	4947.4	1.85E-05	1.13E-05
1.78E-09	11.2	503.5	2.02E-09	1.11E-09	1.40E-05	16.2	5326.5	1.25E-05	5.35E-06
1.78E-09	11.9	539.6	2.03E-09	1.13E-09	3.58E-05	12.2	8520.6	2.64E-05	8.19E-06
4.95E-09	14.4	1647	5.58E-09	3.05E-09	3.58E-05	12.1	8489.6	2.68E-05	8.53E-06
4.95E-09	13.4	1692.5	6.08E-09	3.55E-09	3.58E-05	7.8	5183.2	2.51E-05	6.81E-06
4.95E-09	10.6	1209.1	5.42E-09	2.90E-09	3.58E-05	8.7	5319.4	2.31E-05	4.81E-06
4.95E-09	8.5	1010.5	5.60E-09	3.07E-09	5.78E-05	11.2	11040.9	3.74E-05	7.90E-06
1.45E-08	11.7	3669.6	1.56E-08	8.20E-09	5.78E-05	8.4	8297.5	3.74E-05	7.92E-06
1.45E-08	9.7	3538.7	1.78E-08	1.04E-08	5.78E-05	7	7606.7	4.64E-05	1.69E-05
1.45E-08	5.6	1757.7	1.54E-08	7.98E-09	5.78E-05	11.4	12146.5	4.19E-05	1.24E-05
1.45E-08	5.7	1969.7	1.67E-08	9.29E-09	7.76E-05	11.5	16605.1	5.53E-05	1.57E-05
4.44E-08	13.2	12574.2	4.71E-08	2.45E-08	7.76E-05	17.6	24359.5	5.29E-05	1.33E-05
4.44E-08	12.5	13981.8	5.53E-08	3.27E-08	7.76E-05	6.8	9137.9	5.09E-05	1.13E-05
4.44E-08	10.1	9659.3	4.77E-08	2.51E-08	7.76E-05	6.7	9099.8	5.14E-05	1.19E-05
4.44E-08	16.6	16322.5	4.87E-08	2.60E-08	1.01E-04	10.7	21491.5	7.70E-05	2.58E-05
1.29E-07	11	24678.2	1.11E-07	4.51E-08	1.01E-04	11.8	25886.8	8.34E-05	3.21E-05
1.29E-07	20.1	61890.5	1.54E-07	8.75E-08	1.01E-04	6	12327.1	7.79E-05	2.67E-05
1.29E-07	12.1	38375	1.57E-07	9.12E-08	1.01E-04	10.7	24964.6	9.04E-05	3.91E-05
1.29E-07	11.6	29572.4	1.26E-07	6.03E-08	1.22E-04	13.9	23932.5	6.54E-05	3.24E-06
3.98E-07	15.5	109663	3.51E-07	1.48E-07	1.22E-04	9.6	18189.8	7.27E-05	1.05E-05
3.98E-07	20.5	200150	4.82E-07	2.80E-07	1.44E-04	11.8	26957.9	8.69E-05	1.35E-05
3.98E-07	6.6	72600.6	5.46E-07	3.43E-07	1.44E-04	15.5	32884.7	8.07E-05	7.29E-06
3.98E-07	13.8	94187.1	3.39E-07	1.36E-07	1.44E-04	12.4	27749.6	8.51E-05	1.17E-05
1.19E-06	6.3	176993	1.44E-06	8.32E-07	1.44E-04	15	31781.3	8.06E-05	7.18E-06

Equilibrium Distribution Data (con't)

Adventitia I

C_{bulk} (M)	Tissue wet wt (mg)	Tissue DPM	C_T (M)	C_b (M)	C_{bulk} (M)	Tissue wet wt (mg)	Tissue DPM	C_T (M)	C_b (M)
1.42E-11	24.1	69.1	5.77E-11	4.65E-11	7.08E-07	34.9	349777	5.87E-07	2.95E-08
1.42E-11	32.1	84.3	7.38E-11	6.26E-11	7.08E-07	20.7	233052	6.54E-07	9.62E-08
1.42E-11	7.1	88.6	3.88E-10	3.76E-10	5.27E-06	13.7	854.1	4.98E-06	8.31E-07
1.42E-11	23.2	71.5	6.95E-11	5.83E-11	5.27E-06	39	1727.1	3.58E-06	-5.69E-07
2.97E-10	15.6	200.6	5.99E-10	3.65E-10	5.27E-06	24.6	1340.3	4.41E-06	2.56E-07
2.97E-10	20.1	99.6	1.63E-10	-7.09E-11	5.27E-06	14.6	914.7	4.41E-06	2.63E-07
2.97E-10	26	171.7	2.88E-10	5.41E-11	1.14E-05	49.4	6538.3	1.10E-05	2.03E-06
2.97E-10	19.8	186.8	4.30E-10	1.96E-10	1.14E-05	42.8	5886.6	1.14E-05	2.45E-06
9.86E-10	23.3	430	9.79E-10	2.03E-10	1.14E-05	15.9	2475.7	1.28E-05	3.83E-06
9.86E-10	24.7	518.8	1.12E-09	3.40E-10	1.14E-05	31.6	4375.2	1.15E-05	2.57E-06
9.86E-10	12	253.8	1.02E-09	2.48E-10	3.74E-05	27.7	10579	3.18E-05	2.40E-06
9.86E-10	13.3	256.3	9.56E-10	1.80E-10	3.74E-05	31.4	12846.5	3.45E-05	5.13E-06
3.03E-09	11.9	849.1	4.10E-09	1.72E-09	3.74E-05	49.6	18671.1	3.14E-05	2.00E-06
3.03E-09	28	1442.6	2.91E-09	5.29E-10	3.74E-05	40.3	15381.3	3.21E-05	2.66E-06
3.03E-09	31.6	1956.5	3.61E-09	1.22E-09	6.00E-05	38.5	18209.7	3.99E-05	-7.38E-06
3.03E-09	28.4	1449.5	3.02E-09	6.41E-10	6.00E-05	29.6	17435.4	4.91E-05	1.88E-06
9.42E-09	38.2	6029	9.55E-09	2.13E-09	6.00E-05	25.2	14893.9	4.93E-05	2.03E-06
9.42E-09	26.1	4155.2	9.32E-09	1.91E-09	6.00E-05	49.4	24201.9	4.11E-05	-6.10E-06
9.42E-09	18	2818.5	9.48E-09	2.06E-09	8.30E-05	18.9	12822.6	5.74E-05	-7.90E-06
9.42E-09	21.2	3175.3	9.14E-09	1.72E-09	8.30E-05	15.4	43847.1	2.41E-04	1.76E-04
2.53E-08	25.6	9823.4	2.28E-08	2.89E-09	8.30E-05	29.4	23982.6	6.81E-05	2.74E-06
2.53E-08	32.1	12822.4	2.31E-08	3.20E-09	8.30E-05	37.4	33219.7	7.46E-05	9.22E-06
2.53E-08	27.2	10280.7	2.30E-08	3.12E-09	1.00E-04	16.1	14366.6	7.44E-05	-4.46E-06
2.53E-08	9.3	4117.5	2.60E-08	6.08E-09	1.00E-04	61.6	63984.6	8.73E-05	8.51E-06
8.24E-08	26.9	41803.2	9.08E-08	2.60E-08	1.00E-04	28.9	30734.8	8.88E-05	9.95E-06
8.24E-08	18	24026.5	7.74E-08	1.25E-08	1.00E-04	27.3	29440.4	9.00E-05	1.12E-05
8.24E-08	34.4	44785.6	7.55E-08	1.07E-08	1.29E-04	41.3	40691.2	8.25E-05	-1.87E-05
8.24E-08	12.2	16339	7.75E-08	1.27E-08	1.29E-04	29.9	38166.8	1.07E-04	5.45E-06
2.38E-07	21.2	70837.8	1.95E-07	7.81E-09	1.29E-04	37.1	51334	1.16E-04	1.44E-05
2.38E-07	29.3	104593	2.09E-07	2.16E-08	1.29E-04	21.8	23977.2	9.18E-05	-9.36E-06
2.38E-07	14.1	54355.4	2.25E-07	3.82E-08	1.43E-04	24.6	36593.3	1.26E-04	1.29E-05
2.38E-07	22	82981.8	2.22E-07	3.49E-08	1.43E-04	30.7	38944	1.06E-04	-6.61E-06
7.08E-07	27.2	262038	5.59E-07	1.90E-09	1.43E-04	38.4	53796.4	1.17E-04	4.14E-06
7.08E-07	18.3	217921	6.99E-07	1.42E-07	1.43E-04	36.5	54804.6	1.25E-04	1.25E-05

Equilibrium Distribution Data (con't)

Adventitia II

C_{bulk} (M)	Tissue wet wt (mg)	Tissue DPM	C_T (M)	C_b (M)	C_{bulk} (M)	Tissue wet wt (mg)	Tissue DPM	C_T (M)	C_b (M)
1.42E-11	16.8	60	5.61E-11	4.53E-11	6.00E-05	28.6	16834.6	4.91E-05	3.59E-06
1.42E-11	25.1	57.7	3.23E-11	2.15E-11	6.00E-05	39.3	25143.3	5.35E-05	8.04E-06
1.42E-11	13.3	54.5	4.75E-11	3.67E-11	6.00E-05	45.2	29594.5	5.49E-05	9.41E-06
1.42E-11	11.8	52	4.07E-11	2.99E-11	8.30E-05	24.2	20405.2	7.15E-05	8.60E-06
2.97E-10	33.6	271.6	4.01E-10	1.76E-10	8.30E-05	34.6	25767	6.22E-05	-7.66E-07
2.97E-10	8.5	121.1	5.47E-10	3.22E-10	8.30E-05	37	33511.8	7.46E-05	1.17E-05
2.97E-10	6	116.3	6.57E-10	4.32E-10	8.30E-05	26.1	22013.2	7.04E-05	7.45E-06
2.97E-10	17.9	120.4	2.52E-10	2.76E-11	1.00E-04	40	41776.3	8.72E-05	1.13E-05
9.86E-10	20	350.7	9.04E-10	1.57E-10	1.00E-04	32.2	33452.4	8.73E-05	1.14E-05
9.86E-10	11	273.6	1.29E-09	5.48E-10	1.00E-04	34.2	32223.5	7.89E-05	2.97E-06
9.86E-10	16.7	315.4	9.67E-10	2.20E-10	1.00E-04	20	16144.9	6.73E-05	-8.62E-06
9.86E-10	16	306	9.34E-10	1.86E-10	1.29E-04	12	12549.2	8.71E-05	-1.03E-05
3.03E-09	35.8	1905.9	3.08E-09	7.87E-10	1.29E-04	31.2	35817.6	9.59E-05	-1.54E-06
3.03E-09	10.8	762.6	3.86E-09	1.57E-09	1.29E-04	25.9	36331.3	1.18E-04	2.06E-05
3.03E-09	10.1	654.1	3.51E-09	1.21E-09	1.43E-04	27.4	34779.5	1.06E-04	-2.73E-06
9.42E-09	41.2	5874.5	8.10E-09	9.56E-10	1.43E-04	34.8	44556.9	1.07E-04	-1.47E-06
9.42E-09	15	2350.2	8.81E-09	1.67E-09	1.43E-04	40.4	43174.7	8.95E-05	-1.92E-05
9.42E-09	4	930.5	1.20E-08	4.83E-09	1.43E-04	7.8	11513.3	1.25E-04	1.58E-05
9.42E-09	23.2	3478.8	8.52E-09	1.38E-09	5.27E-06	10.5	548.5	3.94E-06	-5.34E-08
2.53E-08	39.2	17524.1	2.60E-08	6.78E-09	1.14E-05	39.5	5836.3	1.23E-05	3.66E-06
2.53E-08	15.7	6226.4	2.29E-08	3.68E-09	1.14E-05	40.5	4879.7	9.98E-06	1.35E-06
2.53E-08	32.5	12295.6	2.18E-08	2.64E-09	1.14E-05	7.4	1217.4	1.40E-05	5.39E-06
8.24E-08	39.3	53564.3	7.93E-08	1.69E-08	3.74E-05	13.6	5425.4	3.36E-05	5.26E-06
8.24E-08	30.6	40290.1	7.64E-08	1.39E-08	3.74E-05	46.1	15767.8	2.86E-05	3.26E-07
8.24E-08	17.7	23308.1	7.59E-08	1.35E-08	3.74E-05	46.9	16985.9	3.03E-05	2.02E-06
2.38E-07	38.1	137942	2.11E-07	3.12E-08	3.74E-05	33.7	13270	3.30E-05	4.69E-06
2.38E-07	12.3	48732.9	2.30E-07	4.97E-08	6.00E-05	30	18543.4	5.16E-05	6.06E-06
2.38E-07	16	60016.8	2.32E-07	5.21E-08	6.00E-05	39.3	25143.3	5.35E-05	8.04E-06
7.08E-07	20	216700	6.29E-07	9.22E-08	6.00E-05	45.2	29594.5	5.49E-05	9.41E-06
7.08E-07	17.6	207348	6.84E-07	1.47E-07	8.30E-05	34.6	25767	6.22E-05	-7.66E-07
7.08E-07	19.6	225170	6.67E-07	1.30E-07	8.30E-05	37	33511.8	7.46E-05	1.17E-05
5.27E-06	20.2	1345.2	5.47E-06	1.47E-06	8.30E-05	26.1	22013.2	7.04E-05	7.45E-06
5.27E-06	16.6	938.5	4.48E-06	4.82E-07	1.00E-04	40	41776.3	8.72E-05	1.13E-05
5.27E-06	10.5	548.5	3.94E-06	-5.34E-08	1.00E-04	34.2	32223.5	7.89E-05	2.97E-06
1.14E-05	17	2419.6	1.18E-05	3.12E-06	1.00E-04	20	16144.9	6.73E-05	-8.62E-06
1.14E-05	39.5	5836.3	1.23E-05	3.66E-06	1.29E-04	12	12549.2	8.71E-05	-1.03E-05
1.14E-05	40.5	4879.7	9.98E-06	1.35E-06	1.29E-04	31.2	35817.6	9.59E-05	-1.54E-06
1.14E-05	7.4	1217.4	1.40E-05	5.39E-06	1.29E-04	25.9	36331.3	1.18E-04	2.06E-05
3.74E-05	13.6	5425.4	3.36E-05	5.26E-06	1.29E-04	11.6	13768.7	9.98E-05	2.37E-06
3.74E-05	46.1	15767.8	2.86E-05	3.26E-07	1.43E-04	27.4	34779.5	1.06E-04	-2.73E-06
3.74E-05	46.9	16985.9	3.03E-05	2.02E-06	1.43E-04	34.8	44556.9	1.07E-04	-1.47E-06
3.74E-05	33.7	13270	3.30E-05	4.69E-06	1.43E-04	40.4	43174.7	8.95E-05	-1.92E-05
6.00E-05	30	18543.4	5.16E-05	6.06E-06	1.43E-04	7.8	11513.3	1.25E-04	1.58E-05

8.6. Urinary Inulin Clearance Following Perivascular Administration

Native				
Rat #	L9	L11	L12	L13
DPM Injected	53,788	53,788	53,788	53,788
		Urine Samples		
time (min)	DPM	DPM	DPM	DPM
15	84.9	213.2	210.2	113.0
30	429.7	712.3	100.6	593.8
45	107.9	864.6	1078.8	1044.2
60	1189.7	818.8	1191.5	1478.7
75	1287.6	898.8	1247.4	1532.1
90	1044.7	1490.7	1438.7	1615.4
105	1208.0	1233.8	1450.3	
120	1221.2	1190.7	1308.7	3310.6
135	1194.9	1084.1	1298.7	
150	1210.6	1140.4	1513.2	2599.5
165	1026.5	790.8	1535.9	
180	761.1	1259.5	1215.5	3151.9
195	1309.8	1104.2	1276.5	
210	1100.3	849.2	1216.3	2659.5
225	981.3	898.2	1257.9	
240	968.6	1244.4	1353.3	1822.0

Ligature Occluded				
Rat #	L7	L15	L16	L17
DPM Injected	53,788	12,616	12,616	12,616
		Urine Samples		
time (min)	DPM	DPM	DPM	DPM
15	286.5	485.4	39.5	36.4
30	828.3	202.7	138.5	180.8
45	1047.2	251.3	179.5	219.8
60	1344.1	294.0	166.6	495.5
75	1274.7	305.3	209.7	
90	1368.5	293.5	213.3	631.6
105	1245.5			
120	1274.9	602.5	347.0	633.3
135	1212.4			
150	928.7	578.6	384.6	603.4
165	691.1			
180	819.6	511.9	314.1	611.2
195	1235.1			
210	983.0	467.7	454.4	518.2
225	1159.6			
240	984.6	471.1	347.1	464.8

Urinary inulin clearance following perivascular administration (con't)

Wrapped				
Rat #	L39	L41	L43	L42
DPM Injected	77,992	77,992	77,736	77,992
		Urine Samples		
time (min)	DPM	DPM	DPM	DPM
15	24.8	37.4	123.0	51.1
30	25.8	40.7	430.7	35.3
45	19.3	29.9	422.0	22.4
60	33.2	35.4	689.3	52.4
90	60.5	37.4	1559.1	56.9
120	50.5	28.7	1580.0	60.0
150	100.6	41.4	792.9	59.7
180	80.1	198.6	773.9	40.7
210	108.3	47.9	180.2	53.6
240	85.6	46.8	1354.2	66.5

Wrapped & Occluded				
Rat #	L35	L36	L38	L40
DPM Injected	78,423	78,423	78,423	78,423
		Urine Samples		
time (min)	DPM	DPM	DPM	DPM
15	40.1	44.4	53.2	26.7
30	79.1	59.5	58.7	176.0
45	152.1	56.8	59.0	174.9
60	222.1	72.1	50.4	189.5
90	591.5	126.8	80.9	609.0
120	639.3	227.3	73.3	602.3
150	792.6	82.3	64.6	990.9
180	751.2	85.4	53.7	686.9
210	737.6	94.2	77.5	736.7
240	676.4	107.1	57.0	503.8

Background		28.7	DPM

8.7. Heparin Deposition Following Administration from Poloxamer

Native					
Rat #		r16	r17	r18	r19
Deposited DPM	L carotid	34555.1	16237.4	14517.2	36537.4
	A Aorta	256.1	169.6	345.3	224
	Iliac		119.5	151.6	341.7
	Femoral	115.1	73.8	176.9	122.1
	Liver	833.6	339.8	408.2	400.1
Dry Mass (mg)	L carotid	1.2	1.2	1.1	1.8
	A Aorta	4.9	2.8	4.3	2.4
	Iliac		1.8	4.3	2.1
	Femoral	1.0	0.7	1.3	0.4
	Liver	26.2	10.5	28.8	13.8
Deposition (μg/mg/mg)	L carotid	13.2281	6.2032	6.0475	9.3255
	A Aorta	0.0182	0.0177	0.0303	0.0310
	Iliac		0.0147	0.0096	0.0613
	Femoral	0.0244	0.0077	0.0406	0.0690
	Liver	0.0136	0.0122	0.0055	0.0113

Ligature Occluded					
Rat #		r21	r22	r23	r32
Deposited DPM	L carotid	21813.9	14357.9	17429.1	45058.8
	A Aorta	149.0	226.0	264.2	185.9
	Iliac	173.7	227.4	143.2	192.2
	Femoral	809.2	104.4	91.3	144.4
	Liver	820.7	427.7	414.3	350.6
Dry Mass (mg)	L carotid	1.3	0.7	1.7	1.0
	A Aorta	2.0	4.1	4.4	3.2
	Iliac	3.6	7.9	3.2	2.4
	Femoral	0.7	1.3	0.9	1.0
	Liver	25.9	18.1	21.3	22.9
Deposition (μg/mg/mg)	L carotid	7.700	9.398	4.701	20.707
	A Aorta	0.020	0.018	0.021	0.018
	Iliac	0.014	0.010	0.012	0.025
	Femoral	0.491	0.015	0.015	0.038
	Liver	0.013	0.009	0.008	0.006

Heparin Deposition Following Administration from Poloxamer (con't)

Wrapped Rat #		r23	r26	r28	r30
Deposited DPM	L carotid	56322.3	16367.6	61945.2	53077.9
	A Aorta	448	535.7	125.1	182.8
	Iliac	148.7	105.8	80.4	190.7
	Femoral	82.1	72.4	65.2	107.2
	Liver	258.5	282	201	300.6
Dry Mass (mg)	L carotid	2.2	1.3	1.2	1.7
	A Aorta	4.6	3.5	8.4	3.9
	Iliac	2	1.5	4	4.5
	Femoral	1.1	0.5	0.6	0.8
	Liver	17.8	19.3	20.6	21.1
Deposition (μg/mg/mg)	L carotid	11.603	5.772	23.732	14.352
	A Aorta	0.039	0.062	0.003	0.014
	Iliac	0.020	0.013	0.002	0.013
	Femoral	0.008	0.009	0.002	0.026
	Liver	0.005	0.005	0.003	0.005

Intraperitoneal Rat #		r25	r27	r29	r31
Deposited DPM	L carotid	126.9	73.3	95.7	228
	A Aorta	108.3	135.5	662.8	850.1
	Iliac	131.8	100.9	171.1	243.7
	Femoral	85	91.2	64.2	210.2
	Liver	325	331.9	238.5	659.2
Dry Mass (mg)	L carotid	1.2	1.1	1.3	0.9
	A Aorta	4	8.4	4	5.5
	Iliac	4.6	7.2	5.4	4.8
	Femoral	0.7	0.8	0.6	0.7
	Liver	20.4	28.4	13.9	33.8
Deposition (μg/mg/mg)	L carotid	0.025	0.005	0.012	0.085
	A Aorta	0.005	0.004	0.069	0.066
	Iliac	0.007	0.002	0.009	0.017
	Femoral	0.015	0.017	0.002	0.097
	Liver	0.006	0.004	0.006	0.008

INJECTED DOSE	2,172,969	DPM
BACKGROUND	62.1	DPM

8.8 Perivascular Vs Endovascular Heparin Delivery to Rabbit iliac Arteries

Rabbit #	Artery #	<------Artery------> dry mass (mg)	DPM	<-------- mass (mg)	Initial Gel DPM	--------> activity (DPM/mg)	Deposition / [Gel]o DPM/mg / (DPM / mg)
Perivascular							
FR13	7	1.3	1789.8	100	7123630.7	71162.2	0.02213
	8	0.9	1354.3	100	7048050.8	71162.2	0.02396
	9	1.1	2837.2	100	7176988.1	71162.2	0.04189
	10	1	2476.7			71162.2	0.04012
Fr14	8	1.3	1148	100	7123630.7	71162.2	0.01396
	9	1.1	656.8	100	7048050.8	71162.2	0.00912
	10	1.1	1829.2	100	7176988.1	71162.2	0.02674
	11	1.1	992.5			71162.2	0.01417
FR24	8	1.8	2981	100	6541863.9	62829.7	0.03049
	9	1.8	1943.2	100	6407135.8	62829.7	0.01969
	10	1.6	2961.8	145	8554870.0	62829.7	0.03408
	11	1.4	2327.1			62829.7	0.03046
Endovascular							
FR15	4	1.9	3018.9	50	949761.1	18995.2	0.09678
	5	2.2	7972.2	50	949761.1	18995.2	0.22303
	6	1.2	3140.9	50	949761.1	18995.2	0.15953
	7	2.1	7721.1			18995.2	0.22624
	9	1.1	695.1			18995.2	0.03632
	10	1.1	5505.8			18995.2	0.30719
FR25	4	1.5	457	100	2055120.7	20551.2	0.01553
	5	1.7	3714.1	50	1027560.3	20551.2	0.12338
	6	1.9	9963.9	50	1027560.3	20551.2	0.29870
	7	1.5	3536.8			20551.2	0.13307
	8	1.5	14286.7			20551.2	0.54333
FR28	4	1.5	4478	100	2319000.0	23190.0	0.14976
	5	1.7	6978	100	2319000.0	23190.0	0.20675
	6	2	7686.4	100	2319000.0	23190.0	0.19370
	7	1.5	12079.1			23190.0	0.40684
Bkmd			50	DPM			

8.9. Code for Simulations of Arterial Deposition and Distribution

```
% Matlab Code of Simulations of Heparin Delivery to LAD from Endovascular Hydrogel

clear
hold off
tic
%μm, mg, s units
dgel = 2.37e-7*1e4*1e4;          % Diffusivities :    gel
dmed = 7.73e-8*1e4*1e4;          %                   media
dadv = 1.21e-7*1e4*1e4;          %                   adventitia
dmyo = dadv;                     %                   myocardium

cgi= 1/3        ;                % mg/ml = g/l       initial gel concentration

mw = 14000          ;
cgi = cgi / mw ;        % M
epm =.612           ;            %fractional volume of distribution:    media
epa = 0.846     ;                %                                      adventitia
epy =.612           ;            %                                      myocardium
epg = 1             ;            %                                      gel
btm = 2.67e-6   ;       % M      %Binding site density
bta = 2.21e-9   ;       % M
bty = bta ;
kdm = 5.30e-6   ;       % M      %average binding affinity
kda = 8.09e-9   ;       % M
kdy = kda ;

outt = [];
time = [];
lgel = 70   ;                    % Length of each layer
lmed = 160;
ladv = 40  ;
lmyo = 200;

ngel = 5;                        % N
nmed = 20;
nadv = 5;
nmyo=  10;

tci = log(2) * 20*60 ;           % time constant for heparin internalization
tau      = 4.18E+01      ;       % time constant for myocardial clearance
cyinf0  = 1.58E-07 ; %   (M)    % initial myocardial loading

dxa = ladv/nadv ;                % Width of computational element
dxg = lgel/ngel;
dxm = lmed/nmed ;
dxy = lmyo/nmyo ;

dtg = dxg^2/dgel/2.01 ;          % time step appropriate for each layer
dtm = dxm^2/dmed/2.01 ;
dta = dxa^2/dadv/2.01 ;
dty = dxy^2/dmyo/2.01 ;

dt = min([dta dtm dtg dty])
%dt = round(dt*10)/10  ;
%dt = 6
% initial concentration of drug in gel
```

```
cas= zeros(1,nadv);                    % concentrations        : soluble
cab= zeros(1,nadv);                    %                      : bound
cat= zeros(1,nadv);                    %                      : total
cmb= zeros(1,nmed);
cmt= zeros(1,nmed);
cms=zeros(1,nmed);
cint = cms;
cyns= zeros(1,nmyo);
cyb=  zeros(1,nmyo);
cyt=  zeros(1,nmyo);
cys=  zeros(1,nmyo);
cg =  zeros(1,ngel);
time = [];
avgtot= [];
avgsol = [];
avgint=[];
 for i= 1:ngel , cg(i)=cgi ; , end
%  for i= 1:ngel , cg(i)=0  ; , end    %     for cg in gel is zero

%  set up dimensional coordinates of each element
for i = 1: ngel,     x(i)=dxg*(i-1/2) ; , end
for i = 1 : nmed, x(i+ngel) =dxg*ngel+dxm*(i-1/2) ; xb(i) =x(i+ngel);, end
for i = 1 :nadv, x(i+ngel+nmed) = dxg*ngel+dxm*nmed+dxa*i-dxa/2 ;
                              xb(i+nmed)= x(i+ngel+nmed); , end
for i = 1 :nmyo, x(i+ngel+nmed+nadv) = dxg*ngel+dxm*nmed+dxa*nadv+dxy*(i-1/2);
                              xb(i+nmed+nadv)= x(i+ngel+nmed+nadv); , end

outt = [xb'] ;
outb = [xb'];

coefg = dt*dgel/dxg/dxg ;
coefm = dt*dmed/dxm/dxm ;
coefa = dt*dadv/dxa/dxa ;
coefy = dt*dmyo/dxy/dxy ;

ntime = 3600* 1/dt  * 180/60
ct = 0 ;

termm = 2*dmed/dxm;
terma = 2*dadv/dxa;
termy = 2*dmyo/dxy;
termg = 2*dgel/dxg;
          cg1i = 0;

for j = 1:ntime
          cyinf = cyinf0*exp(-j*dt/3600/tau)   ;

% Interfaces:  lower edge
          cy1i  = (terma*cas(nadv)+termy*cys(1))/(terma*epa/epy+termy);
          ca1i  = (termm*cms(nmed)+terma*cas(1))/(termm*epm/epa+terma);
          cm1i  = (termg* cg(ngel)+termm*cms(1))/(termg*epg/epm+termm);

% Interfaces:  upper edge
          cani  = cy1i *epa/epy;
          cmni  = ca1i *epm/epa;
          cgni  = cm1i *epg/epm;
```

```
        cgn(1) = cg(1) + coefg*(2*cg1i-3*cg(1)+cg(2)) ;
        cmns(1) = cms(1) + coefm*(2*cm1i-3*cms(1)+cms(2)) ;
        cans(1) = cas(1) + coefa*(2*ca1i-3*cas(1)+cas(2)) ;
        cyns(1) = cys(1) + coefy*(2*cy1i-3*cys(1)+cys(2)) ;

        cyns(nmyo) = cys(nmyo) + coefy*(cys(nmyo-1) - 3* cys(nmyo) +2* cyinf);
        cans(nadv) = cas(nadv) + coefa*(cas(nadv-1) - 3* cas(nadv) +2* cani);
        cmns(nmed) = cms(nmed) + coefm*(cms(nmed-1) - 3* cms(nmed) +2* cmni);
        cgn(ngel)  = cg(ngel)  + coefg*(cg(ngel-1)  - 3* cg(ngel) +2* cgni);

        dfg = coefg * diff(cg)  ;
        dfm = coefm * diff(cms) ;
        dfa = coefa * diff(cas) ;
        dfy = coefy * diff(cys) ;

        cgn(2:ngel-1) = cg(2:ngel-1) + diff(dfg(1:ngel-1));
        cmns(2:nmed-1) = cms(2:nmed-1) + diff(dfm(1:nmed-1));
        cans(2:nadv-1) = cas(2:nadv-1) + diff(dfa(1:nadv-1));
        cyns(2:nmyo-1) = cys(2:nmyo-1) + diff(dfy(1:nmyo-1));

        cg = cgn;

% Redistribution between soluble and bound phases
        cmt = cmns + cmb ;
        b =  btm - cmt+epm*kdm  ;
        c = - cmt *epm*kdm      ;
        cms = (-b +sqrt(b.^2 - 4 * c))/ 2 ;
        cmb = cmt - cms                   ;

        cat = cans + cab ;
        b =  bta - cat+epa*kda  ;
        c = - cat *epa*kda      ;
        cas = (-b +sqrt(b.^2 - 4 * c))/ 2 ;
        cab = cat - cas     ;

        cyt = cyns + cyb ;
        b =  bty - cyt+epy*kdy  ;
        c = - cyt *epy*kdy      ;
        cys = (-b +sqrt(b.^2 - 4 * c))/ 2 ;
        cyb = cyt - cys     ;

% internalization, assume 0.5% of bound is internalized with t1/2 = 15 minutes
% this is applicable if all binding sites are on SMC surface and therefore
% is an over estimation

        interf = cmb * 0.005      * (1- exp(-dt/tci)) ;
        cint = cint + interf        ;
        cmb = cmb - interf          ;
        if ~rem(j,100)
                time = [time j*dt/3600 ];
                avgint = [ avgint sum(cmt+cint)/length(cmt)/cgi ];
                avgtot = [ avgtot sum(cmt)/length(cmt)/cgi ];
                avgsol = [avgsol sum(cms)/length(cms)/cgi ] ;
        end
end
outt = [time' avgint' avgtot' avgsol' ];
plot (x, [cg (cmt+cint) cat cyt]/cgi,'r',x, [cg (cms) cas cys]/cgi,'b')
toc
```

9. NOMENCLATURE

A_l	Cross sectional area of arterial lumen
b_{end}	Coefficient of endothelial resistance, (0- absent, 1- present)
B	Binding site density (specific and nonspecific) of compound in a tissue
c	Concentration of compound in a volume of tissue or fluid
d	Hydraulic diameter of arterial cross section
D	Effective diffusivity of compound in a tissue or solution
f^C	Convective hindrance coefficient
f^D	Diffusive hindrance coefficient
j	Mass transfer rate of solute
j''	Mass flux of solute
k_{on}	Rate of association of a compound to the average binding site
k_{off}	Rate of dissociation of a compound from the average binding site
K_d	Dissociation constant of ligand from receptor
K'	Dissociation constant of compound from average binding site in a tissue
l	Average thickness of a tissue layer, length scale
L	Length of an artery
N	Total number of computational elements in a tissue layer
P	Perimeter of arterial cross section, length of Internal Elastic Lamina (IEL)
Pe	Peclet number, nondimensional ratio of convective to diffusive forces
R	Resistance to (diffusive) transport
t	Time
U	Convective velocity of solute in hydraulic flow
u	Convective hydraulic velocity in transmural direction
$\bar{v}_l$	Average fluid velocity flowing in arterial lumen
V_a	Tissue Volume
x	Transmural coordinate
ΔH	Hydrostatic head of the perfusate in the artery
ΔP	Hydrostatic pressure difference
ε'	Fractional space in which drug can distribute through a tissue
ψ	Measured mass transfer dondimensionalized by the diffusive driving potential and diffusive resistance

Subscripts

a	Accessible space in tissue for solute
adv	Adventitial
aq	Aqueous solutions
b	Reversibly bound drug phase or occupied binding sites
bl	Boundary layer
bulk	Bulk phase or external solution
ec	Extracellular
end	Endothelial
f	Free or unoccupied binding sites
gel	Photopolymerized hydrogel
h	Heparin
*h**	^{3}H-heparin
ic	Intracellular, internalized
init	Initial, in uniformly loaded artery and photopolymerized hydrogel
med	Medial
mem	Membrane
myo	Myocardial
n	Index for computational elements in a tissue layer
P	Perfusate, endovascular compartment
plasma	Plasma
s	Soluble
T	Total noninternalized (soluble and reversibly bound) drug phase
pv	Perivascular
κ	Partition coefficient of drug into the accessible volume

10. REFERENCES

1. Wolinsky H, Glagov S. Nature of species differences in the medial distribution of aortic vasa vasorum in mammals. *Circ Res.* 1967;20:409-421.

2. Rubanyi GM. Endothelium-derived relaxing and contracting factors. *J Cell Biochem.* 1991;46:27-36.

3. Ohno M, Gibbons GH, Dzau VJ, Cooke JP. Shear stress elevates endothelial cGMP. Role of a potassium channel and G protein coupling. *Circulation.* 1993;88:193-197.

4. Furchgott RF, Vanhoutte PM. Endothelium-derived relaxing and contracting factors. *FASEB J.* 1989;3:2007-2018.

5. Schweigerer L, Nuefeld G, Friedman J, Abraham JA, Fiddes JC, Gospodarowicz D. Capillary endothelial cells express basic fibroblast growth factor, a mitogen that stimulates their own growth. *Nature (lond).* 1987;325:257-259.

6. Conolly DT, Stoddard BL, Harakas NK, Feder J. Human fibroblast-derived growth factor is a mitogen and chemoattractant for endothelial cells. *Biochem Biophys Res Comm.* 1987;144:705-712.

7. Lidner V, Majack RA, Reidy MA. Basic fibroblast growth factor stimulates endothelial regrowth and proliferation in denuded arteries. *J Clin Invest.* 1990;85:2004-2008.

8. Lidner V, Reidy MA. Proliferation of smooth muscle cells after vascular injury is inhibited by an antibody against basic fibroblast growth factor. *Proc Natl Acad Sci USA.* 1991;88:3739-3743.

9. Lidner V, Lappi DA, Baird A, Majack RA, Reidy MA. Role of basic fibroblast growth factor in vascular lesion formation. *Circ Res.* 1991;68:106-113.

10. Clowes AW, Clowes MM. Kinetics of cellular proliferation after arterial injury. II: Inhibition of smooth muscle cell growth by heparin. *Lab Invest.* 1985;52:611-616.

11. Castellot JJJ, Addonizio ML, Rosenberg RD, Karnovsky MJ. Cultured endothelial cells produce a heparin-like inhibition of smooth muscle growth. *J Cell Biol.* 1981;90:372-379.

12. Castellot JJJ, Cochran DL, Karnovsky MJ. Effect of Heparin on Vascular Smooth Muscle Cells. I. Cell Metabolism. *J Cell Physiol.* 1985;124:21-28.

13. Clowes AW, Karnovsky MJ. Suppression by heparin of smooth muscle cell proliferation in injured arteries. *Nature.* 1977;265:625 - 626.

14. Ross R. The pathogenesis of atherosclerosis: a perspective for the 1990s. *Nature.* 1993;362:801-809.

15. Ross R. The pathogenesis of atherosclerosis. *New Eng J Med.* 1986;314:488-500.

16. Ip JH, Fuster V, Badimon L, Badimon J, Taubman MB, Chesebro JH. Syndromes of accelerated atherosclerosis: Role of vascular injury and smooth muscle proliferation. *J Am Coll Cardiol.* 1990;15:1667-1687.

17. Reidy MA, Ringerle J, Lindner V. Factors controlling the development of arterial lesions after injury. *Circulation.* 1992;86:III43-III46.

18. Clowes AW, Reidy MA. Prevention of restenosis after vascular reconstruction: Pharmacologic control of intimal hyperplasia. *J Vasc Surg.* 1991;13:885-891.

19. Landau C, Lange RA, Hillis D. Percutaneous transluminal coronary angioplasty. *New Eng J Med.* 1994;330:981-993.

20. Faxon DP, Currier JW. Prevention of post-PTCA restenosis. *Ann NY Acad Sci.* 1995;748:419-427.

21. Castellot JJJ, Wright TC, Karnovsky MJ. Regulation of vascular smooth muscle cell growth by heparin and heparan sulphate. *Semin Thromb Hemost.* 1987;13:489-503.

22. Hoover RL, Rosenberg R, Haering w, Karnovsky MJ. Inhibition of rat arterial smooth muscle cell proliferation by heparin. II. in vitro studies. *Circ Res.* 1980;47:578-583.

23. March KL, Mohanraj S, Ho PPK, Wilensky RL, Hathaway DR. Biodegradable microspheres containing a colchicine analogue inhibit DNA synthesis in vascular smooth muscle cells. *Circulation.* 1994;89:1929-1933.

24. Weissberg PL, Grainger DJ, Shanahan CM, Metcalfe JC. Approaches to the development of selective inhibitors of vascular smooth muscle cell proliferation. *Cardiovasc Res.* 1993;27:1191-1198.

25. Naftilan AJ. The role of angiotensin II in vascular smooth muscle cell growth. *Journal of Cardiovascular Pharmacology.* 1992;20 (Suppl I):S37-S40.

26. Edelman ER, Adams DA, Karnovsky MJ. Effect of controlled adventitial heparin delivery on smooth muscle cell proliferation following endothelial injury. *Proc Natl Acad Sci USA.* 1990;87:3773-3777.

27. Guyton J, Rosenberg R, Clowes A, Karnovsky M. Inhibition of rat arterial smooth muscle cell proliferation by heparin I. In vivo studies with anticoagulant and non-anticoagulant heparin. *Circ Res.* 1980;46:625-634.

28. Muller DWM, Gordon D, Topol EJ, Levy RJ, Golomb G. Sustained-release local hirulog therapy decreases early thrombosis but not neointimal thickening after arterial stenting. *Am Heart J.* 1996;131:211-218.

29. Villa A, Guzman L, Chen W, Golomb G, Levy R, Topol E. Local delivery of dexamethasone for prevention of neointimal proliferation in a rat model of balloon angioplasty. *J Clin Invest.* 1994;93:1243-1249.

30. Muller DWM, Golomb G, Gordon D, Levy RJ. Site-specific dexamethasone delivery for the prevention of neointimal thickening after vascular stent implantation. *Coron Art Dis.* 1994;5:435-442.

31. Powell JS, Clozel JP, Muller RKM, Kuhn H, Hefti F, Hosang M, Baumgartner HR. Inhibitors of angiotensin-converting enzyme prevent myointimal proliferation after injury. *Science.* 1989;245:186-188.

32. Muller DWM, Ellis SG, Topol EJ. Colchicine and antineoplastic therapy for the prevention of restenosis after percutaneous coronary interventions. *J Am Coll Cardiol.* 1991;17:126B-131B.

33. Gradus-Pizlo I, Wilensky RL, March KL, Fineberg N, Michaels M, Sandusky GE, Hathaway DR. Local delivery of biodegradable microparticles containing colchicine or a colchicine analogue: effects on restenosis and implications for catheter-based drug delivery. *J Am Coll Cardiol.* 1995;26:1549-1557.

34. Lambert T, Dev V, Rechavia E, Forrester JS, Litvack F, Eigler NL. Localized arterial wall drug delivery from a polymer-coated removable metallic stent. Kinetics, distribution, and bioactivity of forskolin. *Circulation.* 1994;90:1003-1011.

35. Strauss BH, Wilson RA, Houten Rv, Suylen Rv, Murphy ES, Escaned J, Verdouw PD, Serruys PW, Giessen WJvd. Late effects of locally delivered mitomycin c on formation of neointima and on vasomotor response to acetylcholine. *Coron Art Dis.* 1994;5:633-641.

36. Hansson GK, Holm J. Interferon-gamma inhibits arterial stenosis after injury. *Circulation.* 1991;84:1266-1272.

37. Edelman ER, Simons M, Sirois MG, Rosenberg RD. C-myc in vasculoproliferative disease. *Circ Res.* 1995;359:69-73.

38. Shi Y, Fard A, Galeo A, Hutchinson HG, Vermani P, Dodge GR, Hall DJ, Shaheen F, Zalewski A. Transcatheter delivery of c-myc antisense oligomers reduces neointimal formation in a porcine model of coronary artery balloon injury. *Circulation.* 1994;90:9440951.

39. Simons M, Edelman ER, Langer R, DeKeyser JL, Rosenberg RD. Antisense *c-myb* oligonucleotides inhibit intimal arterial smooth muscle accumulation *in vivo. Nature.* 1992;359:69-73.

40. Pastore CJ, Isner JM, Bacha PA, Kearney M, Pickering JG. Epidermal growth factor receptor-targeted cytotoxin inhibits neointimal hyperplasia in vivo. *Circ Res.* 1995;77:519-529.

41. Katzung BG. *Basic and clinical pharmacology.* Ed. 6 ed. Norwalk, CT: Appleton and Lange, 1995.

42. Gervin AS. Complications of heparin therapy. In: Kg S, al. e, eds. *Venous surgery in the lower extremities.* St. Louis: Green; 1975:307-25.

43. Porter J, Fick H. Drug-related deaths among medical in patients. *JAMA.* 1977;237:879.

44. Mitchel JF, Fram DB, Palme DF, Foster R, Hirst JA, Azrin MA, Bow LA, Eldin AM, Waters DD, Mckay RG. Enhanced Intracoronary thrombolysis with urokinase using a novel, local drug delivery system. *Circulation.* 1995;91:785-793.

45. Hong MK, Wong SC, Farb A, Mehlman MD, Virmani R, Barry JJ, Leon MB. Feasibility and drug delivery efficiency of a new balloon angioplasty catheter capable of performing simultaneous local delivery. *Coron Art Dis.* 1993;4:1023-1027.

46. Wolinsky H, Thung SN. Use of perforated balloon catheter to deliver concentrated heparin into the wall of the normal canine artery. *J Am Coll Cardiol.* 1990;15:475-81.

47. Wilensky RL, March KL, Hathaway DR. Direct intraarterial wall injection of microparticles via a catheter: a potential drug delivery strategy following angioplasty. *Am Heart J.* 1991;122:1136-1140.

48. Sawhney AS, Pathak CP, Hubbell JA. Bioerodible hydrogels based on photopolymerized poly(ethylene glycol)-co-poly(alpha-hydroxy acid) diacrylate macromers. *Macromolecules.* 1993;26:581-587.

49. Hill-West JL, Chowdhury SM, Slepian MJ, Hubbell JA. Inhibition of thrombosis and intimal thickening by in situ photopolymerization of thin hydrogel barriers. *Proc Natl Acad Sci USA.* 1994;91:5967-5971.

50. Slepian MJ. Polymeric endoluminal paving: Evolving therapeutic methods extending the spectrum of local endovascular interventions. In: Liermann D, eds. *Stents: State of the art and future developments.* Morin Heights, Canada: Polyscience Publications, Inc.; 1995:339-355.

51. Rogers C, Karnovsky MJ, Edelman ER. Inhibition of experimental neointimal hyperplasia and thrombosis depends on the type of vascular injury and the site of drug administration. *Circulation.* 1993;88:1215-1221.

52. Rogers C, Edelman ER. Controlled release of heparin reduces neointimal hyperplasia in stented rabbit arteries: Ramifications for local therapy. *J Interv Cardiol.* 1992;5:195-202.

53. Lovich MA, Edelman ER. Tissue average binding and equilibrium distribution: an example with heparin in arterial tissues. *Biophys J.* 1996;70:1553-1559.

54. Dayton S, Hashimoto S. Recent advances in molecular pathology: a review. *Exp Mol Path.* 1970;13:253-268.

55. Zilversmit DB. Cholesterol flux in the atherosclerotic plaque. *Ann NY Acad Sci.* 1968;149:710-724.

56. Rutledge JC, Curry F-RE, Lenz JF, Davis PA. Low density lipoprotein transport across a microvascular endothelial barrier after permeability is increased. *Circ Res.* 1990;66:486-495.

57. Lin S-J, Jan K-M, Schuessler G, Weinbaum S, Chien S. Enhanced macromolecular permeability of aortic endothelial cells in association with mitosis. *Atherosclerosis.* 1988;73:223-232.

58. Chien S, Lin S-J, Weinbaum S, Lee MML, Jan K-M. The role of arterial endothelial cell mitosis in macromolecular permeability. *Adv Exp Med Bio.* 1988;242:59-73.

59. Truskey GA, Roberts WL, Hermann RA, Malinauskas RA. Measurment of endothelial permeability to 125I-low density lipoproteins in rabbit arteries by use of en face preparations. *Circ Res.* 1992;71:883-897.

60. Morrel EM, Holland JA, Pritchard KA, Colton CK, Stemerman MB. Endothelial cell perturbation and low-density lipoprotein: Quantitative autoradiography. *Ann NY Acad Sci.* 1987;516:412-417.

61. Chuang PT, Cheng HJ, Lin SJ, Jan KM, Lee MML, Chien S. Macromolecular transport across arterial and venous endothelium in rats: Studies with Evans Blue-albumin and horseradish peroxidase. *Arteriosclerosis.* 1990;10:188-197.

62. Bell FP, Adamson IL, Schwartz CJ. Aortic endothelial permeability to albumin: Focal and regional patterns of uptake and transmural distribution of 131I-albumin in the young pig. *Exp Mol Path.* 1974;20:57-68.

63. Bratzler RL, Chisolm GM, Colton CK, Smith KA, Zilversmit DB, Lees RS. The distribution of labeled low-density lipoproteins across the rabbit thoracic aorta in vivo. *Atherosclerosis.* 1977;28:289-307.

64. Tompkins RG, Yarmush ML, Schnitzer JJ, Colton CK, Smith KA, Stemerman MB. Low-density lipoprotein transport in blood vessel walls of squirrel monkeys. *Am J Physiol.* 1989;257:H452-H464.

65. Curmi PA, Juan L, Tedgui A. Effect of transmural pressure on low density lipoprotein and albumin transport and distribution across the intact arterial wall. *Circ Res.* 1990;66:1692-1702.

66. Scott PJ, Hurley PJ. The distribution of radio-iodinated serum albumin and low-density lipoprotein in tissues and the arterial wall. *Atherosclerosis.* 1971;11:77-103.

67. Ghosh S, Finkelstein JN, Moss DB, Schweppe JS. Evaluation of the permeability parameters (influx, efflux, and volume of distribution) of arterial wall for LDL and other proteins. In: Day CE, eds. *Atherosclerosis:Drug Discovery.* New York: Plenum Press; 1976:191-204.

68. Bretherton KN, Day AJ, Skinner SL. Effect of hypertension on the entry of 125I-labeled low denisty lipoprotein into the aortic intima in normal-fed rabbits. *Atherosclerosis.* 1976;24:99-106.

69. Calvert GD, Scott PJ, Sharpe DN. The plasma and tissue turnover and distribution of two radio-iodine labelled pig plasma low dendity lipoproteins. *Atherosclerosis.* 1975;22:601-628.

70. Duncan LE, Buck K, Lynch A. Lipoprotein movement through canine aortic wall. *Science.* 1963;142:972-973.

71. Fry DL, Cornhill JF, Sharma H, Pap JM, Mitschelen J. Uptake of low density lipoprotein, albumin, and water by deendothelialized in vitro minipig aorta. *Arteriosclerosis.* 1986;6:475-490.

72. Okishio T. Studies on the transfer of 131I-labelled serum lipoproteins into the aorta of rabbits with experimental atherosclerosis. *Med J Osaka Univ.* 1961;11:367-381.

73. Stemerman MB, Morrel EM, Burke KR, Colton CK, Smith KA, Lees RS. Local variation in arterial wall permeability to low density lipoprotein in normal rabbit aorta. *Arteriosclerosis.* 1986;6:64-69.

74. Virag S, Pozsonyi T, Denes R, Gero S. Uptake of 125I-labeled β-lipoprotein by the aortas of animals differently susceptible to cholesterol induced atherosclerosis. *Atherosclerosis Res.* 1968;8:859-860.

75. Adams CWM, Morgan RS, Bayliss OB. The differntial entry of [125I]albumin into mildly and severely atheromatous rabbit aortas. *Atherosclerosis.* 1970;11:119-124.

76. Bratzler RL, Chisolm GM, Colton CK, Smith KA, Zilversmit DB, Lees RS. The distribution of labeled albumin across the rabbit thoracic aorta in vivo. *Circ Res.* 1977;40:182-190.

77. Caro CG, Ebel W, Laver-Rudich Z, Liron N, Meyer F. Steady albumin transport in the rabbit common caraotid artery. *J Phys.* 1979;289:497-511.

78. Caro CG, Lever MJ, Laver-Rudich Z, Meyer F, Liron N, Ebel W, Parker KH, Winlove CP. Net albumin transport across the wall of the rabbit common caraotid artery perfused in situ. *Atherosclerosis.* 1980;37:497-511.

79. Colton CK, Schneiderman G, Ramirez CA, Smith KA, Lees RS, Stemerman MB. Labeled albumin transport into normal and de-endothelialized rabbit thoracic aorta in vivo. In: Nerem RM, Guyton JR, eds. *Hemodynamics and the arterial wall, proceedings from a specialists meeting.* Houston: University of Houston; 1980:42-46.

80. Duncan LE, Cornfield J, Buck K. Circulation of iodonated albumin through the aortic and other connective tissues of the rabbit. *Circ Res.* 1958;6:244-245.

81. Duncan LE, Cornfield J, Buck K. Circulation of labeled albumin through the aortic wall of the dog. *Circ Res.* 1959;7:390-397.

82. Duncan LE, Buck K. Passage of labeled albumin into canine aortic wall in vivo and in vitro. *Am J Physiol.* 1960;200:622-624.

83. Duncan LE, Cornfield J, Buck K. The effect of blood pressure on the passage of labelled plasma albumin into canine aortic wall. *J Clin Invest.* 1962;41:1537-1545.

84. Fry DL, Mahley RW, Wersgraber KH, Oh SY. Simultaneous accumulation of Evans blue dye and albumin in canine aortic wall. *Am J Physiol.* 1977;233:H66-H79.

85. Fry DL, Melchior GW, Mitschelen J. Effect of serum and stirring on diffusive 125I-albumin and Evans Blue Dye uptake. *Am J Physiol.* 1982;243:H708-H712.

86. Fry DL. Effect of pressure and stirring on in vitro aortic transmural ^{125}I-albumin transport. *Am J Physiol.* 1983;245:H977-H991.

87. Ramirez CA, Colton CK, Smith KA, Stemmerman MB, Lees RS. Transport of 125I-albumin across normal and deendothelialized rabbit thoracic aorta in vivo. *Arteriosclerosis.* 1984;4:283-291.

88. Tedgui A, Lever J. The interaction of convection and diffusion in the transport of ^{131}I-Albumin within the media of the rabbit thoracic aorta. *Circ Res.* 1985;57:856-863.

89. Tedgui A, Merval R, Esposito B. Albumin transport characteristics of rat aorta in early phase of hypertension. *Circ Res.* 1992;71:932-942.

90. Weinberg PD. Application of fluorescence densitometry to the study of net albumin uptake by the rabbitaortic wall up- and downstream of intercostal ostia. *Atherosclerosis.* 1988;74:139-148.

91. Goldman B, Blamke H, Wolinsky H. Influence of pressure on permeability of normal and diseased muscular arteries to horseradish peroxidase. *Atherosclerosis.* 1987;65:215-225.

92. Penn MS, Koelle MR, Schwartz SM, Chisolm GM. Visualization and quantification of transmural concentration profiles of macromolecules across the arterial wall. *Circ Res.* 1990;67:11-22.

93. Penn MS, Chisolm GM. Relation between lipopolysaccharide-induced endothelial cell injury and entry of macromolecules into the rat in vivo. *Circ Res.* 1991;68:1259-1269.

94. Penn MS, Saidel GM, Chisolm GM. Vascular injury by endotoxin: changes in macromolecular transport parameters in rat aortas in vivo. *Am J Physiol.* 1992;262:H1563-H1571.

95. Penn MS, Saidel GM, Chisolm GM. Relative significance of endothelium and internal elastic lamina in regulating the entry of macromolecules into arteries in vivo. *Circ Res.* 1994;74:74-82.

96. Karnovsky MJ, Shea SM. Transcapillary transport by pinocytosis. *Microvasc Res.* 1970;2:353-360.

97. Bratzler RL, Colton CK, Smith KA. Endothelium and permeability: theoretical models for transport of low-density lipoproteins in the arterial wall. In: Manning GW, Daria-Haust M, eds. *Atherosclerosis: metabolic, morphologic, and clinical aspects.* New York: Plenum; 1975:943-951.

98. Fry DL. Mathematical models of arterial transmural transport. *Am J Physiol.* 1985;248:H240-H263.

99. Saidel GM, Morris ED, Chisolm GM. Transport of macromolecules in arterial wall in vivo: A mathematical model and analytical solutions. *Adv Exp Med and Bio.* 1987;49:153-169.

100. Truskey GA, Colton CK, Smith KA. Quantitative analysis of protein transport in the arterial wall. In: Schwartz CJ, Werthessen NT, Wolf S, eds. *Structure and Function of the Circulation.* New York: Plenum Press; 1981:287-355.

101. Weinbaum S, Caro CG. A macromolecule transport model for the arterial wall and endothelium based on the ultrastructural specialization observed in electron microscopic studies. *J Fluid Mech.* 1976;74:611-640.

102. Fry DL, Vaishnav RN. Mass transport in the arterial wall. In: Patel DJ, Vaishnav RN, eds. *Basic Hemodynamics and its Role in Disease Processes.* Baltimore: University Park Press; 1980:425-485.

103. Krishnan L, Krishnan EC, Jewell WR. Theoretical treatment of the distribution and degradation of vascular interstitial, and intracellular albumin. *J Theor Biol.* 1977;67:609-623.

104. Fry DL. Response of the arterial wall to certain physical fators. In: Scheinberg P, eds. *Atherogenesis: Initiating factors, Ciba. symposium.* Amsterdam: Associated Scientific Publishers; 1973:93-124.

105. Lovich MA, Edelman ER. Mechanisms of transmural heparin transport in the rat abdominal aorta after local vascular delivery. *Circ Res.* 1995;77:1143-1150.

106. Caro CG. Transport of 14C-cholesterol between intraluminal serum and artery wall in isolated dog common carotid artery. *J Phys.* 1973;233:37P-38P.

107. Nerem RM, Polsey JS, Robinson DL, Carey WE. *Shear dependent transport of albumin between blood and the arterial wall. 26th annual conference on engineering in medicine and biology.* Ed. Maryland: 1973. 15: 413.

108. Weinbaum S. Mathematical models for transport across the endothelial cell layer. *Ann NY Acad Sci.* 1983;416:92-114.

109. Yuan F, Chien S, Weinbaum S. A new view of convective-diffusive transport processes in the arterial intima. *J Biomech Eng.* 1991;113:314-329.

110. Tzeghai G, Ganatos P, Pfeffer R, Weinbaum S, Nir A. A theoretical model to study the effect of convection and leaky junctions on macromolecule transport in artery walls. *J Theor Biol.* 1986;121:141-162.

111. Weinbaum S, Tzeghai G, Ganatos P, Pfeffer R, Chien S. Effect of cell turnover and leaky junctions on arterial macromolecular transport. *Am J Physiol.* 1985;248:H945-H960.

112. Nir A, Pfeffer R. Transport of macromolecules across arterial wall in the presence of local endothelial injury. *J Theor Biol.* 1979;81:685-711.

113. Weinbaum S, Ganatos P, Pfeffer R, Wen GB, Lee M, Chien S. On the time-dependent diffusion of macromolecules through transient open junctions and their subendothelial spread I. Short-time model for cleft exit region. *J Theor Biol.* 1988;135:1-30.

114. Wen GB, Weinbaum S, Ganatos P, Pfeffer R, Chien S. On the time-dependent diffusion of macromolecules through transient open junctions and their subendothelial spread 2. Long time model for interaction between leakage sites. *J Theor Biol.* 1988;135:219-253.

115. Lin S-J, Jan K-M, Weinbaum S, Chien S. Transendothelial transport of low density lipoprotein in association with cell mitosis in rat aorta. *Arteriosclerosis.* 1989;9:230-238.

116. Caplan BA, Schwartz CJ. Increased endothelial cell turnover in areas of in vivo evans blue uptake in the pig aorta. *Atherosclerosis.* 1973;17:401-417.

117. Smith EB, Staples EM. Distribution of plasma proteins across the human aortic wall. *Atherosclerosis.* 1980;37:579-590.

118. Fung YC. *Biomechanics: Mechanical properties of living tissues.* second edition ed. New York: Springer-Verlag, 1993.

119. Tedgui A, Lever MJ. Effect of pressure and intimal damage on 131I-albumin and [14C]sucrose spaces in aorta. *Am J Physiol.* 1987;253:H1530-H1539.

120. Tedgui A, Lever MJ. Filtration through damaged and undamaged rabbit thoracic aorta. *Am J Physiol.* 1984;247:H784-H791.

121. Whale MD, Grodzinsky AJ, Johnson M. The effect of aging and pressure on the specific hydraulic conductivity of the aortic wall. *Biorheology.* 1995;33:17-44.

122. Caro CG, Lever MJ. Effect of vasoactive agents and applied stress on the albumin space of excised rabbit caraotid arteries. *Atherosclerosis.* 1983;46:137-146.

123. Curry FE, Michel CC. A fiber matrix model of capillary permeability. *Microvasc Res.* 1980;20:96-99.

124. Curry FE. Mechanics and thermodynamis of transcapillary exchange. In: Renkin EM, Michel CC, Geiger SR, eds. *THe handbook of physiology, Section 2, The Cardiovascular System.* Bethesda, MD: American Physiological Society; 1984:351-363.

125. Curry FE. Determinants of capillary permeability: a review of mechanisms based on single capilary studies in the frog. *Circ Res.* 1986;59:367-380.

126. Kim W-S, Tarbell JM. Macromolecular transport through the deformable porous media of an artery wall. *Transactions of the ASME.* 1994;116:156-163.

127. Clowes AW, Clowes MM. Kinetics of cellular proliferation after arterial injury. IV. Heparin inhibits rat smooth muscle mitogenesis and migration. *Circ Res.* 1986; 58:839-845.

128. Nugent MA, Karnovsky MJ, Edelman ER. Vascular cell-derived heparan sulfate shows coupled inhibition of basic fibroblast growth factor binding and mitogenesis in vascular smooth muscle ell. *Circ Res.* 1993;73:1051-1060.

129. Clowes AW, Reidy MA, Clowes MM. Kinetics of cellular proliferation after arterial injury. I: Smooth muscle cell proliferation following endothelial injury. *Lab Invest.* 1983;49:327-333.

130. Rohsenow WM, Choi HY. Mass transfer in turbulent flow and experimental results. In: Rohsenow WM, Choi HY, eds. *Heat, Mass, and Momentum Transfer.* Englewood Cliffs, NJ: Prentice-Hall, Inc.; 1961:410-424.

131. Mills AF. Forced convection. In: Mills AF, eds. *Heat Transfer.* Homewood, IL: Richard D. Irwin, Inc.; 1992:269-293.

132. Vargas CB, Vargas FF, Pribyl JG, Blackshear PL. Hydraulic conductivity of endothelial and outer layers of the rabbit aorta. *Am J Physiol.* 1979;236:H53-H60.

133. Bungay PM, Brenner H. The motion of a closely-fitting sphere in a fluid-filled tube. *Int J Multiphase Flow.* 1973;1:25-56.

134. Deen WM. Hindered transport of large molecules in liquid-filled pores. *AICHE J.* 1987;33:1409-1425.

135. Granath KA, Kvist BE. Molecular weight distribution analysis by gel chromotography on sephadex. *J Chromot.* 1967;28:69-81.

136. Siflinger A, Parker K, Caro CG. Uptake of ^{125}I albumin by the endothelial surface of the isolated dog common carotid artery: effect of certain physical factors and metabolic inhibitors. *Cardiovasc Res.* 1975;9:478-489.

137. Meyer G, Merval R, Tedgui A. Effects of pressure-induced strectch and convection on low-density lipoprotein and albumin uptake in the rabbit aortic wall. *Circ Res.* 1996;79:532-540.

138. Okada T, Bark DH, Mayberg MR. Localized release of perivascular heparin inhibits intimal proliferation after endothelial injury without systemic anticoagulation. *Neurosurg.* 1989;25:892-898.

139. Fry DL. Mass transport, atherogenesis, and risk. *Arteriosclerosis.* 1987;7:88-100.

140. Casu B. Heparin structure. *Haemostasis.* 1990;20 Suppl 1:62-73.

141. Ferro D, Provasoli A, Ragazzi M, Casu B, Torri G, Bossennec V, Perly B, Sinay P, Petitou M, Choay J. Conformer populations of L-iduronic acid residues in glycosaminoglycan sequences. *Carbohyd Res.* 1990;195:157-167.

142. Edelman ER, Nugent MA, Karnovsky MJ. Perivascular and intravenous bFGF administration: Vascular and solid organ deposition. *Proc Natl Acad Sci USA.* 1993;30:1513-1517.

143. Nugent MA, Edelman ER. Kinetics of basic fibroblast growth factor binding to its receptor and heparan sulfate proteoglycan: A mechanism for cooperativity. *Biochemistry*. 1992;31:8876-8883.

144. Pukac L, Ottlinger ME, Karnovsky M. Heparin suppresses specific second messenger pathways for protooncogene expression in rat vascular smooth muscle cells. *J Biol Chem*. 1992;267:3707-3711.

145. Castellot JJJ, K.Wong, Herman B, Hoover RL, Albertini DF, Wright TC, Caleb BL, Karnovsky MJ. Binding and internalization of heparin by vascular smooth muscle cells. *J Cell Physiol*. 1985;124:13-20.

146. Barzu T, Molho P, Tobelem G, Petitou M, Caen J. Binding and endocytosis of heparin by endothelial cells in culture. *Biochimica et Biophysica Acta*. 1985;845:196-203.

147. Psuja P. Affinity of radiolabeled (125I) Heparin and low molecular weight heparin fraction CY 222 to endothelium in culture. *Folia Haematol*. 1987;114:429-436.

148. Vannucchi S, Pasquali F, Chiarugi V, Ruggiero M. Internalization and metabolism of endogenous heparin by cultured endothelial cells. *Biochem Biophys Res Commun*. 1986;1140:294-301.

149. San Antonio JD, Slover J, Lawler J, Karnovsky MJ, Lander AD. Specificity in the interactions of extracellular matrix proteins with subpopulations of the glycosaminoglycan heparin. *Biochemistry*. 1993;32:4746-4755.

150. Press W, Flannery B, Teukolsky S, Vetterling W. Modeling of data: Nonlinear models. In: eds. *Numerical Recipes*. Cambridge, England: Cambridge University Press; 1986:521-528.

151. Haas K, Phillips S, Comerota A, White J. The architecture of adventitial elastin in the canine infrarenal aorta. *Anat Rec*. 1991;230:86-96.

152. Murata K, Motayama T, Kotake C. Collagen types in various layers of the human aorta and their changes with the atherosclerotic process. *Atherosclerosis*. 1986;60:251-262.

153. Barzu T, Rijn JLMLV, Petitou M, Molho P, Tobelem G. Endothelial binding sites for heparin: specificity and role in heparin neutralization. *Biochem J*. 1986;238:847-854.

154. Glimelius B, Busch C, Hook M. Binding of heparin on the surface of cultured human endothelial cells. *Thromb Res*. 1978;12:773-782.

155. Hiebert LM, McDuffie NM. The intracellular uptake and protracted release of exogenous heparins by cultured endothelial cells. *Artery*. 1989;16:208-222.

156. Brown LR, Wei CL, Langer R. In vivo and In vitro release of macromolecules from polymeric drug delivery systems. *J Pharm Sci*. 1983;72:1181-1185.

157. Slepian MJ. Polymeric endoluminal gel paving: Therapeutic hydrogel barriers and sustained drug delivery depots for local arterial wall biomanipulation. *Semin Intervent Cardiol*. 1996;1:103-116.

158. Mayberg MR. Localized release of perivascular heparin. *Persp Neuro Surg*. 1990;1:77-95.

159. Booth RFG, Martin JF, Honey AC, Hassall DG, Beesley JE, Moncada S. Rapid development of atherosclerotic lesions in the rabbit artery induced by perivascular manipulation. *Atherosclerosis.* 1989;76:257-268.

160. Huth F, Kojimahara M, Franken T, Rhedin P, Rosenbauer KA. Aortic alterations in rabbits following sheathing with silastic and polyethylene tubes. *Curr Top Pathol.* 1975;60:1-32.

161. Cardin AD, Weintraub HJR. Molecular modelling of protein-glycosaminoglycan interactions. *Arteriosclerosis.* 1989;9:21-32.

162. Letourneur D, Caleb BL, Castellot JJJ. Heparin binding, internalization, and metabolism in vascular smooth muscle cells: II. Degradation and secretion in sensitive and resistant cells. *J Cell Physiol.* 1995;165:687-695.

163. Slepian MJ, Weselcouch E, Cambell P, Roth L, Massia SP, Kieras M, Philbrook M. Endoluminal hydrogel polymer layers provide prolonged heparin delivery to porcine coronary artery wall in vivo. *J Am Coll Cardiol.* 1996;27 (Supplement A):85A.

164. Holman JP. *Heat Transfer.* Ed. 6th ed. New York: McGraw-Hill Book Co., 1963. 131-133.

165. Lincoff AM, Topol EJ, Ellis SG. Local Drug Delivery for the prevention of restenosis: Fact, fancy and future. *Circulation.* 1994;90:2070-2084.

166. Ruoslahti E, Yamaguchi Y. Proteoglycans as modulators of growth factor activity. *Cell.* 1991;64:867-869.

167. Burgess WH, Maciag T. The heparin binding (fibroblast) growth factor family of proteins. *Am Rev Biochem.* 1989;58:575-606.

168. Imai H, Connell CE, Lee KT, Kim DN, Thomas WA. Differential counts by electron microscopy of cell types in normal intimal cell masses in swine abdominal aortas. *Exp Mol Path.* 1985;42:377-388.

169. Scott RF, Thomas WA, Lee WM, Reiner JM, Florentin RA. Distribution of intimal smooth muscle cell masses and their relationship to early atherosclerosis in the abdominal aortas of young swine. *Atherosclerosis.* 1979;34:291-301.

170. Letourneur D, Caleb BL, Castellot JJJ. Heparin binding, internalization, and metabolism in vascular smooth muscle cells: I. Upregulation of heparin binding correlates with antiproliferative activity. *J Cell Physiol.* 1995;165:676-686.

171. Fingerle J, Au YPT, Clowes AW, Reidy MA. Intimal lesion formation in rat carotid arteries after endothelial denudation in absence of medial injury. *Arteriosclerosis.* 1990;10:1082-1087.